Data assimilation of GRACE terrestrial water storage data into a hydrological model using the Ensemble Kalman Smoother

A case study of the Rhine river basin

Endang Widiastuti

17 August 2009

Title:
Data assimilation of GRACE terrestrial water storage data into a hydrological model using the Ensemble Kalman Smoother: A case study of the Rhine river basin

Name: Endang Widiastuti
Student number: 13094142
Master programme: Geomatics

Graduation professor:
Prof. dr. ir. Nick C. van de Giesen
Water Resources Management, Faculty of Civil Engineering and Geosciences, TU Delft.
Daily supervisor:
Dr. ir. Susan C. Steele-Dunne
Water Resources Management, Faculty of Civil Engineering and Geosciences, TU Delft.
Committee members:
Dr. Brian C. Gunter
Physical and Space Geodesy, Faculty of Aerospace Engineering, TU Delft.
Dr. Albrecht Weerts
Deltares

Date: August 17th 2009

Abstract

Terrestrial water storage (TWS) can be defined as the storage of water on and below the land surface, and includes snow, ice, surface water, soil moisture, and ground water. TWS is a key component of the terrestrial and global hydrological cycles, which have important control over the water, energy and biogeochemical fluxes, and plays a major role in the Earth's climate. An accurate estimation of terrestrial water storage is thus important for improved water management. However, direct determination of TWS is difficult due to insufficient in-situ data. TWS estimation can be obtained through hydrological modelling, although models are not free from uncertainties due to inaccurate forcing data and weak modelling assumptions. However, the launch of the Gravity Recovery and Climate Experiment (GRACE) twin satellite mission has provided the first space based dataset for TWS estimates, although with coarse resolution and limited accuracy. It is expected that combining GRACE observations and estimates from a model could improve TWS estimates, and one way to this through data assimilation.

In this thesis, the ensemble Kalman filter (EnKF) and the ensemble Kalman smoother (EnKS) have been applied to assimilate the GRACE TWS variation data into the HBV-96 model, a conceptual rainfall-runoff model over the Rhine river basin, for the study period of February 1st 2003 to January 31st 2004. Two TWS variation estimates were inferred from two sets of GRACE solutions, one from DEOS – TU Delft, and another from CSR - University of Texas. Both solutions use different filtering methods which yield different estimates, and therefore can be expected to have different effect on the data assimilation.

The EnKF and EnKS have been successfully applied, fulfilling the expectation of having a new estimate with lower variance than both the prior model estimate and the GRACE observation estimate. The model estimated discharge after the data assimilation was compared with measured discharge at several stations. The discharge estimates were improved at the beginning of the experiment, but the degree of improvement decreased with time. Both of the GRACE data sets gave comparable results. Longer experiment period and comparison with other validation data could lead to a more definitive conclusion.

Preface

It has been a long journey to get to the point of finishing this thesis. Starting from a near 14 hours flight from Jakarta to Schipol back in September 2007 to start my master study in the Geomatics master programme in TU Delft, followed by what is easily the most exciting two years of my life, and wrapping it up with the most gruelling and yet exciting phase of my study, the graduation project. This thesis was conducted at the Water Resources Management Chair of Civil Engineering and Geosciences faculty in TU Delft, with cooperation with the Department of Earth Observations and Space Systems, Faculty of Aerospace Engineering in TU Delft, and the Deltares institute in Delft.

Having my bachelor degree in Geodetic engineering and working in Indonesia's national mapping agency for a couple of years, spatial data acquisition and processing have become my profession. But this graduation research has taken my knowledge into a different level. Data assimilation and hydrological modelling is not the mainstream study field in Geomatics, but this thesis has shown me a different way of using spatial data than what I was familiar with, and in improving our knowledge on the Earth systems, more specifically in water resources.

That being said, first and foremost I would like to sincerely thank my thesis supervisor, Dr. Susan Steele-Dunne, who came up with this topic, for her tireless support, education, encouragement and most of all patience in teaching and supervising me who is a novice in hydrology and data assimilation and getting me through this research. I found this interesting thesis topic through Prof. Nick van de Giesen who is also my thesis professor and Dr. Olivier Hoes from the Water Resources Management chair, and to them I'd like to extend my gratitude. This research wouldn't have happened without the support of my other two committee members: Dr. Albrecht Weerts from Deltares who had provided me with the HBV-96 model and the supporting data, and Dr. Brian Gunter who had provided me with the GRACE data and to them I extend my gratitude for all their support and help throughout this research.

During my master study and this thesis in particular, my colleague, friend and partner, Koen Duijnmayer has been a tremendous supporter, helping me numerous times with problem solving discussions and MATLAB scripting, and I sincerely thank him. The past two years of my studies wouldn't have been as nice without the education and assistance from the academic staff involved in Geomatics. Next to it, my fellow Geomatics students have been wonderful friends and colleagues during the lectures, synthesis project and also in everyday life and fun activities. I'd like to give my warm thanks to all of them. This thesis and my studies in general wouldn't have been possible without the Stuned scholarships programme and the staff of NESO Indonesia, and I'd like to thank them for this precious opportunity. Last but not least, I would like to thank my parents and family for their endless support and prayers throughout these years.

Endang Widiastuti

Delft, August 2009.

Table of contents

List of figures

List of tables

1 Introduction

1.1 Motivation

Terrestrial water storage (TWS) is a concept based on the water balance, which can be defined as the storage of water on and below the land surface, and includes snow, ice, surface water, soil moisture, and ground water. The temporal change in TWS is the closure term in the balance between precipitation, runoff, and evapotranspiration.

TWS is a key component of the terrestrial and global hydrological cycles, which have important control over the water, energy and biogeochemical fluxes, and play a major role in the Earth's climate. An accurate estimation of terrestrial water storage is thus important for improved water management. However, direct determination of TWS is difficult due to insufficient in-situ data on space-time variability of hydrologic stores (snow, soil moisture, and groundwater) and fluxes (precipitation, evapotranspiration). Until a few years ago, direct measurements of terrestrial water storage over large areas were nonexistent. However, the launch of the Gravity Recovery and Climate Experiment (GRACE) twin satellite mission in March 2002 has provided the first space based dataset for large scale TWS estimates. Although primarily aimed at accurately mapping time variations in Earth's gravity field at 30 day intervals, a lot of studies has shown the ability to infer water mass changes from GRACE observation.

The estimation of TWS changes at a river basin scale has been one of the most documented applications of the GRACE mission. It is expected that GRACE observations closes the water balance at river basin scale and allows the verification, improvement and modelling of the related hydrological processes by combining GRACE estimates with hydrological model output and in-situ data. The majority of studies to date in focus more on using GRACE estimates for comparison or validation of hydrological model (Güntner, 2008). However another way of utilising GRACE estimates is by using data assimilation to combine the GRACE TWS estimates with the model estimates into a single best estimate (Zaitchik, et al., 2008).

1.2 Research objective

The objective of this thesis is to perform an optimal data assimilation of GRACE derived terrestrial water storage change into a hydrological model, using the ensemble Kalman smoother. Some research questions involved with this objective are:

- How to map the coarse temporal and spatial resolution GRACE observations into the fine resolution hydrological model?
- How to separate the contribution of the TWS components from GRACE observation?
- Does assimilating GRACE into hydrological model improve the model's predictions?

1.3 Readers guide

This thesis starts by giving background information on terrestrial water storage, the GRACE derived monthly mean water storage variation, and a short review of recent comparisons between GRACE and hydrological models (Chapter 2). Next, a brief explanation of the basic

tenet of data assimilation is given in Chapter 3, focusing on the Ensemble Kalman Filter and Smoother. Chapter 4 describes the case study used in this thesis, which is the Rhine river basin modelled with the HBV-96 rainfall-runoff model and assimilated with GRACE observation. As a perquisite in using an existing hydrological model, a sensitivity study on the HBV-96 model was done and described in Chapter 5. In Chapter 6, the implementation of the Ensemble Kalman Filter and Smoother in this research is explained, followed by the results and discussion in Chapter 7. Finally conclusions are drawn in Chapter 8.

2 Background

This Chapter provides background information about terrestrial water storage, its importance to water management, and how it can be estimated by means of hydrological modelling and gravity field observations, including the GRACE satellite mission. The description is followed by a review on how information from both hydrological modelling and GRACE observation can be combined to provide a better estimate of terrestrial water storage.

2.1 Terrestrial water storage

Terrestrial water storage (TWS) can be defined as all forms of water stored above and underneath the surface of the Earth (Syed, et al., 2008), which can include water in vegetation surfaces, snow, ice, soil water, groundwater, and surface water in rivers, lakes, wetlands and man-made reservoirs.

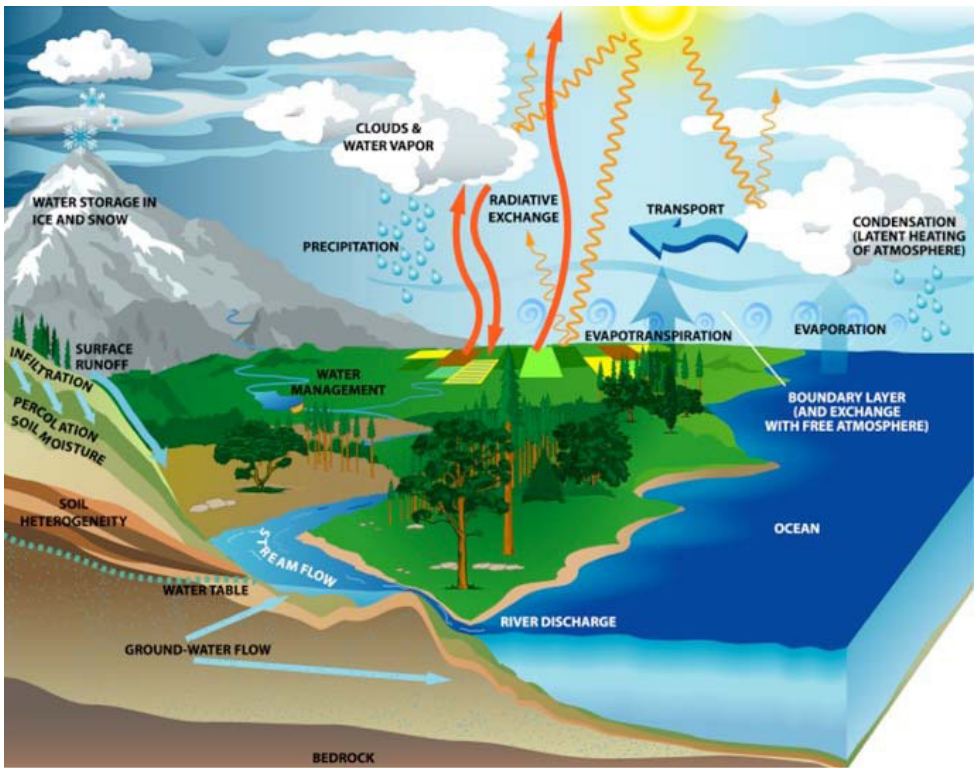

Figure 2-1 Water cycle **(Famiglietti, 2007)**

Although TWS only represent about 3.5% of the total amount of water on Earth (Riegger, et al., 2005), it is an important part of the terrestrial water cycle. Figure 2-1 illustrates the water cycle. Precipitation occurrs on land as snow and rain. Snow and ice are water in temporary terrestrial storage. Rain over land surfaces may be intercepted by vegetation and evaporate back to the atmosphere. Some of it infiltrates into soil and percolates into the ground water beneath the water table, which flows slowly through intermediate storages such as lake or wetlands, to river channels or directly to the sea. The water that infiltrate also feeds

vegetations where transpiration takes place. The remaining water on the surface is mostly directed as surface runoff to the river. This process can be generalized in the terrestrial water-balance equation:

$$P = Q + E + \Delta S \tag{2-1}$$

Where P is precipitation, Q is runoff, E is evapotranspiration, and ΔS is the storage change (i.e. TWS variation).

Here TWS can be seen as an integrated measure of surface and groundwater availability, which provides water supply for usage in domestic, industrial, and agricultural sectors. Soil moisture and snow are important memory components of the climate system, and soil moisture-precipitation, as well as soil moisture-temperature feedbacks appear relevant both for global and regional climate (Koster, et al., 2004). The ability to simulate present-day TWS is essential for predicting future changes in the hydrological cycle, stream flow and water availability, and related impacts on the occurrence of droughts, heat waves, or floods (Hirschi, et al., 2007).

Despite its importance, knowledge on spatial and temporal variations of TWS and its components are lacking, particularly on a large scale due to the lack of large-scale monitoring system. Ground based measurements only provide point estimates. Large spatial coverage can be provided from remote sensing observations, however in the case of soil water, these are limited to the upper soil layer and to areas free from dense vegetation cover. Variation in surface water can be observed with satellite altimetry or radar remote sensing, but it is still limited to large target areas (Güntner, et al., 2007)

Estimation of TWS is possible by using hydrological models. A large number of hydrological models are available, and vary in terms of process description, temporal resolution, spatial resolution, and the detail in process representation, see e.g. (Singh, et al., 2002). With respect to terrestrial water storage components, models vary in how they represent the individual component of TWS, or which components are included in the model.

A land surface model (LSM), for example, commonly represents the energy and water fluxes at the interface of atmosphere and land surface based on heat and mass balance equations. Most LSMs are constrained to a limited depth of soil and exclude model components for groundwater and water transport and surface storage. A water balance model on the other hand, which usually includes all components of hydrological cycle to close the water balance for area of interest, uses simplified conceptual approaches to simulate the water fluxes and storage (Güntner, 2008).

Hydrological modelling is constrained by the accuracy of the forcing data and the model formulations and parameterisation in representing the physics of the water cycle, i.e. model calibration. Therefore one cannot expect identical or similar results when different models are used at the same location and propagated using the same set of forcing data. However, the advantage of using a model is in its ability to obtain spatially distributed estimates, differentiate the different water storage components, and simulate changing boundary conditions.

An alternative way of measuring changes in terrestrial water storage is by observing the time variation of the Earth's gravity field, which has been realised by the launch of GRACE satellite mission, described in the following section.

2.2 TWS change in gravity

The earth's gravitational field varies in space and time as the result of the changes in the distribution of mass in the earth. Geophysical properties such as topography and density govern the spatial variations in surface gravity. Meanwhile, the temporal variations of gravity are caused by a variety of phenomena, including a time dependent gravitational constant and variations of the earth's rotation, tidal accelerations, and variations caused by terrestrial mass displacement. Hydrology has an important role in this mass distribution, since the earth's system consists of a fluid and mobile atmosphere and oceans, and a continuously changing distribution of ice, snow, soil moisture, and ground water (Hasan, 2009).

This temporal variation can be detected through repeated gravity measurements, using a ground based gravity meter such as a superconductive gravimeters (Kroner, et al., 2006). However, for large scale monitoring (e.g. at a river basin), this would require a vast network of monitoring stations.

On the other hand, changes in gravity field also affect the orbital motion of satellites, and thus conceptually it is possible to infer the change in gravity from the deviation of an orbiting satellite from its designed course at an epoch. This is the idea behind the Gravity Recovery and Climate Experiment (GRACE) mission.

GRACE is a twin satellite mission managed jointly by the United States National Aeronautics and Space Administration (NASA) and the German Aerospace Centre (DLR)[1] (Tapley, et al., 2004). The main objective of this mission is to obtain accurate estimates of the mean and time variable components of the earth's gravity field variations, with a temporal resolution of one month or better and a spatial resolution of ~ 400 km. The mission was launched in March 2002 and it is expected to provide data until 2010.

The two satellites are approximately 220 km from each other, and as they move along the orbit, a K-band microwave ranging system is used to calculate the inter-satellite range. The satellites are placed on a low orbit with initial altitude of ~ 500 km to allow the detection of the gravity signal. The orbit altitude is not kept fixed and decreases due to air drag at an average rate of ~2.7 km/year, and therefore the satellites do not have a fixed repeated ground track. A near polar orbit inclination of 89.5° is selected to allow a global coverage. Absolute positioning of the satellites is done using multi-channel dual frequency GPS receiver onboard each satellite. Next to this, absolute and relative orientations of the observations are determined using onboard star cameras. An accelerometer is used to account for non-conservative contributions to the inter-satellite ranges and range rates. The GRACE Science Data System (SDS) uses these measurements, to estimate a sequence of gravity estimates representing corrections to a well-defined background gravity model used in GRACE data processing (10,11).

During the GRACE data post processing, various time-variable gravity effects are already reduced from the data using models (e.g. 12); therefore the remaining gravity signal should mainly represent changes in terrestrial water storage, as well as mass changes in the polar ice caps and inland glaciers. GRACE provides the first direct observations of large scale TWS. However it is important to note that it is not possible to identify whether the inferred mass variation at a given time and region is due to changes in surface water or ground water, for example.

[1] *Deutsches Zentrum für Luft- und Raumfahrt e.V.*

The teams of the SDS provide time series of monthly GRACE gravity field models. This team consists of the Centre for Space Research (CSR)[2] , the GeoForschungsZentrum Postdam (GFZ)[3], and the Jet Propulsion Laboratory (JPL)[4]. Other than the SDS team, the Centre National d'Etudes Spatiales (CNES)[5] and the Delft Institute of Earth Observation and Space System (DEOS)[6] at Delft University of Technology also provide monthly gravity field solution. These solutions are provided in time series consisting of monthly and long-term mean sets of spherical harmonic coefficients. A more complete explanation on the mathematics of the spherical harmonic solutions can be found in e.g. Wahr, et al. (Wahr, et al., 1998).

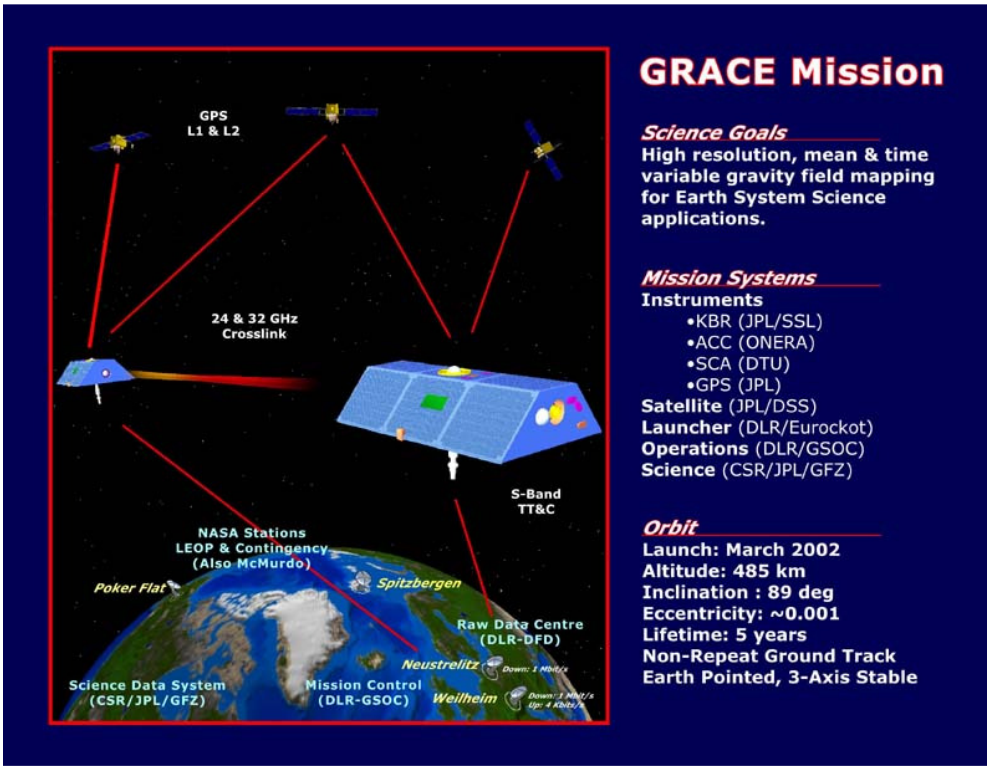

Figure 2-2 GRACE mission flight configuration **(CSR, 2004)**

Next to the monthly global GRACE models provided by these analysis centres, some other centres computes the so-called regional solutions using data over the region of interest as an alternative to the spherical harmonic solutions, see e.g Klees et al (Klees, et al., 2008b).

For both the monthly global solutions and regional solutions, the different analysis centres uses different approaches and yields to different sets of solutions. Klees, et al. (Klees, et al., 2008a) investigated the differences between the monthly spherical harmonic models and also between global models and regional models, and showed that the terrestrial water storage variations from these solutions agree with each other. The study also shows the impact that the choice of spatial filtering can have on the solution quality.

[2] http://www.csr.utexas.edu/grace/
[3] http://op.gfz-potsdam.de/grace/index_GRACE.html
[4] http://podaac.jpl.nasa.gov/grace/
[5] http://bgi.cnes.fr:8110/geoid-variations/README.html
[6] http://www.lr.tudelft.nl/live/pagina.jsp?id=613adfde-c9a6-4bc2-9bd6-80442f6e01d7&lang=en

As the GRACE solutions are interpreted as estimates of terrestrial water storage variation, errors in the estimates should not be neglected. One source of error is the error in the monthly gravity field solutions, which includes by the measurement and processing errors. Another source of error is due to changes in the true monthly mass averages caused by things other than the terrestrial water storage, which can include gravity signals cause by e.g. unmodeled mass variations in the Earth's interior (Wahr, et al., 2006). The typical accuracy of current GRACE solution river basins above 1 million km^2 is 20 mm equivalent water height (Klees, et al., 2008a).

2.3 GRACE vs. hydrological models

The previous sections have highlighted the advantages and shortcomings of using either hydrological model or GRACE observation to estimate TWS variation. It would be advantageous if one could combine the best of both methods and come up with the best estimates of TWS and its individual components.

The majority of publications to date on GRACE TWS variation with respect to hydrological models are focused on the evaluations of models by comparison with GRACE data. Güntner (Güntner, 2008) compiled an extensive list of these studies, and it was concluded that in general the comparisons show reasonable agreement between model predictions and GRACE-based data, in terms of the seasonal dynamics and their continental scale spatial patterns. However, some differences in amplitudes and phase of seasonal variations were found. The correspondence between models and GRACE generally tends to degrade when going to smaller spatial scales. The differences found in these comparisons can provide a valuable hint about existing model deficiencies, although it should be noted that the differences are also due to limitations of GRACE monitoring technique and data error. In this sense, GRACE can be used as additional information to constrain model calibration or model validation.

Another way of integrating GRACE data with hydrological models prediction is through data assimilation. Using data assimilation techniques, the model states can be continuously updated, taking into account the errors estimated for both model states and GRACE observations, resulting in an improved model prediction which is closer to the truth while at the same time minimising the error. This is an attractive method, as data assimilation can provide a mean to utilise the full potential of GRACE TWS variation estimates, by downscaling GRACE observation in time and space and separating GRACE TWS variation into individual storages, as opposed to a mere comparison.

However, the fact is that GRACE data has a couple of fundamental shortcomings with respect to typical hydrological models:

- GRACE data gives an integral value of water storage variations from all individual water storage components, while models represent a selection of, if not all, water storage components.
- GRACE data is monthly time averaged while hydrological models typically have much finer temporal resolution, up to hourly time steps.

Based on the recent studies, Güntner (Güntner, 2008) highlighted that a sound comparison or integration between hydrological model and GRACE should be achieved by:

- Using a model which incorporates the full set of storage components to simulate total water storage changes as in the GRACE data.

- Separating the storage component to be improved in the hydrological model from the integral GRACE signal, or
- Excluding components of the model if reliable information exists that supports the assumption that these components do not significantly contribute to water storage variations in the area of interest.

Assimilating GRACE data into a hydrological model therefore requires a careful strategy in handling the vertical and temporal disaggregation to achieve an outcome which combines the best estimates out of the two.

While data assimilation has been used for updating hydrological elements with remote sensing data (e.g. (Reichle, et al., 2002), (Dunne, et al., 2006)), the study for the use of GRACE data for updating a hydrological model is still in early stage. The only documented application of data assimilation of GRACE data to date is the study by Zaitchik, et al. (2008). In this study, GRACE data is assimilated into the Catchment Land Surface Model for the Mississippi river basin, using a uniform monthly smoother referred in their publication as Ensemble Kalman Smoother (EnKS)-GRACE. The results are promising, as the experiment led to increased correlation between TWS estimates and gauged river flow.

This thesis attempts to look at the capability of using data assimilation methods to integrate GRACE TWS variation data into a different kind of hydrological model, namely the HBV, a conceptual rainfall-runoff model. The experiment takes place at Western Europe's largest river basin, the Rhine, as will be explained further in Chapter 4.

3 Data assimilation

Hydrological systems are complex and difficult to observe. In situ observations are limited in time and even more in space. For example in groundwater measurement, a piezometric well needs to be dug to observe the piezometric head. Locations of these wells are restricted to where it is possible to set them up and is only a sample at a small scale. Therefore a model serves as an interpolator at locations where necessary information is not available.

Models are at a certain level a conceptual model, i.e. they simplify the processes that occur in reality. This is due to the lack of knowledge about certain processes and their interaction, the lack of mathematical tools to solve analytically the set of equation and/or differential equations describing the system's behaviour, and the computing power which limits the size of data that can be handled(Drécourt, 2004).

From the limited in-situ observations to the simplifications of reality, models are thus suffering from uncertainties. The major uncertainties encountered in hydrological modelling are ((Melching, 1995) in (Drécourt, 2004)):

- Natural uncertainties: random temporal and spatial fluctuations. It is only possible to evaluate the magnitude of the uncertainties.
- Data uncertainties (forcing term): The main problem comes from the discretisation in time and space of the measurements (e.g. rainfall), and the necessity of spatial interpolation to get these measurements over the whole domain of study from the information given by point measurements.
- Model-parameter uncertainties: It is impossible to find one set of parameters that represent reality properly. This uncertainty is related to the problem of equifinality (Beven, et al.): During a model calibration, different combinations of parameters can yield to a good model performance, but still users would not be sure if the model is doing it for the right reasons.
- Model structure uncertainty: It is impossible to truly represent the physical processes by model simulation.

Next to this, there is the issue of scale to take into account. Hydrological processes behave differently at different scales, and it is difficult to observe hydrological behaviour at the appropriate scale of our modelling (Savenije, 2007). Scaling uncertainties can be related to (Drécourt, 2004):

- The scale at which the differential equation represents the system.
- The scale of the model, i.e. the size of the discretisation grid that is used to evaluate the equations.
- The scale of the observations used to build and calibrate the model. They can be point observations (e.g. rainfall gauge) or zone observation (remote sensing data).

The existence of these uncertainties motivates the need to combine the model with other existing observation to obtain a better representation of the system's behaviour. Remote sensing data in particular are abundant compared to in situ measurements, but still there are limitations and uncertainties surrounding these data, at which using remote sensing data alone is not sufficient in representing the hydrological system.

Remote sensing data are affected by the sensor errors and extraneous noises. As remote sensing instruments typically observe electromagnetic properties of the Earth system as opposed to directly measuring the feature of interest (e.g. measuring microwave radiation to obtain soil moisture), the data are dependent on the inversion of the observed properties to the real physical value. This in turn may include some approximation in the inversion model and affects the accuracy of the data.

In the case of GRACE, extraction of terrestrial water storage variation involves spatial filtering procedure to reduce GRACE errors, but at the same time yields biased amplitude estimates (Klees, et al., 2007). A number of studies are being conducted in improving the GRACE solutions, which at present the typical accuracy reaches 20 cm equivalent water heights for river basins above 1 million km^2 (Klees, et al., 2008a).

Next to this, the spatial and temporal resolution and observability of remote sensing observations are still limited. Hydrological models can work up to hourly time steps, and current satellite sensors are unable to provide such rapid dataset. GRACE for example, has a monthly temporal resolution. It provides terrestrial water storage variation as a whole, whilst hydrological model represents the individual storages. Its spatial resolution is dependent on the spatial filtering method, but it is typically >1.5 million km^2, while the spatial resolution of models can be in the order of km.

The existence of uncertainties and limitations of both the model and the observation requires a certain technique to combine the different information, one of which is data assimilation.

3.1 What is data assimilation?

Data assimilation can be loosely defined as the combination the complementary information from reliable observations and dynamic model into an optimal estimate of an unknown true state.

In data assimilation, observations can be interpolated or extrapolated, aggregated or downscaled to resolve the scale of interest, both in time and in space. States that are not directly observed are inferred by the updated model state, or can be included in the state vector and updated through the covariance matrix. This is done by taking into account the uncertainties from both the model and the observation. When a reliable observation becomes available, the estimate from data assimilation will draw close to the observations. At other times when such observation is unavailable, the estimate will be closer to the model solution, but still be influenced by the observation available at a different time.

A group of data assimilation techniques which have been used in hydrologic application is the variational method (e.g. (Reichle, et al., 2001)). In this method, the past observations, from the start of modelling until the present time, are used simultaneously to correct the initial conditions of the model and obtain the best overall fit of the state of observations, illustrated in Figure 3-1. Example of variational method is the 1DVAR, 3DVAR and 4DVAR method. In this technique, the model error is generally assumed to be time-invariant. The core of this method is the derivation of the adjoint model, which is obtained by linearization of the hydrologic model. The assumption of time-invariant model covariance can be considered unrealistic (Seo, et al., 2003), and the derivation of adjoint model adds to the complexity of implementing this method.

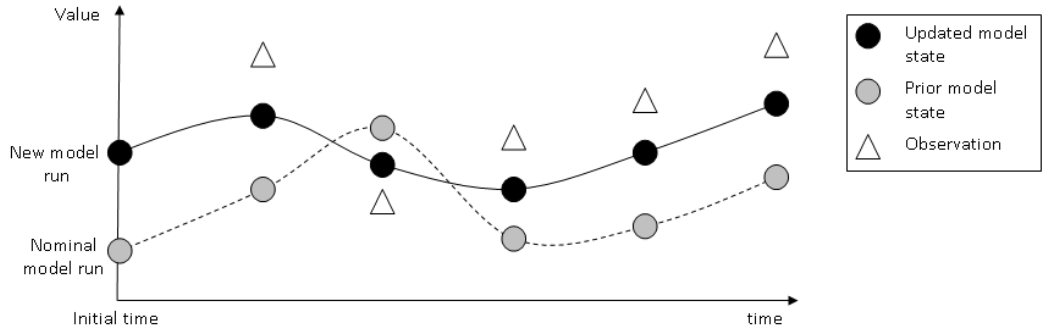

Figure 3-1 Variational data assimilation method. The initial model run is given better initial condition that leads to a new model run that is closer to the observations (after **(Drécourt, 2004)**).

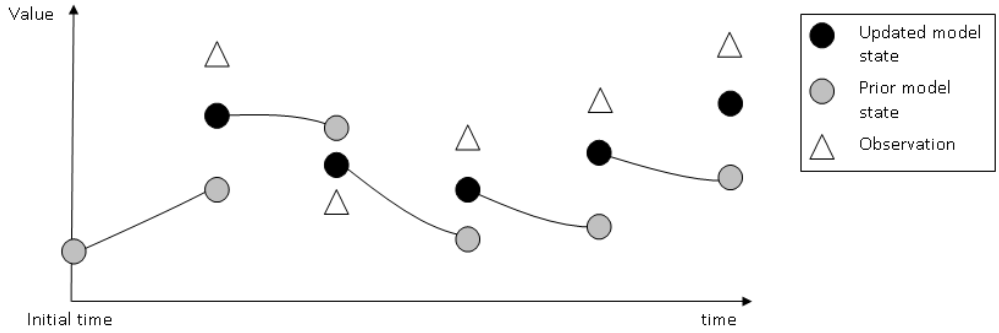

Figure 3-2 Sequential data assimilation method. When an observation is available, the model state is updated to a value closer to the observation that is used to make the next model state (after **(Drécourt, 2004)**)

Another group of data assimilation method which has gathered a lot of attention in hydrological applications is the sequential methods, derived from the classic linear Kalman filter. In sequential data assimilation, observations are used when they became available to correct the present state of the model. In contrast to the variational method, sequential methods lead to discontinuities in the time series of the corrected state, as illustrated in Figure 3-2.

The classic linear Kalman filter itself is rarely used in hydrological application, as it is designed for linear models, while hydrological models are rarely linear. For non-linear model, the extended Kalman filter (EKF) is available and hase been successfully applied, e.g. (Crosson, et al., 2002). The equations are the same as the linear Kalman filter, assuming that the model state variables are differentiable. In the EKF, the state is modelled forward with the full non-linear model. The error is propagated forward using the tangent linear model, so the state equation must be differentiable. The assumption of differentiable model is often difficult to apply for strong nonlinear hydrological models, and this approximation can lead to unstable results.

Table 3-1 Advantages and disadvantages of ensemble-based methods compared to variational methods (after **(Dunne, et al.)**)

	Ensemble-based methods	Variational methods
Advantages	Any model can be used. Model does not need to be differentiable. Noise can be placed anywhere, e.g. on uncertain parameters and forcing data Noise can be non-Gaussian and non-additive.	Uses all data in a batch window to estimate the state
Disadvantages	Estimates are conditioned on past measurements only (for filters, e.g. EnKF)	Model must be differentiable to obtain tangent linear model. Process noise can only be additive and Gaussian. Changes to model require that adjoint be obtained again.

An alternative sequential method is the ensemble methods, where using the Monte Carlo method, a sample population is drawn from a desired probability distribution, creating an ensemble of model states. Such Monte Carlo approximation of the Kalman filter was proposed by Evensen (Evensen, 2004), known as the ensemble Kalman filter (EnKF). This method is popular due to its ease of use and computational burden is less demanding. Dunne and Entekhabi (Dunne, et al.) provided a comparison of the advantages and disadvantages of the ensemble based methods compared to variational methods (Table 3-1).

Next to the ease of implementation, EnKF has an advantage compared to the EKF, in which the the tangent linear model is not needed to propagate the covariance; instead it can be calculated from the ensemble. For these reasons, the EnKF and its extension, the ensemble Kalman smoother (EnKS) is used in this thesis work and the mathematical formulations are described further in the following sections. For a much more detailed explanation, readers are referred to Evensen (Evensen, 2003).

3.2 Ensemble Kalman Filter

In the EnKF, an ensemble of model states is integrated forward in time using the non-linear forward model, with replicates of system noise. At update times, the error covariance is calculated from the ensemble. The notations being used here follow those of (Dunne, et al., 2006).

The non-linear model can be expressed in a generic form as follows:

$$y(t) = A[y(\tau), \alpha, u(\tau), w(\tau)] \tag{3-1}$$

The state variables of interest are gathered in the vector y , the non-linear model is expressed by A , which has parameters in the vector α , forcing data in the vector $u(\tau)$, vector of system uncertainty $\omega(\tau)$, and where $t > \tau > 0$.

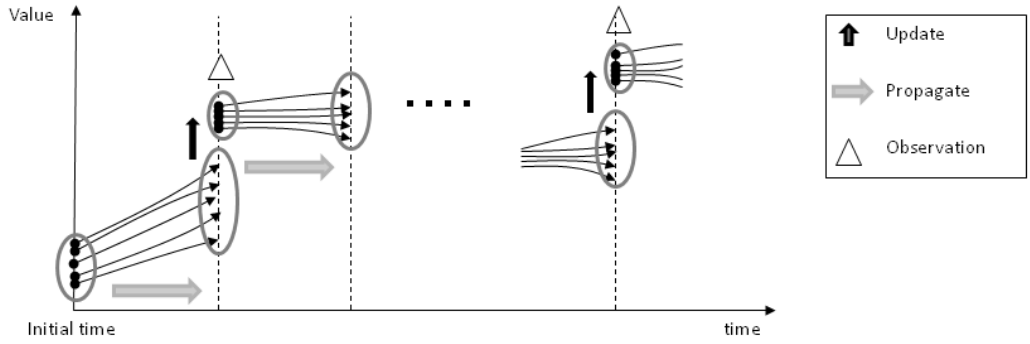

Figure 3-3 Ensemble filtering: each replicate is propagated forward until a new observation is available and then updated (after **(McLaughin, 2002)**).

If the observations available at a measurement time t are gathered in a vector of observations z, the measurement can be expressed as:

$$z(t) = \mathrm{M}[y(t)] + e(t) \quad (3\text{-}2)$$

M is operator which relates the true state to the measured variable. The uncertainty in the observation is given in the vector e, which is assumed to be zero mean with covariance matrix $R_e R_e$ as a probabilistic interpretation of uncertainty is adopted.

The EnKF moves sequentially from one measurement time to the next and works in two steps, a forecast step and an update step (Figure 3-3). In the initial forecast step, first the EnKF is initialised by generating an ensemble of N realisation of the state vector $y_j(t=0), j=1...N$ around a mean $y(t=0)$with covariance C_{y0}. This reflects the prior knowledge of the state at initial time. In addition to uncertainty in the initial guess, the parameters and forcing data can be uncertain. Therefore each ensemble member is drawn from a distribution of possible values.

As each ensemble member is updated with respect to a perturbed observation to ensure that the spread of the updated ensemble is consistent with the true posterior estimation, at the update time $t\,t$, an ensemble of perturbed observations is generated:

$$z_j(t) = z(t) + \epsilon_j(t) \quad (3\text{-}3)$$

Where *j* denotes the *j*-th ensemble member. If the ensemble of perturbations is gathered into the matrix $\gamma = (\varepsilon_1, \varepsilon_2, .. \varepsilon_N)\, \gamma = (\epsilon_1, \epsilon_2, \dots, \epsilon_3)$, the measurement error covariance can be written as:

$$R_e = \frac{\gamma \gamma^T}{N-1} \quad (3\text{-}4)$$

The updated state, denoted by ^{a} which was obtained for each ensemble member during the forecast step is then:

$$y_j^a(t) = y_j(t) + K(t)(z_j(t) - \mathrm{M}[y_j(t)]) \quad (3\text{-}5)$$

Where $K(t)$ is the so-called Kalman gain matrix:

$$K(t) = C_{YM}(C_M R_e)^{-1} \tag{3-6}$$

C_{YM} is the forecast cross covariance between the state vector $y(t)$ and the measurement prediction $\mathcal{M}[y(t)]$. C_M is the forecast error covariance of the measurement predictions. The states, perturbed observations and predicted measurements can be collected into matrices Y, Z, and M respectively. The terms of the Kalman gain matrix can then be written as:

$$C_{YM} = \frac{1}{N-1} Y' M'^T \tag{3-7}$$

$$C_M = \frac{1}{N-1} M' M'^T \tag{3-8}$$

The primed matrices are matrices whose ensemble mean has been removed from each column. Equation 13 can be rearranged and expressed as:

$$Y^a(t) = Y(t) + Y'(t)M'^T(t)\left(M'(t)M'^T(t) + \gamma\gamma^T\right)^{-1}\left(Z(t) - M(t)\right) \tag{3-9}$$

3.3 Ensemble Kalman Smoother

The ensemble Kalman smoother (EnKS) can be considered as an extension of the EnKF. It updates the ensemble at prior times t' every time new observations are available, using:

$$Y^a(t') = Y(t') + Y'(t')M'^T(t)\left(M'(t)M'^T(t) + \gamma\gamma^T\right)^{-1}\left(Z(t) - M(t)\right) \tag{3-10}$$

The EnKS is also a sequential method, where every time a new measurement becomes available, the ensemble at the current time and any previous time can be updated. The terms containing time t can be grouped together, and equation 3-10 be written as:

$$Y^a(t') = Y(t) + Y'(t')B(t) \tag{3-11}$$

$B(t)$is calculated only once at the update time t and can be used to update previous time t', thus the expensive matrix inversion is computed once only.

Each EnKS update changes the ensemble mean and reduces the ensemble variance, and therefore the results are at least as good as the EnKF. However, as more observations in the future are being use, the update becomes negligible as the time between state of interest and the observation time exceed the decorrelation time.

It is important to note that both EnKF and EnKS use the assumption of Gaussian error distribution, as in the classic Kalman filter, and they are thus suboptimal when the prior ensemble has a non Gaussian distribution.

4 Case study

In this Chapter, some facts about the case study area - the Rhine river basin - are given, followed by a brief description of the HBV model and the GRACE observations which have been used in this thesis. All data used and presented in this thesis are in the Gauss Krueger Zone 3 coordinate system, which is a German coordinate system where the majority of the study area lies on.

4.1 Study area

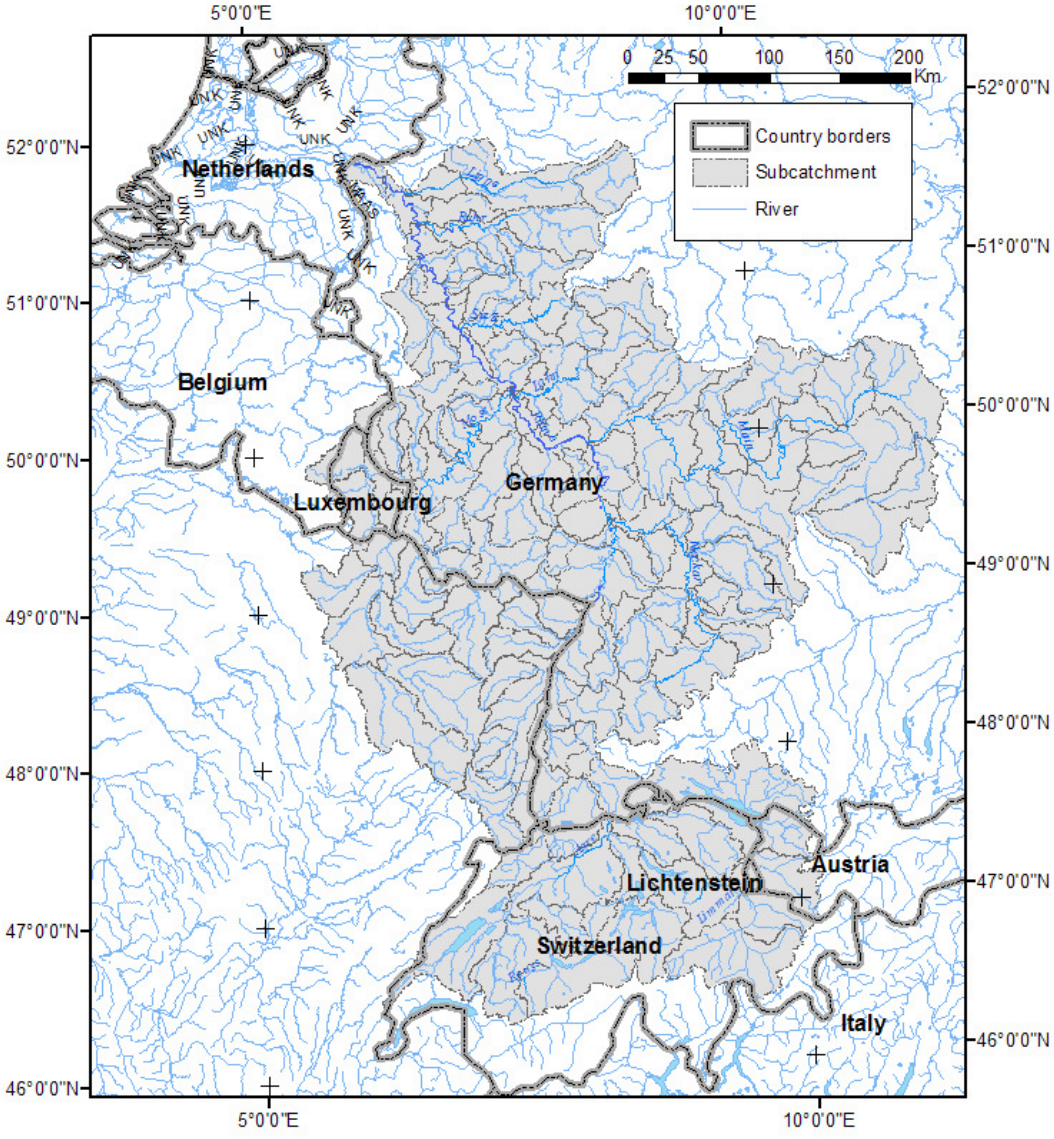

Figure 4-1 The Rhine river basin and its sub catchments (in grey).

The river Rhine is a major river in Western Europe, which originates at the Swiss Alps. The river basin covers several countries: Austria, Belgium, France, Germany, Italy, Liechtenstein, Luxembourg, Netherlands, and Switzerland. Based on its geographical and climatological characteristics, the Rhine river basin can be roughly divided into three areas: the Alpine area

upstream of Basel, the German middle mountains between Basel and Koln, and the lowland region.

At the Alpine area, the main tributaries are the Aare, Reuss, and Limmat rivers. Within this area, large differences in precipitation occur, where the maximum annual precipitation on the mountains can reach 3000 mm, while in the valley it's only 600 mm (International Commission for the Hydrology of the Rhine (CHR), 1997). A substantial part of the precipitation is temporarily stored in snow cover.

At the German middle mountains, the main tributaries are the Neckar, Main, Moselle, Lahn and the Sieg. The climate and its spatial variability of this area are largely determined by the elevation. Average temperatures decrease with elevation, while precipitation generally increases with elevation. With respect to the altitude, average precipitation decreases from north to south.

The lowland region has maritime climate characteristics, with lower annual and daily amplitude of temperature than the upstream part of the basin. The main tributaries are the Lippe, Ruhr, and the Vecht. In the Netherlands, the Rhine splits up into three main distributaries: the Waal, Nederrijn-Lek, and Ijsel.

The discharge of the Rhine is mainly determined by the amount and timing of precipitation, snow storage, and snow melt in the Alps, the evapotranspiration surplus during the summer period, and changes in the amount of groundwater and soil water storage (International Commission for the Hydrology of the Rhine (CHR), 1997).

There are over 50 million people inhabitants in the Rhine river basin (Rhi09). The river is intensively navigated, connecting the world's largest seaport, Rotterdam with the world largest inland port, Duisburg; and a large number of industrial complexes are built along the river. Besides for navigation the river is used for domestic and agricultural water supply, waste water disposal, hydropower generation, fisheries, recreation and other purposes.

The river basin area considered in this case study follows that of the operational forecasting by the German Federal Institute for Hydrology (BfG) and the Dutch Centre for Water Management (WMCN) (Berglöv, et al., 2009), as shown in Figure 4-1. This study area excludes the lowland region, and comprises an area of ~160.000 km^2.

4.2 Hydrological model: HBV-96

The model used in this is thesis is HBV-96, named after the abbreviation of of **H**ydrologiska **B**yråns **V**attenbalansavdelning (Hydrological Bureau Waterbalance-section). This was the former section at SMHI, the Swedish Meteorological and Hydrological Institute, where the model was originally developed in the early 70's. Since then, the HBV model has been used in over 40 countries (SHMI). In 1996, a comprehensive re-evaluation of the HBV model routines was carried out (Lindstorm, et al., 1997), resulted in the HBV-96 version.

The variant of HBV-96 model used in this thesis was set up by BfG in cooperation with WMCN, obtained by the author through Deltares (Weerts, 2009). Since 2005, the hourly model of HBV-96 has been integrated in the forecasting systems FEWS-DE and FEWS-NL respectively. However in studies such as this thesis a daily time step is used. The HBV-96 model used in this thesis was programmed in PCRaster environment (University of Utrecht)

The model was calibrated primarily (period 1990-1999) with REGNIE data from the Deutscher Wetterdienst. The Rhine river basin is subdivided into 134 sub-basins (Figure 4-1) and the model parameters are determined for each sub-basin. Sample of spatial distributions of some parameters are shown in Figure 4-2.

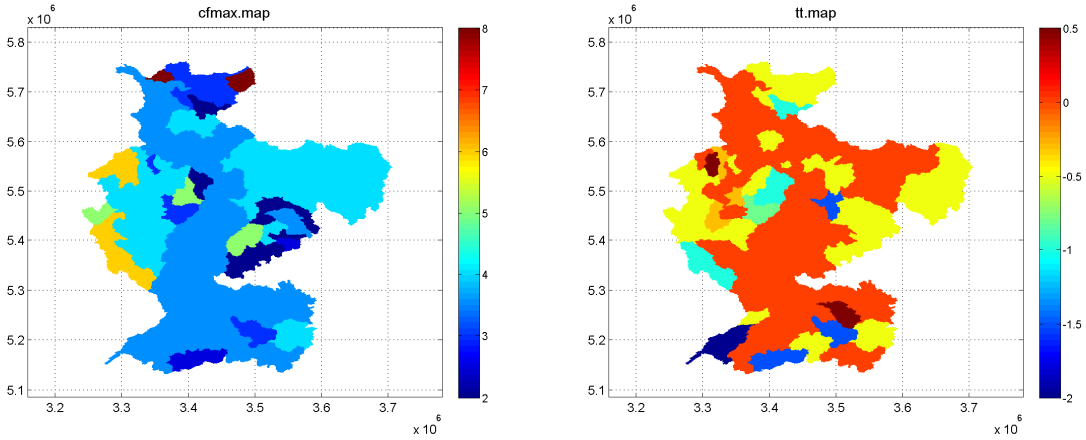

Figure 4-2 Spatial distribution of parameter maps.
Left: cfmax (snow melting factor), right: tt (threshold temperature).

A schematic presentation of the HBV-96 model is given in Figure 4-1. The model consists of three major parts: a snow routine, a soil routine, and a runoff response routine. In the above schematic, the model states are denoted by **S**. The following explanation about the model follows that of Berglöv, et.al. (Berglöv, et al., 2009) .

The snow routine is based on a simple degree day relation. A threshold temperature *tt* (usually about 0 °C) is used to define the temperature above which snow melt occurs. This is controlled by the melting factor *cfmax*:

$$snowmelt = cf \max.(T - tt) \tag{4-1}$$

A different melting factor applies for forest zones, corrected by the parameter *focfmax*. The snowpack is assumed to retain melt water as long as the amount does not exceed a certain fraction given by the parameter *whc*. When temperature decreases below *tt*, the water refreezes with a refreezing factor *cfr*:

$$refreezing = cfr.cf \max.(tt - T) \tag{4-2}$$

The snow storage is calculated from the accumulated snowfall and snow melt.

The soil routine is the main part controlling runoff formation, and controlled by three parameters: β , *lp*, and *fc*. β controls the runoff to soil (i.e. seepage) or the increase in soil moisture storage. *Lp* is a soil moisture value above which evapotranspiration reaches its potential value, and *fc* is the maximum soil moisture storage (in mm) in the model. The parameter *lp* is given as a fraction of *fc*.

The effect of the soil routine is that the contribution to runoff from rain or snow melt is small when the soil is dry and large at wet conditions, thus the runoff coefficient varies with the wetness of the soil. The actual evapotranspiration decreases as the soil dries out.

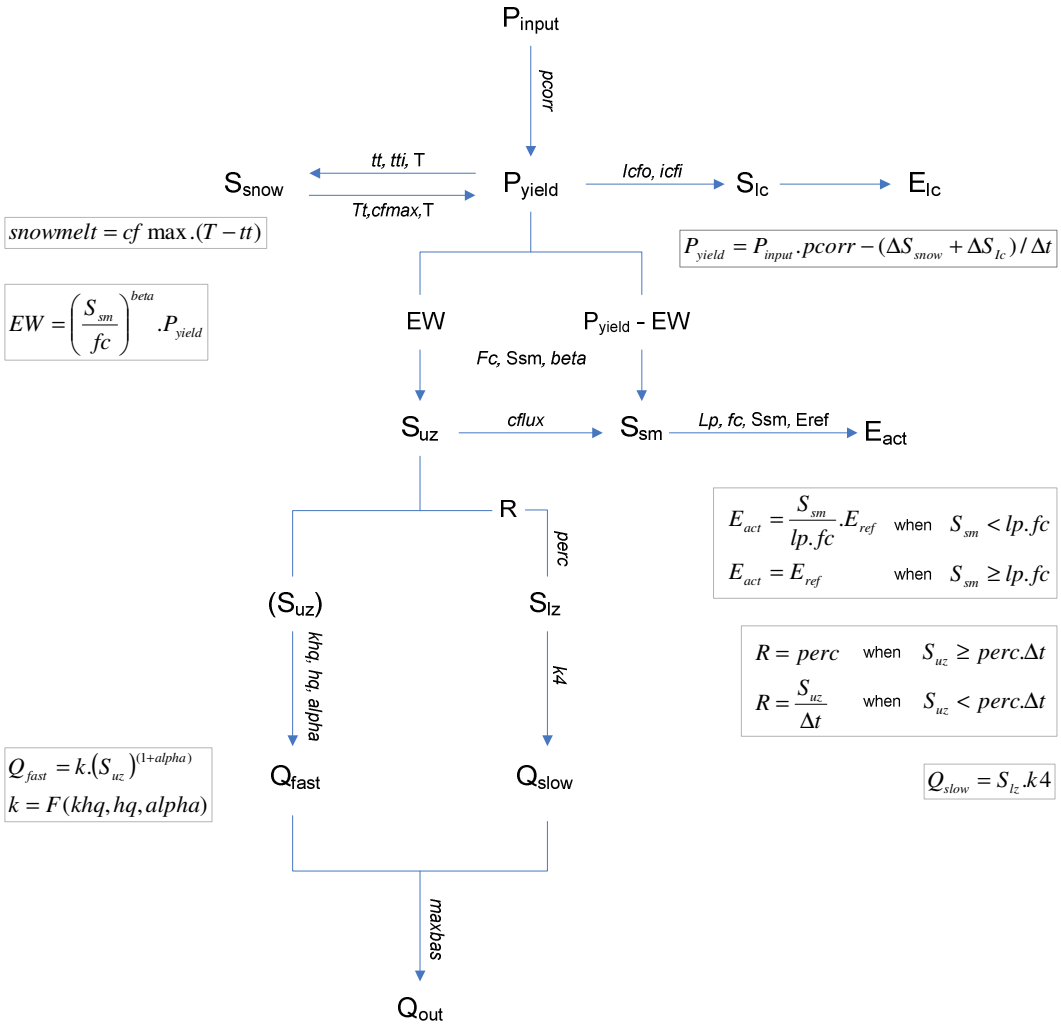

Figure 4-3 Schematic overview of the HBV model**(Weerts, et al., 2006)**.

The runoff routine is the response function which transforms excess water from the soil moisture zone to the runoff. It consists of one upper-nonlinear reservoir (**S_{uz}**) and one lower-linear reservoir (**S_{lz}**), which are the origin of the quick and slow runoff. The yield from the soil moisture zone will be added to the upper reservoir. As long as there is water in the upper reservoir, water will percolate to the lower zone, controlled by the parameter *perc*. When there is high yield from the soil, percolation is not sufficient to keep the upper reservoir empty, the generated discharge will contribute directly from the upper reservoir. The lower reservoir represents the groundwater storage which contributes to the base flow.

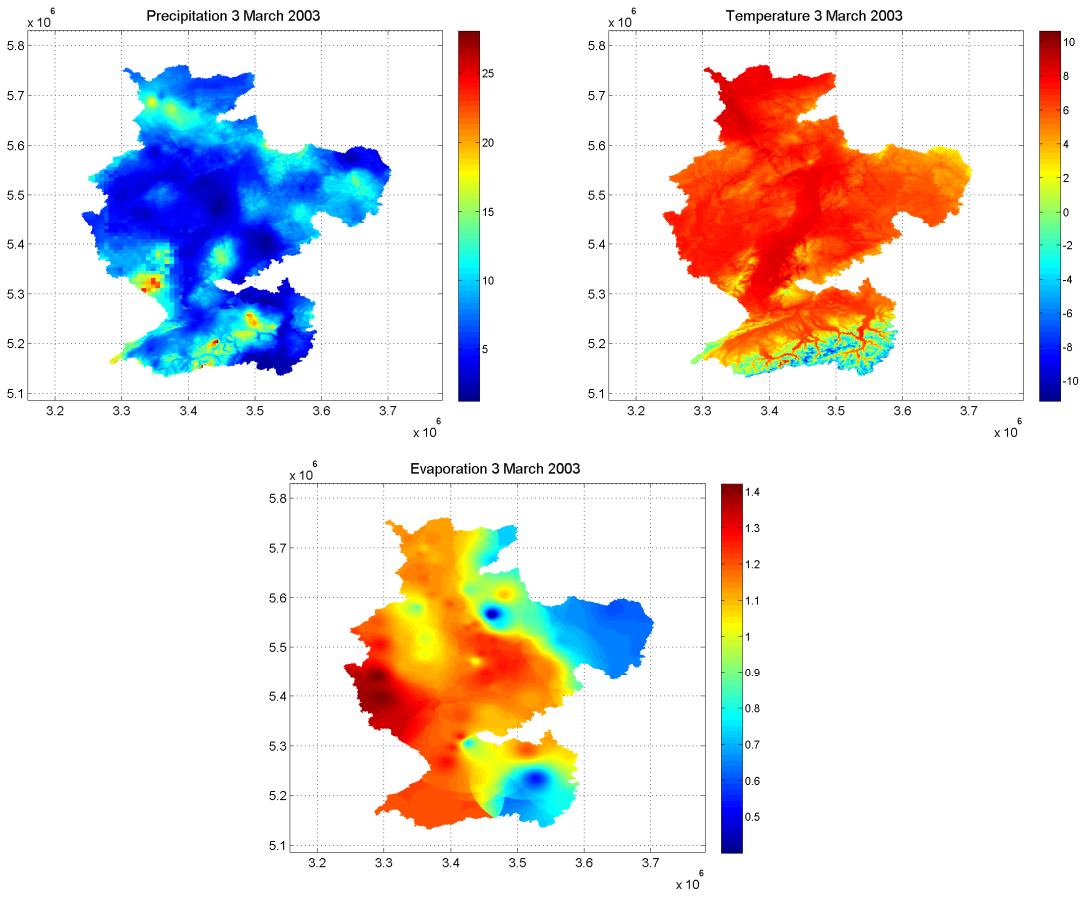

Figure 4-4 Input maps for March 3rd 2003, in mm.

The quick flow from the upper reservoir is calculated with:

$$Q_{fast} = k.(S_{uz})^{(1+alpha)}$$
$$k = F(khq, hq, alpha) \quad \textbf{(4-3)}$$

Where *k* is the recession coefficient of upper reservoir. The outflow from the lower reservoir is calculated with:

$$Q_{slow} = S_{lz}.k4 \quad \textbf{(4-4)}$$

With k4 being the recession coefficient of the lower reservoir.

The input data required by the HBV-96 model are precipitation, air temperature, and evapotranspiration for daily timestep. The available data for this thesis is from January 1st 2001 until December 31st 2005, and the grid size is 1 km (Weerts, 2009).

The input data are available in the form of PC Raster maps, in units of millimetre. The precipitation data originates from observations at 46 stations that provide hourly values of precipitation. Interpolation from these point observations into the whole map was required. This was done by making use of mean monthly precipitation background grids. The measured precipitation is divided by these grids to derive the precipitation anomaly. The anomaly is then

interpolated to a grid with the same size as the background grid, then multiplied with the background grid to derive the interpolated field. This approach corrects for orography and to take into account the orientation of the terrain. The interpolation methodology was developed in Deltares (Weerts, et al., 2008).

The temperature data also originates from observations at temperature (~200 stations), providing hourly values of temperature. Missing temperature data at stations are filled using Kriging, using variogram parameters derived for Switzerland and taking into account the east-west direction of Alps (anisotropic variogram). Next, the temperature is interpolated to mean height of the sub-basin. Then the mean height can be used to calculate the temperature in different elevation zone using the parameter tcalt with a default value of 0.6, resulting in temperature maps for each time step (Weerts, et al., 2008).

Potential evaporation data is derived from long term mean potential evaporation measurements from limited stations, and the potential evaporation is the same for every day of a month (Weerts, et al., 2008).

A sample of the input maps for a given time step is shown in Figure 4-4.

4.3 GRACE data

As mentioned in section 2.3, there are several GRACE processing centres which release solutions of the TWS variations, each using their own method and algorithm in the derivation. For this thesis, two sets of GRACE data are available, provided by DEOS (Gunter, 2009)**.**

The first one is a solution derived from the GRACE Level-2 product version CSR-RL04 4 of the CSR [(GFZ)], from here on denoted as GRACE-GSM. To remove the correlated noise in the spherical harmonic coefficients, a filter was applied. Processed at DEOS, the destriping technique of Swenson and Wahr (Wahr, et al., 2006) was applied, combined with a 400 km half width Gaussian smoothing. This is the so-called DS400 filter (Klees, et al., 2008a).

The second set of data the DEOS DMT1 solution, from here on denoted as GRACE-DMT. This data set was processed with a different kind of filter, namely the anisotropic non-symmetric (ANS) filter (Klees, et al., 2008c). This filter exploits full signal and noise variance-covariance information in an iterative least-square approach, without any destriping. Figure 4-5 shows a sample of both datasets at a given time. Notice the different magnitude between the two data set as a result of the different filtering method.

4.4 Comparison between model and GRACE

A comparison between the two monthly GRACE TWS variation and with the monthly HBV-96 derived TWS variation model is shown in
Figure 4-6. Prior to the comparison period, the HBV-96 model was propagated starting from January 1st 2001 to allow for the model to spin up and the reservoirs to fill up accordingly. The period starting from January 1st 2002 is where the real signal starts to show from the model, and thus comparable to the GRACE data. The result of this model propagation using the original input data and parameters is from here on denoted as open loop (OL).

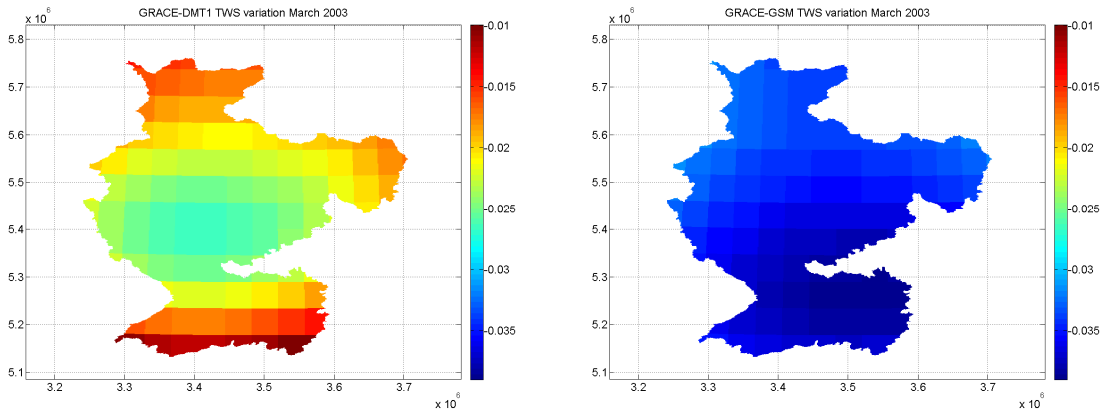

Figure 4-5 Map of GRACE TWS variation for March 2003.
Left: GRACE-DMT1, right: GRACE-GSM.

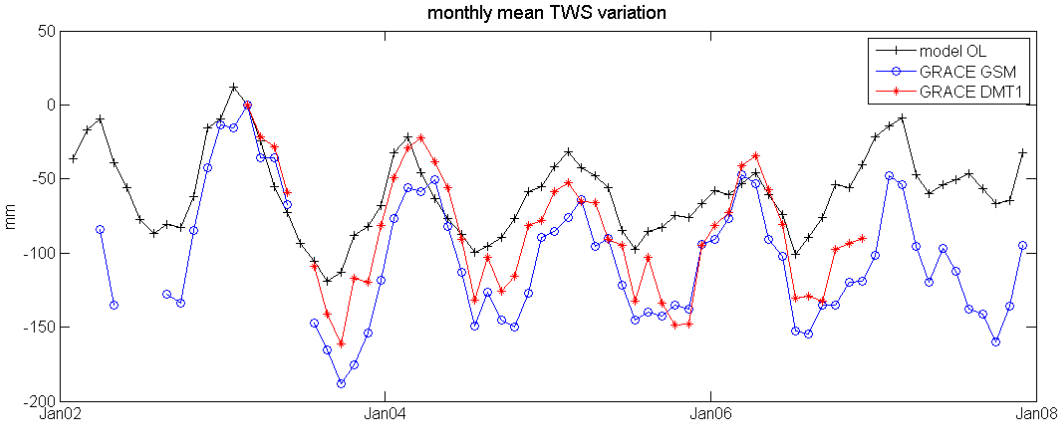

Figure 4-6 Comparison of the monthly mean TWS variation between the model and the two GRACE data.

While the HBV model actually calculate several storages as described previously in section 16, the model TWS is calculated only as the sum of three components: soil moisture, upper zone storage, and lower zone storage, because these three have the most influence on the runoff and also the biggest contribution towards the TWS.

The DEOS-DMT1 data are only available from February 2003 until December 2006. As a result, February 2003 was set as the starting time from which the monthly TWS variations for both dataset were calculated. Therefore the TWS variation from the model open loop also used February 2003 as the reference. Note that there are some data gaps in GSM data for June and July 2002 and in both dataset for June 2003.

While the seasonal pattern of the model and GRACE agree with each other, apparently both GRACE data tend to give larger TWS variation compared to the model. There are also peaks that occur on GRACE on August 2004 and August 2005 that do not occur in the model. Comparing GRACE-GSM and GRACE-DMT1, the former generally estimates lower values than the latter. This can be expected to have different influence on the data assimilation.

5 Sensitivity study

Sensitivity is the rate of change in one factor with respect to change in another. The sensitivity study is an essential tool in the proper use of an existing model because it enables the model user to understand the importance of variables and the effects of errors in inputs on computed outputs.

Within this thesis, sensitivity study of the HBV model is performed to answer these questions:

1. Which are the most important parameters of the model?
2. What is the effect of perturbing a parameter on the model states?
3. Which parameters should be perturbed for the EnKS?
4. What is the effect of perturbing forcing data on the model states?

This is important to understand the impact of uncertainty in the model parametes. The same applies for the forcing data, there is little knowledge of the accuracy of the data measurements, and the fact that the data are interpolated to the whole catchment means there are uncertainties in the forcing maps.

5.1 Perturbing model parameters

The sensitivity study was done using a Monte Carlo sampling approach. For each tested parameter, an ensemble of random noise within a certain normal distribution is applied to the nominal parameter. For each ensemble member $i = 1{:}\,nr$, where nr is the number of replicates:

$$\alpha_i = \alpha_{nom} + \varepsilon_i \tag{5-1}$$

Where α_{nom} is the nominal model parameter, ε_i is the noise, and α_i is the perturbed parameter. This normal distribution uses the nominal value as the mean and a predetermined standard deviation. After the ensemble member generation, each ensemble member are propagated with the model varying one parameter at a time, i.e. as one perturbed parameter is perturbed, the remaining parameters use their nominal values.

As HBV-96 is a complex model with 33 parameters involved, it was not possible to perform analysis on all parameters within the limited time frame. Instead, 10 parameters were chosen to be tested, which are considered to have the most likely influence on the model states. Description of these parameters is presented in Table 5-1.

For each of these parameters, two types of perturbations were applied. The sizes of perturbations are:

- $dev = 0.02 * (\max value - \min value)$
- $dev = 0.05 * (\max value - \min value)$

Table 5-1 Parameters tested in the sensitivity study.
No upper bound is applied on several parameters, indicated with dash (-).

Parameter	**Definition**	**Range of nominal values**		**Suggested range** (Siebert, 2007)		**Range of perturbation**	
		Min	**Max**	**Min**	**Max**	**Min**	**Max**
k4	Recession constant base flow	0.001	0.09	-	-	0	-
khq	Recession rate at flow HQ	0.01	0.3	-	-	0	-
maxbas	Number of days in unit hydrograph (<=10)	0	3	1	5	0	5
beta	Exponent in soil runoff generation equation	0.9	3	1	6	1	6
fc	Total water holding capacity of the soil	100	309	50	500	50	500
perc	Percolation from upper to lower zone (mm/day)	0.1	5	0	6	0	6
cflux	Maximum capillary rise from runoff response routine to soil moisture routine	0	1.5	-	-	0	-
lp	Fraction of field capacity below which actual evaporation = potential evaporation	0.5	0.9	0.3	1	0	1
Icfi	Maximum interception storage in non forested area	1	1.5	-	-	0	-
Icfo	Maximum interception storage in forested area	1.5	4	-	-	0	-

10 ensemble members are generated for each type of perturbation. The ensemble is then propagated with the model for the time period January 1st 2001 until December 31st 2001. To analyse the results, the ensemble mean, standard deviation, and coefficient of variation for the whole catchment at every time step are calculated for the model states. Coefficient of variation (CV) is:

$$CV = \frac{std.deviation}{mean} \tag{5-2}$$

And the model states are:

1. Snow (in mm)
2. Soil moisture (in mm)
3. Interception storage (in mm)
4. Lower zone storage (in mm)
5. Upper zone storage (in mm)
6. Runoff (m3/s)
7. Accumulated discharge (m3/s)
8. Base flow (mm)

Next to the catchment, the statistics of 5 pixels are also analysed, which are spread across the catchment as shown in Figure 5-1. The results are compared with the nominal open loop run.

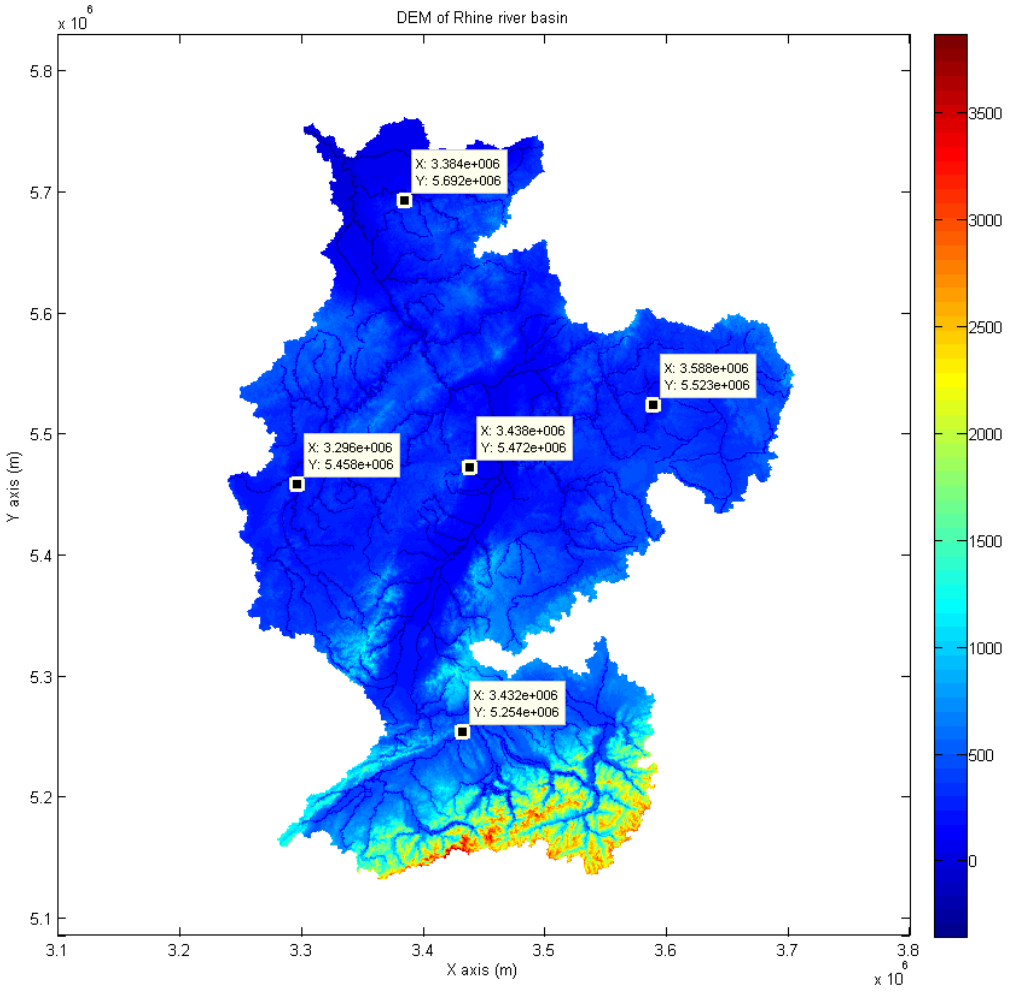

Figure 5-1 Locations of the analysed pixels overlaid on the catchment DEM

Table 5-2 Pixel descriptions

	Location	**Easting (km)**	**Northing (km)**	**Land cover**
Pixel 1	West	3.296 e+06	5.458 e+06	Non-forest
Pixel 2	Centre	3.438 e+06	5.472 e+06	Non-forest
Pixel 3	East	3.566 e+06	5.523 e+06	Non-forest
Pixel 4	North	3.384 e+06	5.569 e+06	Non-forest
Pixel 5	South	3.432 e+06	5.254 e+06	forest

The criteria to choose between these parameters are those which give enough variability and ensemble spread to the model states concerning TWS (i.e. soil moisture, upper zone and lower zone storage), while the ensemble mean of all model states are still physically reasonable and not resulting strange behaviour of the model.

Perturbing individual parameters

Overall, the upper zone storage is the most affected model state by any parameter perturbation. This means that it is the most dynamic part of the water storage. The impact of perturbing these 10 parameters on the model is summarised in **Error! Reference source not found.**. Increasing the size of perturbation 2.5 times in general reflects in the increase of CV at a similar magnitude.

Table 5-3 Summary of parameter perturbations

Parameter	Influenced model state	Highest variability	
K4	LZ, Q, Qacc, Base	LZ	Large impact on lower zone (2.5 times higher than OL). Doesn't impact other storage.
Khq	SM, LZ, UZ, Q, Qacc, Base	UZ	Biggest impact on upper zone.
Maxbas	-	-	No impact and variability for all model states.
Beta	SM, LZ, UZ, Q, Qacc, Base	UZ	Have impact on lower zone, but still small difference to OL. Moderate variability everywhere except upper zone.
Fc	SM, LZ, UZ, Q, Qacc, Base	UZ, SM	Small impact on soil moisture at the pixel, almost no impact on other storages.
Perc	SM, LZ, UZ, Q, Qacc, Base	UZ, LZ, Base	Have impact on upper zone and lower zone, small on others.
Cflux	SM, LZ, UZ, Q, Qacc, Base	UZ	Small impact on soil moisture, upper zone and lower zone
Lp	SM, LZ, UZ, Q, Qacc, Base	UZ	Small to no impact for all model states.
Icfi	SM, IS, LZ, UZ, Q, Qacc, Base	UZ, IS	Influence non-forested area. Small difference to OL at other model states.
Icfo	SM, IS, LZ, UZ, Q, Qacc, Base	UZ, IS	Influence forested area. Small difference to OL at other model states.

Figures highlighting the most affected storage for the perturbed parameters are given in **Appendix A**.

To find out which parameters have the highest overall impact towards the model states, a ranking is done based on the combined results of CV, both from the catchment and pixel statistics. These are given in table 15. Note that snow cover is not affected at all by any of the parameters and therefore not included in the table. The maximum and minimum values of CV for each parameter perturbation can be found in **Appendix A**.

In deciding the final set of parameters to perturb for the EnKS, it is important to take into account not only the variability but also that there is no significant bias in the ensemble mean of the TWS model states (i.e. soil moisture, upper zone storage, and lower zone storage).

Perturbing *k4* has a big impact towards lower zone storage. Even with the smallest deviation, the catchment mean is approximately 2.5 times higher than the unperturbed open loop (OL). The rest of the model states however show no discrete or very small difference with the OL. Looking at CV confirms that while perturbing *k4* leads to high variability to lower zone, it doesn't have any effect on soil moisture and upper zone storage. Seeing its effect on lower zone, including *k4* in the final set of parameters could risk on disturbing the model too much, resulting into a physically impossible model output.

Table 5-4 Rank of resulting variability.

Rank	Base flow	Interception storage	Lower zone storage	Discharge	Runoff	Soil Moisture	Upper zone storage
1	perc	icfi	k4	khq	khq	fc	fc
2	k4	icfo	perc	perc	perc	cflux	perc
3	khq		khq	k4	k4	perc	beta
4	beta		beta	cflux	beta	beta	lp
5	cflux		cflux	beta	cflux	lp	cflux
6	lp		lp	fc	fc	icfi	icfi
7	fc		fc	lp	lp	khq	khq
8	icfi		icfi	icfi	icfi	icfo	icfo
9	icfo		icfo	icfo	icfo		

Perturbing *maxbas* has no effect on the mean model states as all model states remain the same as the OL, and also gives no variability. This could mean that changing *maxbas* affects the rate of water transport across the catchment, but still none of the model output is sensitive for this variable, i.e. all standard deviations remain zero. Therefore there is no need to include *maxbas* in the final set of parameters.

Next, icfi and icfo, which are the paramaters concerned with the interception from precipitation, mainly impact the interception storage, but not the three TWS storage. Therefore they both can be excluded from the final set of parameters.

While individually fc and lp have very small impact towards the storages, they are both related in the model to determined the actual evaporation (see Section 4.1), and therefore the combined effect could potentially have a bigger impact on the storages. *Cflux* has moderate impact on the model states and can be included in the ensemble member generation.

After reviewing the above results, the 6 parameters chosen to be perturbed in the ensemble member generation for the data assimilation are: **khq, beta, fc, perc, cflux, and lp.**

Perturbing parameters together

The next step is to observe the model behaviour when the 6 chosen parameters are perturbed at the same time. Using the same two types of perturbations for the combined set of parameters, 15 ensemble members are propagated forward with the model, from January 1st 2001 until December 31st 2001.

As can be seen in Figure 5-2, 5-3, and 5-4, perturbing the 6 parameters does not show much impact on the mean storages, i.e. small difference between the ensemble mean and the OL. Looking at the values of CV, only snow cover and interception storage are not affected. This is expected as none of the parameters are belong to the snow or interception calculations in the model.

The upper zone again shows the highest value of CV, which confirms that this is the most dynamic storage. The soil moisture and the lower zone storage both show moderate variability. Increasing the perturbation size by 2.5 times again shows an increase in the ensemble standard deviation about 2.5 times.

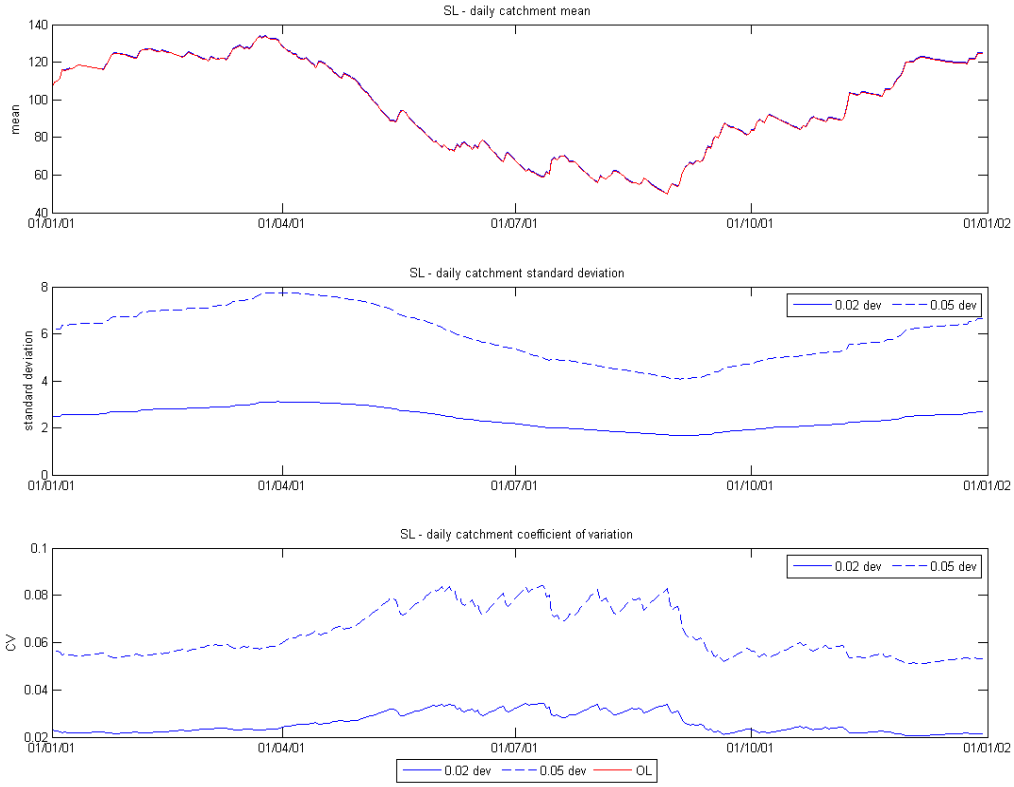

Figure 5-2 Catchment statistics for soil moisture
Perturbed parameter: *khq, beta, fc, perc, cflux,* and *lp*.

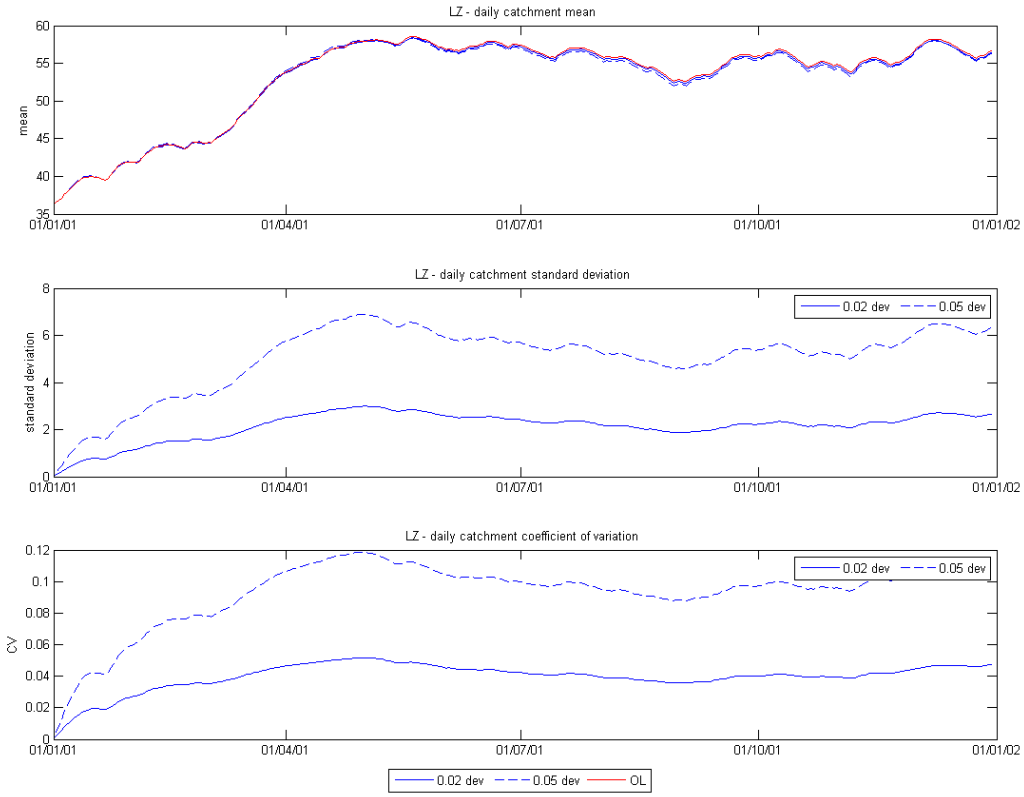

Figure 5-3 Catchment statistics for lower zone storage
Perturbed parameter*: khq, beta, fc, perc, cflux,* and *lp.*

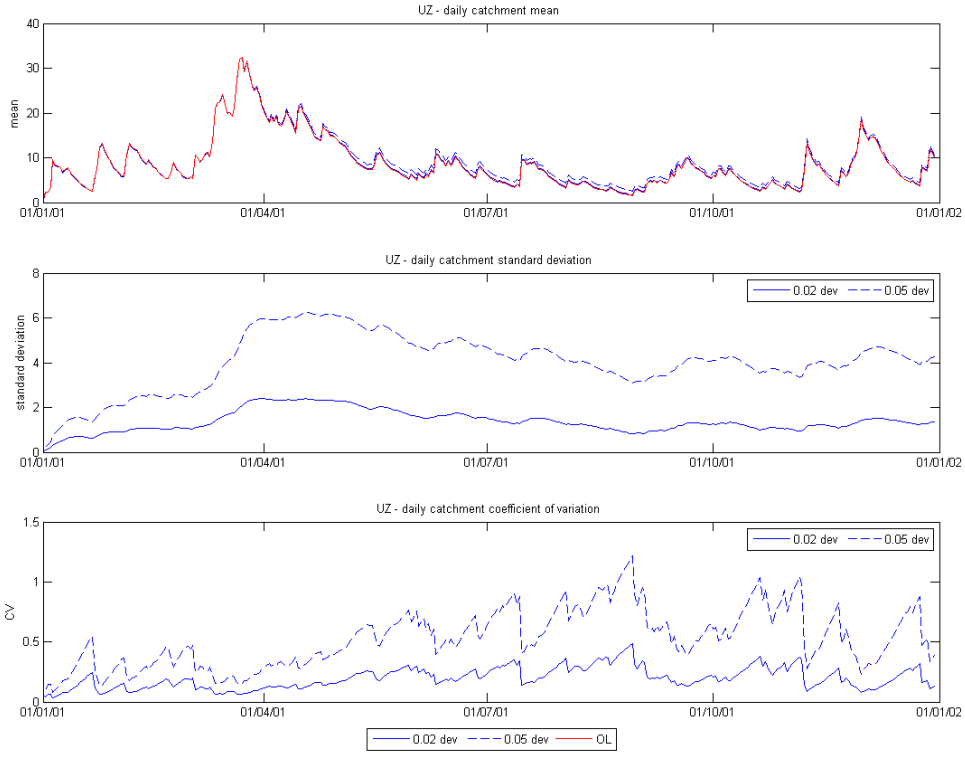

Figure 5-4 Catchment statistics for upper zone storage
Perturbed parameter*: khq, beta, fc, perc, cflux,* and *lp*.

Table 5-5 Coefficient of variation
Perturbed parameter: *khq, beta, fc, perc, cflux,* and *lp*.

	Output (1-4)							
	Snow cover		**Soil Moisture**		**Interception Storage**		**Lower Zone Storage**	
CV	Min	Max	Min	Max	Min	Max	Min	Max
Catchment	0	0	0.0206	0.0839	0	0	0.0007	0.1185
Pixel 1	0	0	0.0239	0.1701	0	0	0.0177	0.7907
Pixel 2	0	0	0.1701	0.0180	0	0	0	0.1404
Pixel 3	0	0	0.0255	0.1868	0	0	0	0.5279
Pixel 4	0	0	0.0181	0.1161	0	0	0.0234	0.7565
Pixel 5	0	0	0.0143	0.0780	0	0	0	0.1600
	Output (5-8)							
	Upper Zone Storage		**Runoff (Q)**		**Discharge (Qacc)**		**Base flow**	
CV	Min	Max	Min	Max	Min	Max	Min	Max
Catchment	0.0329	1.2160	3.10E-03	0.1760	4.11E-05	0.0038	0.0032	0.2183
Pixel 1	0.0227	0.9916	0.0071	0.3867	7.84E-05	0.0030	0.0177	0.7907
Pixel 2	0.0246	3.8729	0	0.3452	0	0.1015	0	0.1404
Pixel 3	0.0448	3.8729	0	0.3280	0	0.0988	0	0.5279
Pixel 4	0.0391	3.1332	0.0061	0.3741	0.00608	0.3741	0.0234	0.7565
Pixel 5	0.0173	3.8729	0	0.4269	0	0.4269	0	0.1600

Perturbing forcing data

In the case of perturbing model parameters, ensemble members are generated by applying random noise to the nominal parameter values. However in the case of perturbing forcing data, exponential spatial correlation functions are used to model the covariances of the forcing data. This is done to ensure that the perturbed maps maintain a reasonable spatial correlation. For example when there's precipitation at one pixel, it can be expected that precipitation also occurs in the neighbouring pixels, although the rate can be different.

In the perturbation, the spatial correlation is applied using an exponential function:

$$C(i,j) = \exp\left(-1 * \left(\frac{\sqrt{\left(X(i)-X(j)\right)^2 + \left(Y(i)-Y(j)\right)^2}}{L}\right)\right) \quad (5\text{-}3)$$

where *C(i,j)* is the spatial correlation, *i* and *j* denotes the row and column respectively, *X* and *Y* denotes the coordinates in *X* and *Y* direction, and *L* is the correlation length. The covariance matrix now becomes:

$$C_{dev} = dev^2 * \left(C + C^T - I\right) \quad (5\text{-}4)$$

where *I* is an identity matrix. The noise map ε_{nr} now a has a distribution with the nominal value as the mean and C_{dev} as the covariance.

As there is little knowledge on the correlation length of the forcing maps, *L* was determined by calculating the variogram of the input maps. *L* here is the mean of the range of the variogram

over the year 2001 (see Appendix B). The range of the input maps varies for each day, so ideally the correlation length should also vary for each day. However the idea is to obtain a value such that the perturbed maps are physically reasonable. Therefore taking a single value L from the mean of the range over one year is considered to be sufficient. The values are 59 km for evapotranspiration, 21 km for precipitation and 21 km for temperature.

From variogram calculation, ideally it would be possible to obtain the variance from the nugget value and use it as the deviation size in generating the noise. However as explained in section 4.2, the input maps were results from interpolation. Apparently the nugget value has been filtered out in the process, since the nugget value is close to zero everywhere. Therefore the same deviation sizes as used for the parameter maps are also used in perturbing the input maps.

The statistics of the model states after propagating 15 replicates with the model are calculated and the catchment statistics of the TWS related model states are shown in Figures 5-5 to 5-7. Again CV is calculated to observe the variability resulted from perturbing forcing data, as given in Table 5-6.

In contrast to perturbing model parameters, perturbing forcing data introduces bias between the ensemble mean of the modes states and the nominal OL, which increase in time. This means that the physics of the model is strongly dependent on the forcing data. The standard deviation and the CV are however not as effected as when perturbing the model parameters.

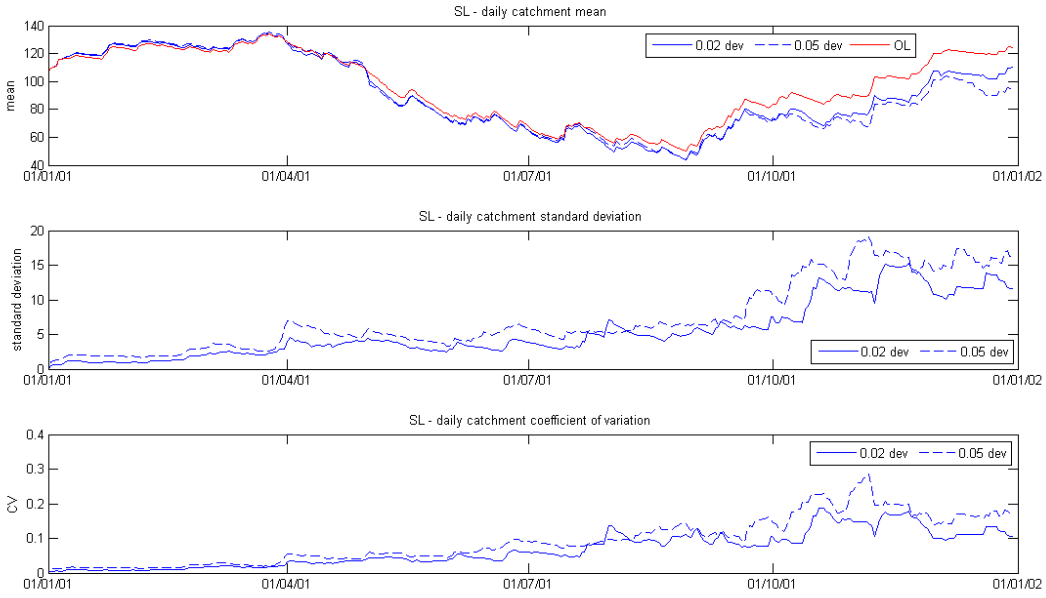

Figure 5-5 Catchment statistics for soil moisture
Perturbed forcing data: evaporation, precipitation, temperature

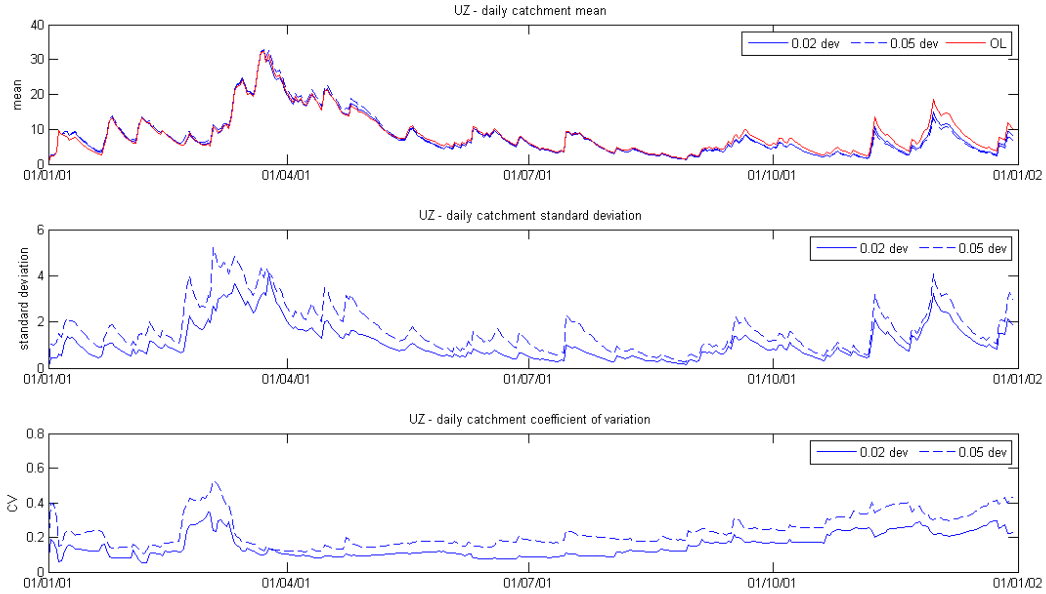

Figure 5-6 Catchment statistics for upper zone storage
Perturbed forcing data: evaporation, precipitation, temperature

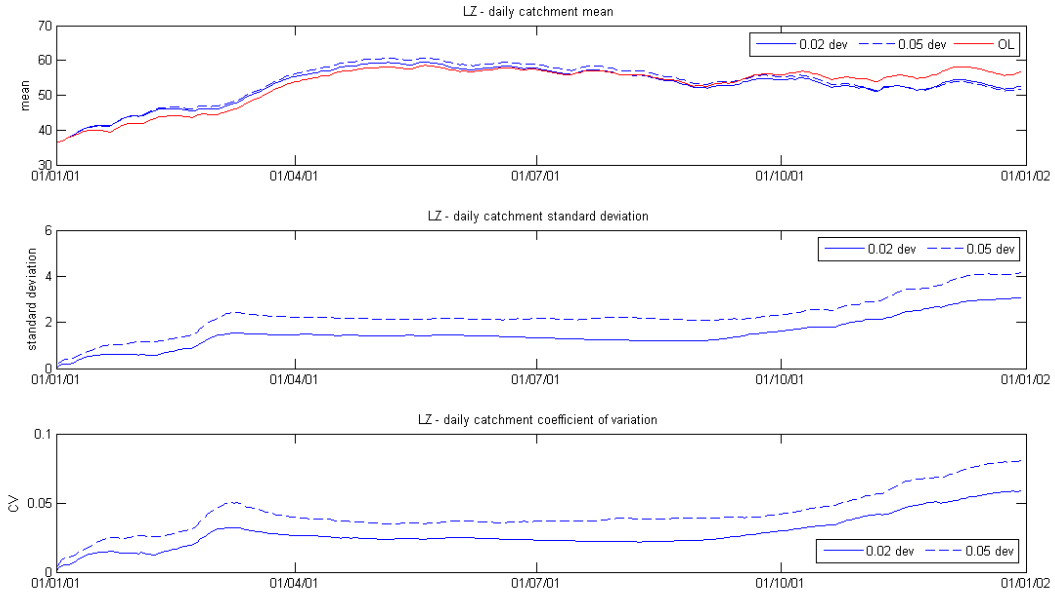

Figure 5-7 Catchment statistics for lower zone
Perturbed forcing data: evaporation, precipitation, temperature

Table 5-6 Coefficient of variation
Perturbed forcing data: *evapotranspiration, precipitation,* and *temperature*

	Output (1-4)							
	Snow cover		**Soil Moisture**		**Interception Storage**		**Lower Zone Storage**	
CV	Min	Max	Min	Max	Min	Max	Min	Max
Catchment	0.0676	4.465	0.0004	0.2858	0.0103	3.9101	0.0002	0.0806
Pixel 1	0.3801	4.4721	0.0007	0.3548	0.0079	4.4721	0	0
Pixel 2	0.0931	4.4721	0.0003	0.3880	0.0036	4.4721	0.00028	0.1513
Pixel 3	0.3452	4.4721	9.24E-05	0.4112	0.0054	4.4721	0	0.2687
Pixel 4	0.0304	4.4721	0.0003	0.2918	0.0053	4.4721	0	0.1854
Pixel 5	0.2032	4.4721	3.82E-05	0.3020	0.0011	4.4721	0	0.1593
	Output (5-8)							
	Upper Zone Storage		**Runoff (Q)**		**Discharge (Qacc)**		**Base flow**	
CV	Min	Max	Min	Max	Min	Max	Min	Max
Catchment	0.0527	0.5288	0.0010	0.4433	0.0003	0.3935	0.0006	0.1279
Pixel 1	0.0171	0.2963	0.0013	0.3459	0.0006	0.3917	0	0
Pixel 2	0.0728	4.4721	0.0002	0.2664	4.66E-05	0.3921	0.0002	0.1513
Pixel 3	0.0967	4.4721	0	0.3999	0	0.4289	0	0.2687
Pixel 4	0.0191	4.4721	0.0015	0.4358	0.0015	0.4358	0	0.1854
Pixel 5	0.0742	4.4721	0	0.6580	0	0.6580	0	0.1593

Perturbing forcing data affected all the model states, and the CV values are particularly higher on the snow cover, interception storage, and the upper zone storage, all of which have the maximum CV value of 4.47. This could be because these three storages are the first ones directly affected by the change in temperature and precipitation, and unlike soil moisture and lower zone storage, there are no actual boundary of the maximum amount of water (or snow in case of snow cover) that these three storages can hold (see the HBV-96 schematics in Figure 4-3).

Comparing the results of perturbing forcing data with perturbing parameters, two conclusions can be drawn:

1. Change in the ensemble mean compared to nominal OL: perturbing forcing data in general have more influence than perturbing parameters.
2. Change in variability when the deviation size is increased: perturbing forcing data in general have less influence than perturbing parameters.

6 Implementation of GRACE EnKF/EnKS

The Ensemble Kalman Filter has been explained in section 3-2. Looking at the update equation (equation 3-9), there are three requirements of the EnKF which can be identified: generating an ensemble of perturbed observations, generating an ensemble of perturbed model states, and obtaining an ensemble of predicted measurement. These three requirements are discussed in this Chapter, before summarising the EnKF/EnKS algorithm which is applied to the experiments in this thesis.

6.1 Ensemble of perturbed observations

In equation 3-3, $Z(t)$ is the ensemble of perturbed observation, in this case it is the GRACE observation. Remember that GRACE data gives an integral value of monthly mean TWS variations instead of a discrete TWS value. For GRACE to be comparable with the model and allowing the data assimilation, the observations need to be converted to absolute TWS values. This is done with respect to the model's nominal open loop for the data assimilation time span. At each month the GRACE data is available, the time mean of the nominal OL and the time mean of GRACE TWS variation is added to the TWS variation of the current month. This way for the whole assimilation period, the average of the model and GRACE is the same. The conversion is treated per sub catchment, to more or less imitate the nature of GRACE observation which has coarser spatial resolution compared to the model; that in a sub catchment scale GRACE observation will most likely to be uniform.

Now that the absolute GRACE TWS value for each month is obtained, it needs to be disaggregated within the corresponding month. As GRACE orbits are irregularly spaced in time, the observation is weighed and averaged over both space and time, see (Winsemius, et al., 2006). A way to disaggregate the observation in a month is to interpolate the values at the satellite overpasses times. In this thesis, the interpolation is simplified, by assuming that the satellites orbits overpasses the study area regularly, and the converted-absolute TWS value is at the middle of the month. This way the interpolation can be easily done at any temporal resolution. However, it would be unrealistic to interpolate in a rapid interval, say in daily interval, and therefore a 5 days interval is used for a more realistic representation of the satellite overpasses, using spline interpolation. This way of interpolation avoids the assumption of a single GRACE TWS value for a month, such that of Zaitchik et.al. (2008), which is slightly unrealistic.

Perturbing the GRACE TWS is done the same way as that of perturbing model parameters in section 5.3, i.e. additive random noise without spatial correlation is applied to the nominal (absolute-interpolated) GRACE observation. The ensemble of perturbation γ in equation 3-9 is generated with the standard deviation of 20 mm, following the typical accuracy of GRACE (Klees, et al., 2008a).

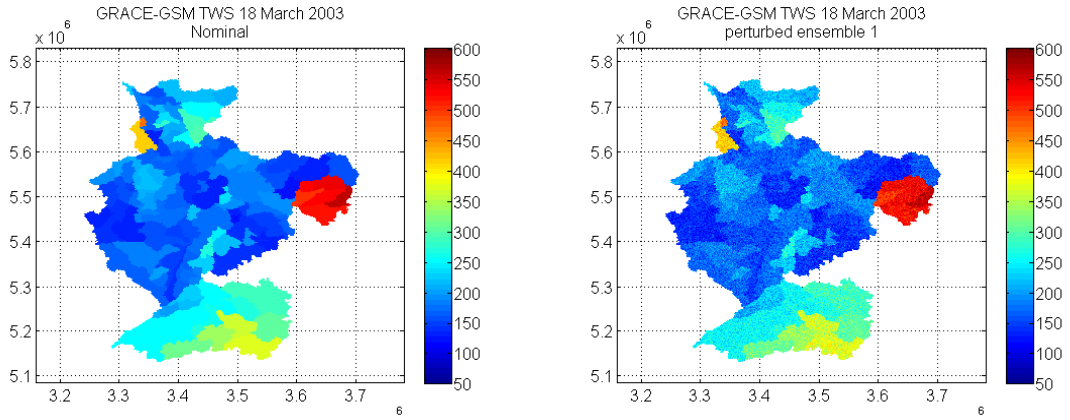

Figure 6-1 The nominal-absolute GRACE GSM observation (left) and the perturbed observation for ensemble 1 (right).

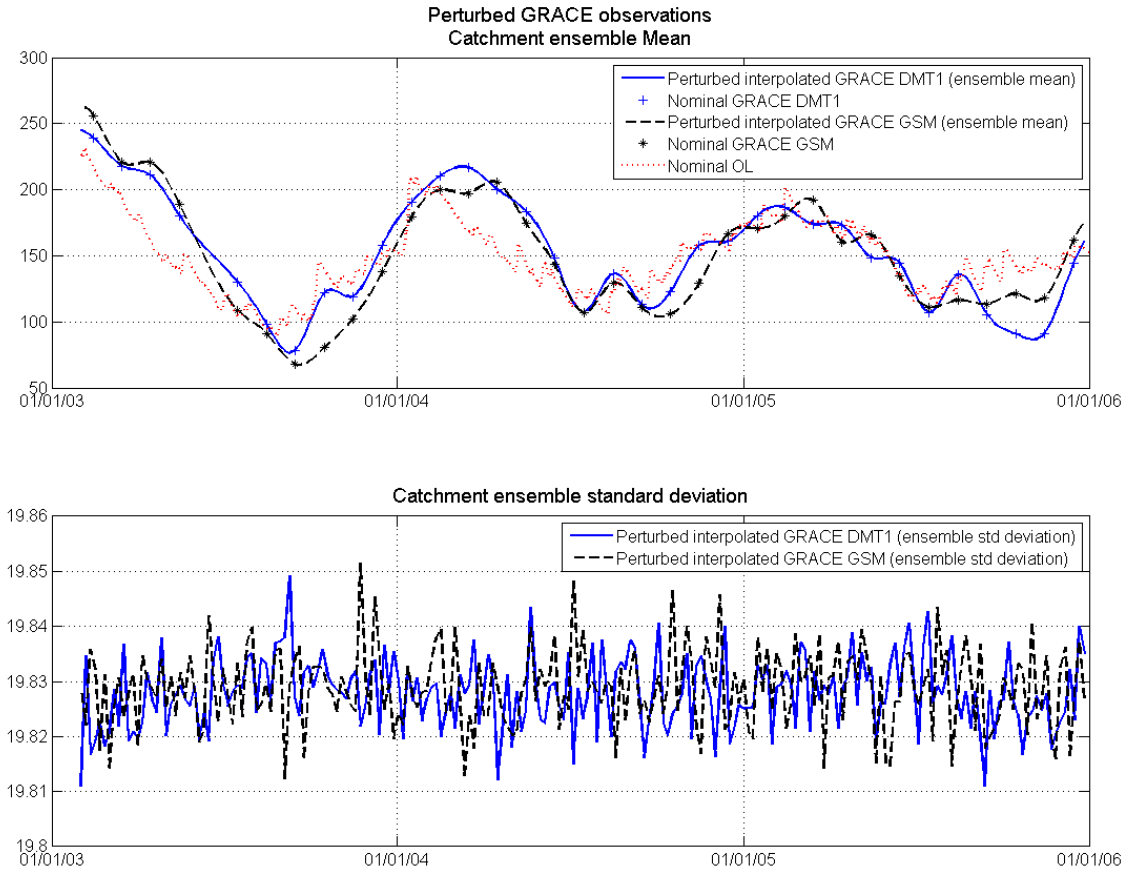

Figure 6-2 Comparison of the perturbed GRACE-DMT1, GRACE-GSM,and the model nominal OL. Top: catchment mean of the ensemble mean. Bottom: catchment mean of the ensemble standard deviation.

In Figure 6-1, a sample of the absolute and the perturbed GRACE TWS maps are shown. Figure 6-2 shows the comparison between the nominal OL, the absolute GRACE TWS and the interpolated GRACE TWS, for both GSM and DMT1 data, at the catchment. The second plot in the figure shows the catchment mean of the ensemble standard deviation. In this figure the standard deviation is a little less than 20 mm, but this is only because it is the mean of the whole catchment. At the individual pixel the standard deviation is more or less than 20 mm, as shown in Figure 6-3 for pixel 1 (see Chapter 5) of both data sets.

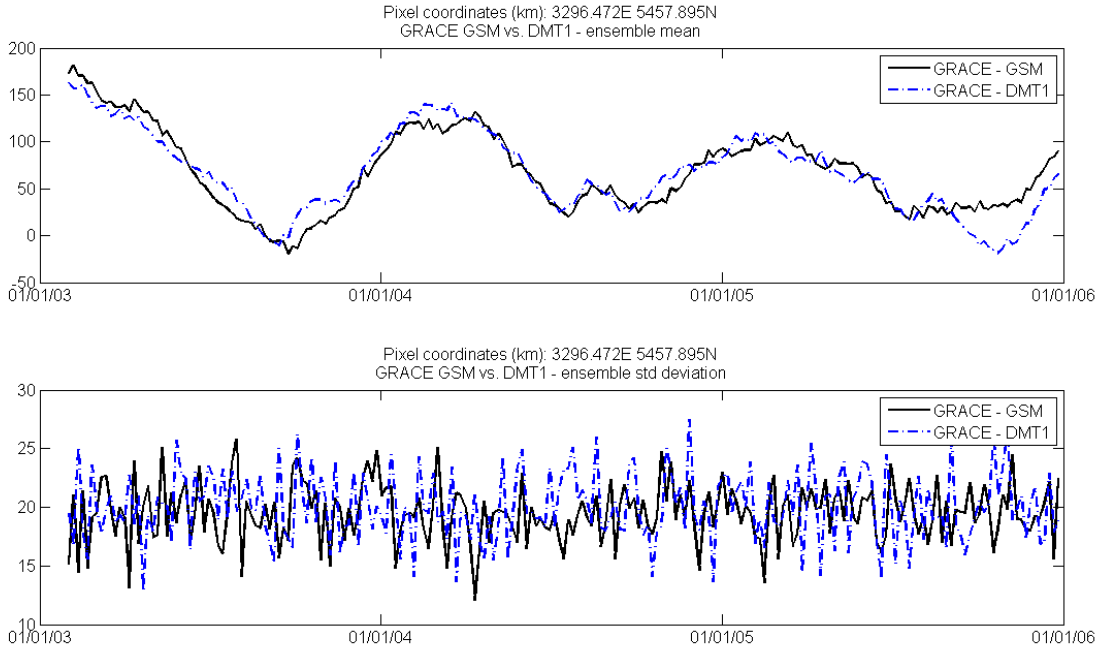

Figure 6-3 Comparison of the perturbed GRACE-DMT1, GRACE-GSM,and the model nominal OL at pixel 1. Top: the ensemble mean. Bottom: the ensemble standard deviation.

As was already visible in figure 4-6 (section 4-4), the seasonal pattern generally agrees with each other, although it appears to have a slight phase shift between GRACE and model from January 2004 to March 2003. Different peaks between the DMT1 data and GSM data also occurs. For example at October 2003 DMT1 shows more water than GSM; at October 2005 DMT shows decreased water storage while GSM shows increased water storage.

6.2 Ensemble of perturbed model states

The ensemble of model state $Y(t)$ in equation 3-9 is the TWS which is calculated as:

$$Y(t) = \sum \left(SM(t) + UZ(t) + LZ(t) \right) \tag{6-1}$$

where SM is soil moisture, UZ is upper zone storage, and LZ is lower zone storage. Figure 6-4 shows the contributions of the three storages to the TWS calculated in the nominal OL.

The generation of the perturbed model state was done by perturbing the model parameters and the forcing data, such that a set of replicates is obtained. The perturbation is created the same way as in the sensitivity study (Chapter 5). However, the perturbation sizes used in the data assimilation is different than those of the sensitivity study, which are as follows:

- Parameter perturbation = 0.1of nominal range
- Forcing data perturbation:
  - Evapotranspiration and temperature = 0.15 of nominal value
  - Precipitation = 0.10 of nominal value.

The reason is that in order to have the EnKF to update properly (i.e. not to assume too high accuracy on either the model or the observation), the ensemble spread of both the model states and the observation should be at a comparable magnitude. In the sensitivity study,

increasing the parameter perturbation size from 2% to 5% already increase the standard deviation at about 2.5 times, therefore increasing the perturbation size to 10% is considered sufficient to achieve a comparable variance to GRACE data. This is still justifiable as none of the parameters are known perfectly in the calibration (Weerts, 2009). Similar assumption applies to the forcing data. Precipitation is given a lower variance since the data generation involved an advance interpolation method compared to temperature data and evapotranspiration, for which the latter is only a monthly value (Weerts, et al., 2008).

An ensemble model propagation using these perturbation sizes, called the ensemble open loop (EnOL) was done for the time span of January 1st 2002 until December 31st 2005. It is necessary to initialise the model a year in advance to allow the model to spin up and filled up the storages.

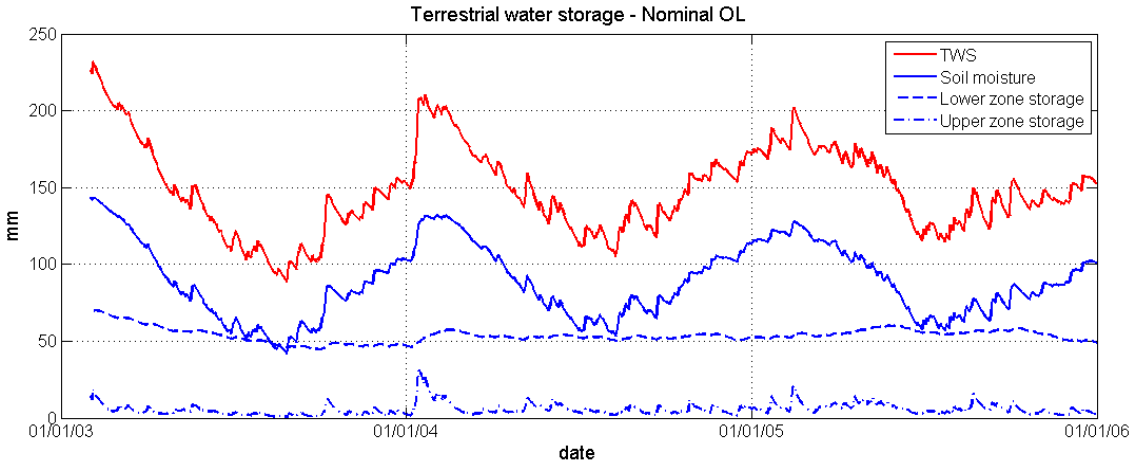

Figure 6-4 Contribution of the individual storages to TWS (nominal open loop)

Figure 6-5 shows the nominal OL for the time span of January 1st 2003 until December 31st 2005, after the spin up period. In this figure, individual storages are also shown to illustrate their contributions to the TWS. Clearly the biggest contribution comes from the soil moisture, which also controls the seasonal behaviour of the TWS. This is true since soil moisture is the first TWS storage affected by any precipitation event, while lower zone storage has slower response to precipitation. The least contribution comes from the upper zone storage, the most dynamic storage which serves more as an intermediate storage from which water either goes to the lower zone storage or directly goes to quick runoff, and thereby not much water is retained in this storage.

Figure 6-5 compares the EnOL to the nominal OL. Ideally the more replicates generated the better the ensemble represents the error covariance of the model state, however in this thesis the ensemble consists of 30 replicates, mainly due to limited processing resources. Clearly pertubing model parameters and forcing data have introduced a bias of the EnOL from the nominal OL, at approximately 20 mm. The model's behaviour however remains generally the same as the nominal OL.

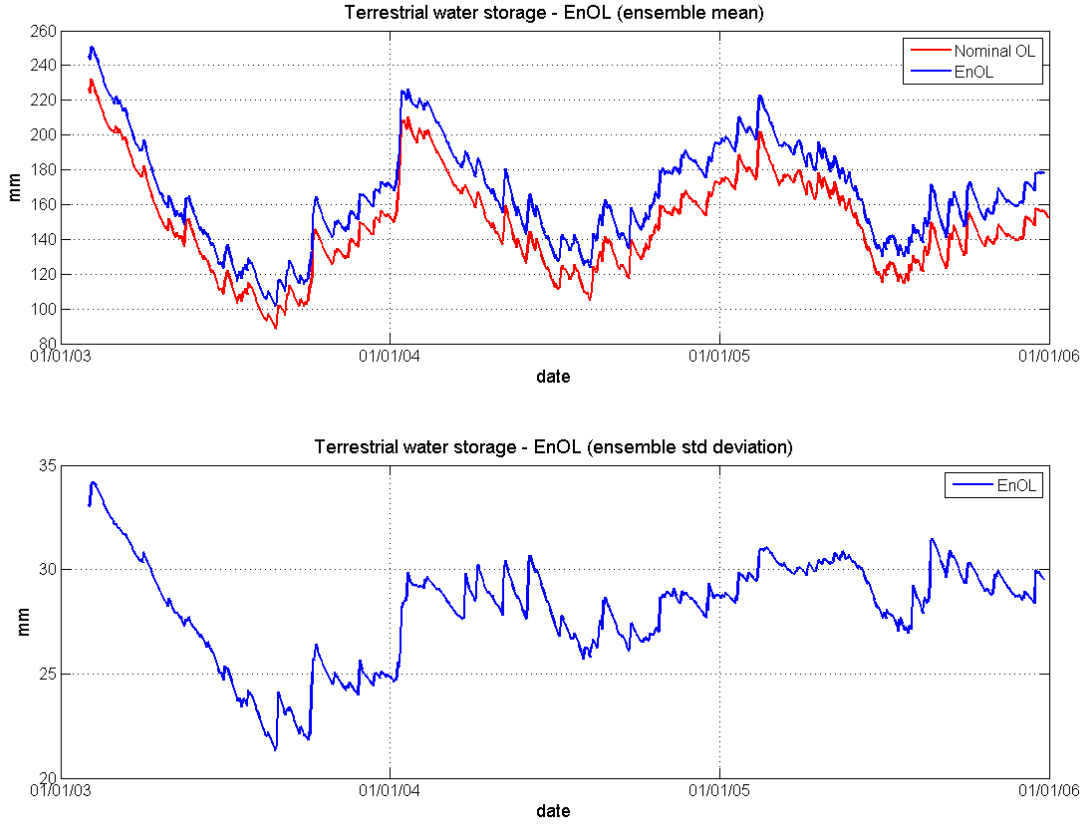

Figure 6-5 Ensemble open loop

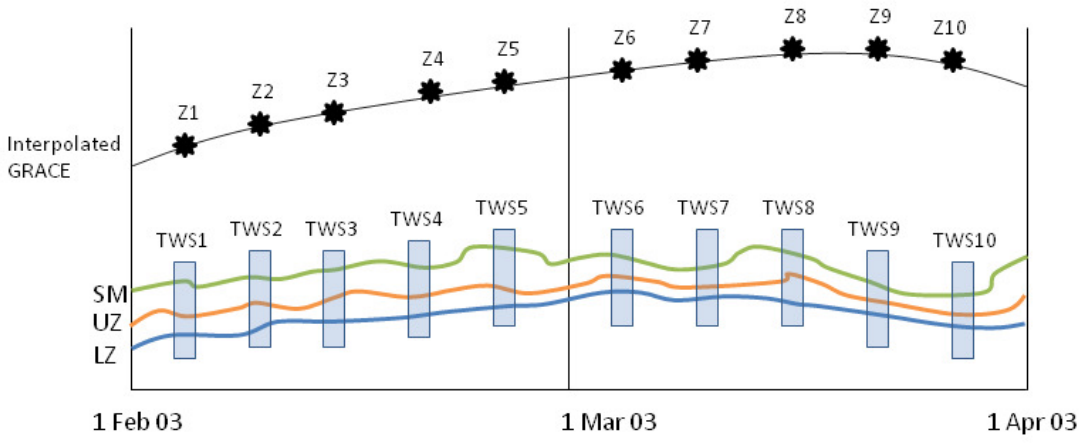

$$TWS_j(t) = \sum\left(SM_j(t) + UZ_j(t) + LZ_j(t)\right)$$
$$Y_j(t) = M_j(t) = TWS_j(t)$$

Figure 6-6 Obtaining the predicted measurement. At times the GRACE observation is interpolated, the predicted measurement is calculated as the sum of soil moisture, upper zone storage, and lower zone storage.

6.3 Ensemble of predicted measurement

Since the GRACE observation is now available for every 5 days, in the data assimilation the predicted measurement M in equation 3-9 must also be available for the same period for each ensemble member. As illustrated in Figure 6-5, this is obtained as simply the sum of the three storages of a given ensemble j at the time of observation t:

$$Y_j(t) = M_j(t) = \sum \left(SM_j(t) + UZ_j(t) + LZ_j(t) \right) \tag{6-2}$$

The non-linear operator which relates the true state to the measured variable M in equation 3-2 now becomes an identity matrix.

6.4 Disaggregating the updated TWS

As the model is propagated forward in time, every five days when the interpolated GRACE TWS data is available, the EnKS updates the prior model state with equation 3-9. The updated model state $Y^a(t)$ is again an integrated value of TWS, therefore the difference between the prior TWS to the updated TWS for every ensemble member needs to be disseminated back to the soil moisture, upper zone storage and the lower zone storage before the model can be reinitiated and the data assimilation can be continued.

Adding (or substracting) the prior values of the storages with the update is limited by the thresholds in the HBV-96 model, which are:

- For soil moisture, *max* (SM) = *field capacity*, provided by the parameter *fc.*
- For lower zone storage, *max* (LZ) = (*k4/perc*) * $LZ_{prior.}$
- For upper zone storage, *min* (UZ) = 0.

The first storage to be updated is the soil moisture, since this is the first storage to be affected by precipitation. When the soil moisture reaches its thresholds (0 or *fc*), the lower zone storage is updated next, again until the lower zone threshold is reached. Lastly the remaining update goes to the upper zone storage.

Although upper zone storage receives the excess water from the soil moisture, this storage is the more dynamic storage where water will percolate to the lower zone until the lower zone storage is full and then excess water will go directly as discharge. Further, the upper zone storage does not have an upper bound, and therefore it is convenient to update the lower zone storage before the upper zone storage. Otherwise at most times when an update needs to be added, the lower zone storage will not receive any update at all. This update disaggregation is illustrated in Figure 6-7.

As explained in Section 3-3, the EnKS uses the same update matrix $B(t)$ in equation 3-11, and thus the same disaggregation applies.

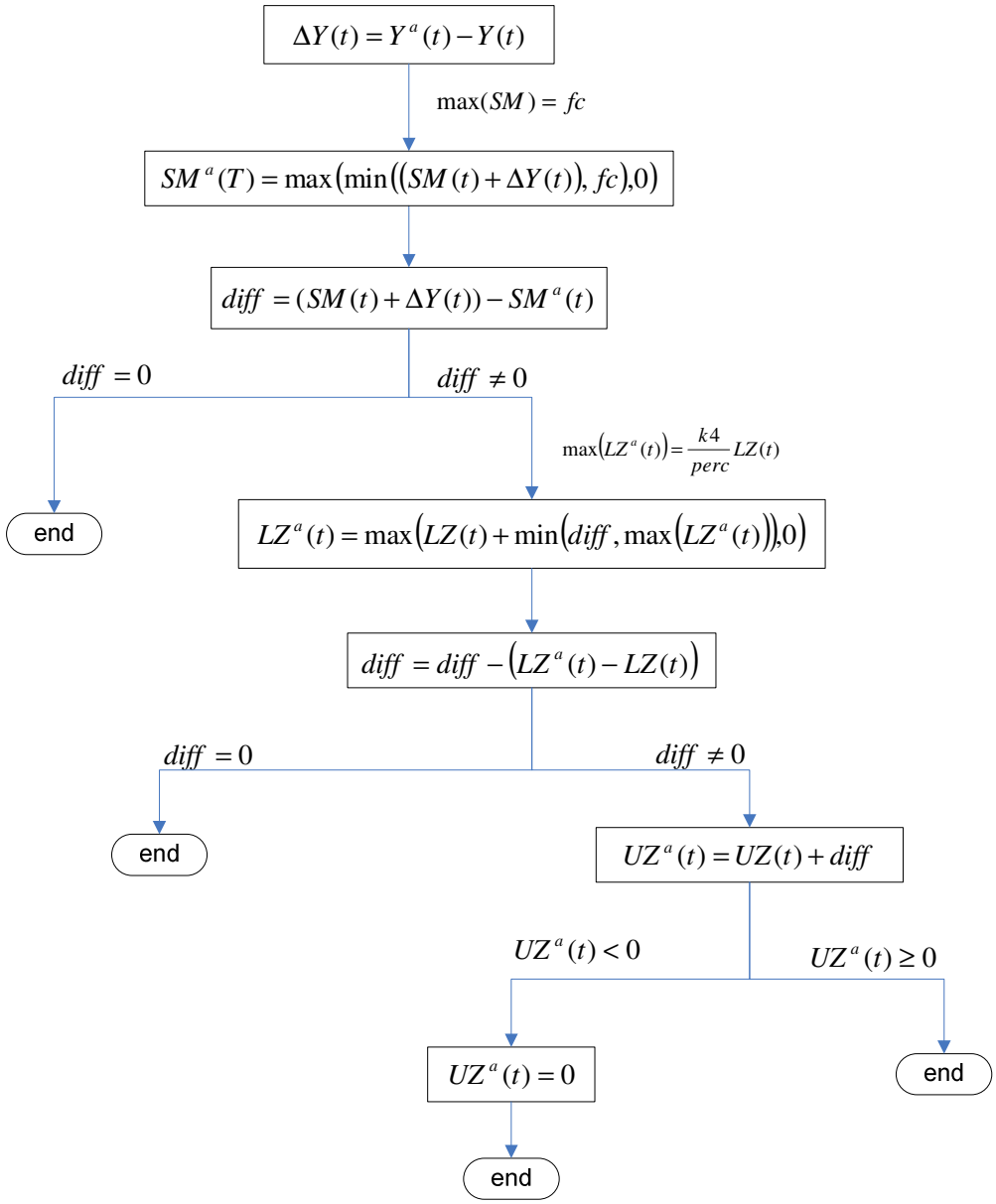

Figure 6-7 Updating soil moisture, lower zone storage, and upper zone storage.

6.5 GRACE EnKF/EnKS application

The algorithm applied in the GRACE EnKF/EnKS is best described in a flow diagram as shown in Figure **6-8**. Initial ensemble of model states is generated by perturbing the model parameters and the forcing data, and propagates the model forward in time until an observation becomes available. At this time an ensemble of perturbed observation is generated, and at the same time the individual storages from the models state is collected into a single model state, i.e. the TWS. The EnKF is used to calculate the update using equation 3-9. At this point the so called $B(t)$ in equation 3-11 has been calculated and can be used to also update the past state in the EnKS. Once the updated model state is calculated, it is disaggregated back to the individual storages and these are used to reinitialise the model.

The main experiments in this thesis are performing the EnKS using the two GRACE data sets, for the period February 1st 2003 until January 31st 2004. For both data assimilation, the ensemble members and the perturbed observations are as explained in this Chapter. The results will be discussed in Chapter 7.

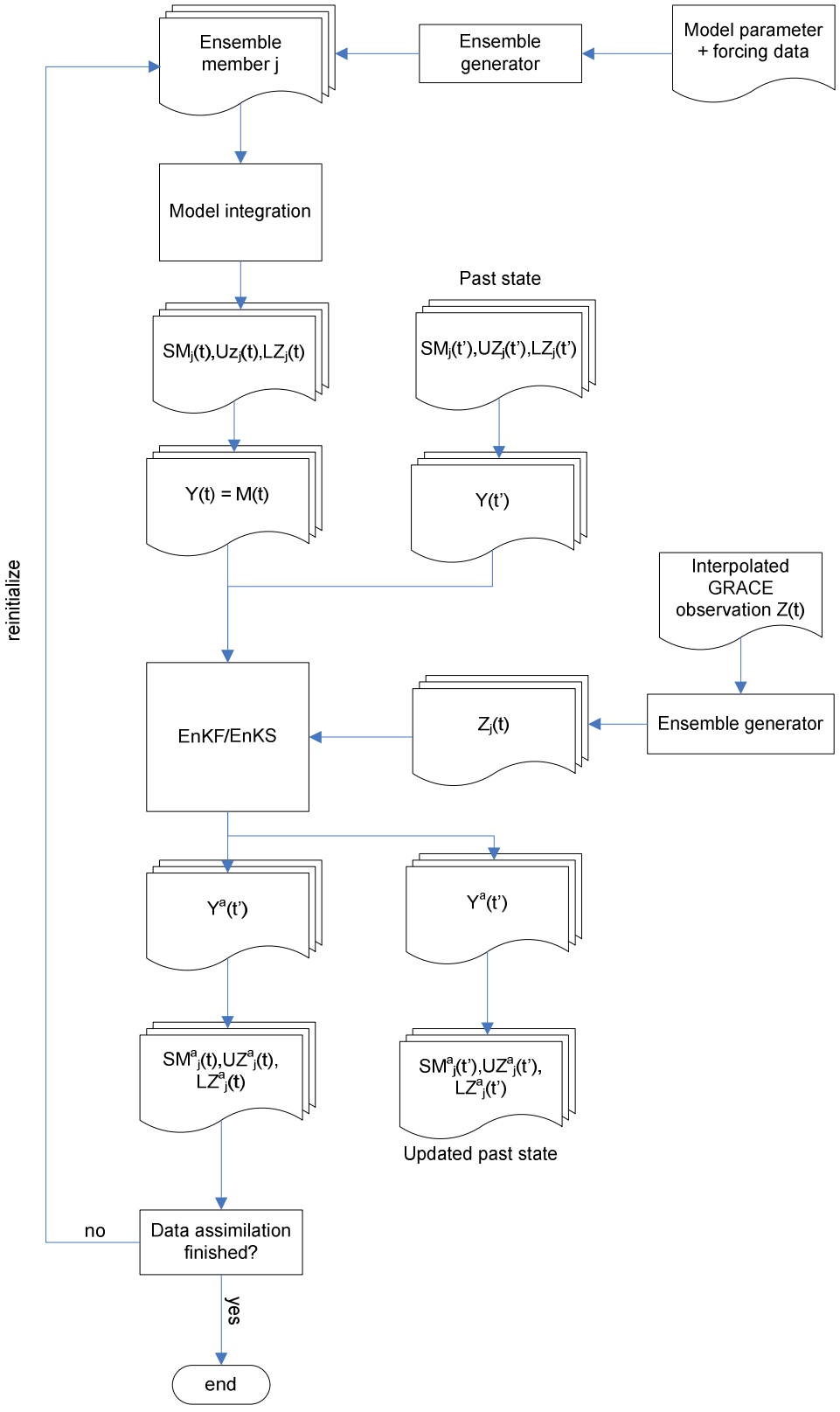

Figure 6-8 Flow diagram of the GRACE EnKF/EnKS

7 Results and discussion

The main experiment in this thesis is using the Ensemble Kalman Filter and Smoother as explained in Chapter 6, to assimilate the two GRACE data sets into the HBV-96 model of the Rhine river basin. Next to it, several shorter experiments were done and will be explained further in this Chapter. At the end of this Chapter, some constrains concerning the computation is discussed.

7.1 GRACE EnKF/EnKS with DMT1 and GSM data.

For the time period of February 1st 2003 until January 31st 2004, the GRACE DMT1 data and DMT1 data are assimilated into the HBV-96 model. Both GRACE observations are interpolated for every 5 days. The 6 model parameters chosen in the sensitivity study (section 5-1) and the forcing data are perturbed as explained in section 6-2. Due to the limitation of time and computing resources, the data assimilation is limited to 30 ensemble members. The EnKS DMT1 and GSM are performed up to lag 3, i.e. the previous three observation intervals.

The resulting TWS estimates from the EnKF/EnKS DMT1 and EnKF/EnKS GSM are shown in Figure 7-1 and Figure 7-2 respectivley. In both figures it can be seen that when the GRACE observation becomes available, the TWS is updated towards the observation. At the same time, the standard deviation is reduced significantly. When the model has been reinitialised and propagated again, the standard deviation increases until the next observation is available, and this pattern is repeated throughout the simulation period. Notice that at the first two update times, the prior TWS standard deviations are much higher than the GRACE's standard deviation, and the updated TWS are reduced so much that they already become lower than the observations standard deviation at these times. This shows that the EnKF fulfils the expectation of reducing the error covariance that the updated model state has lower error covariance than either the model or the observation.

Looking at the results of the EnKF update of the two experiments in Figure 7-1 and Figure 7-2 , three important behaviours could be observed, which holds for both experiments:

- The standard deviation is strongly related to precipitation event. Whenever there is an increase in precipitation (i.e. the catchment becomes wetter), the standard deviation is increased. This is clear for example on the small peak in October 2003, and this is actually already visible in the EnOL run (Figure 6-5).
- The rate of update is affected by the magnitude of difference between the prior model state and the observation. This is visible for example at the period between March 1st 2003 until May 1st 2003, where the differences between prior TWS and the observations are large, and the updates are considerably large.
- The rate of update is also affected by the standard deviation of the prior model stat. If the standard deviation of the prior model state is already low, the observation only adds up a small amount of update, even when the difference between the prior model state and the observation is considerably big. This is visible for example at the period of August 2003.

Next to these, there are also times when the observation and the prior model states are already so close to each other that the update is negligible, for example at the period of September 2003.

The EnKS in general adds more update to the TWS, while the standard deviations are further reduced at the update times. The EnKS lag 1 in general has the biggest size of update towards the observation. The size of update of EnKS lag 2 becomes smaller than lag 1, and subsequently the update of lag 3 is smaller than lag 2. This is true for both experiments. If the EnKS is done on every past days instead of just the past observation days, the result will give a smooth transition between observation days instead of being jumpy as the EnKF.

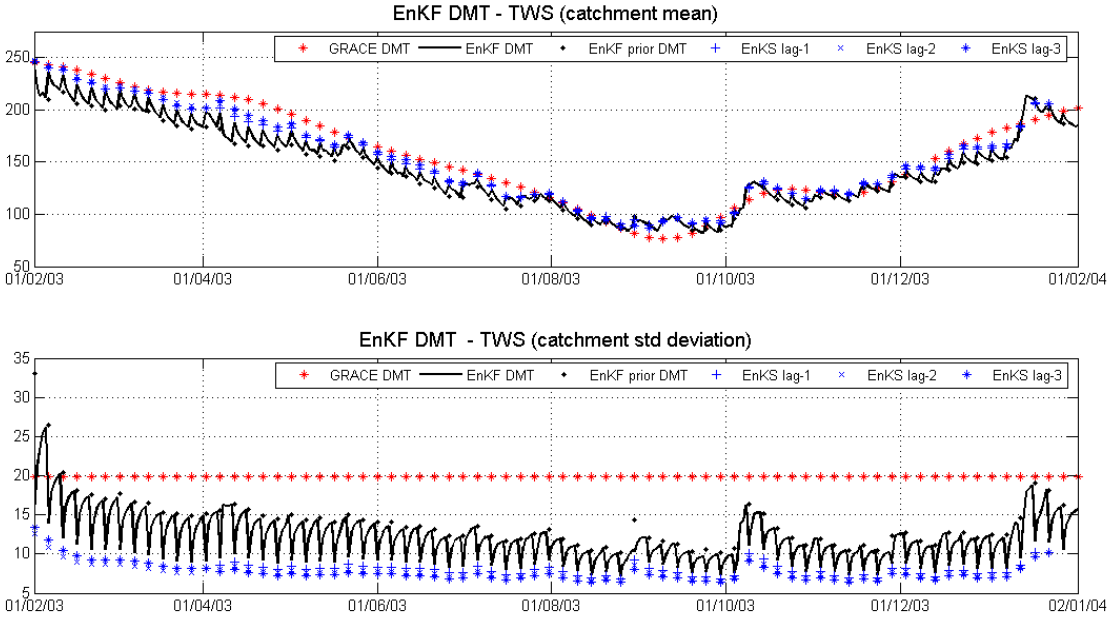

Figure 7-1 EnKF/EnKS DMT1.

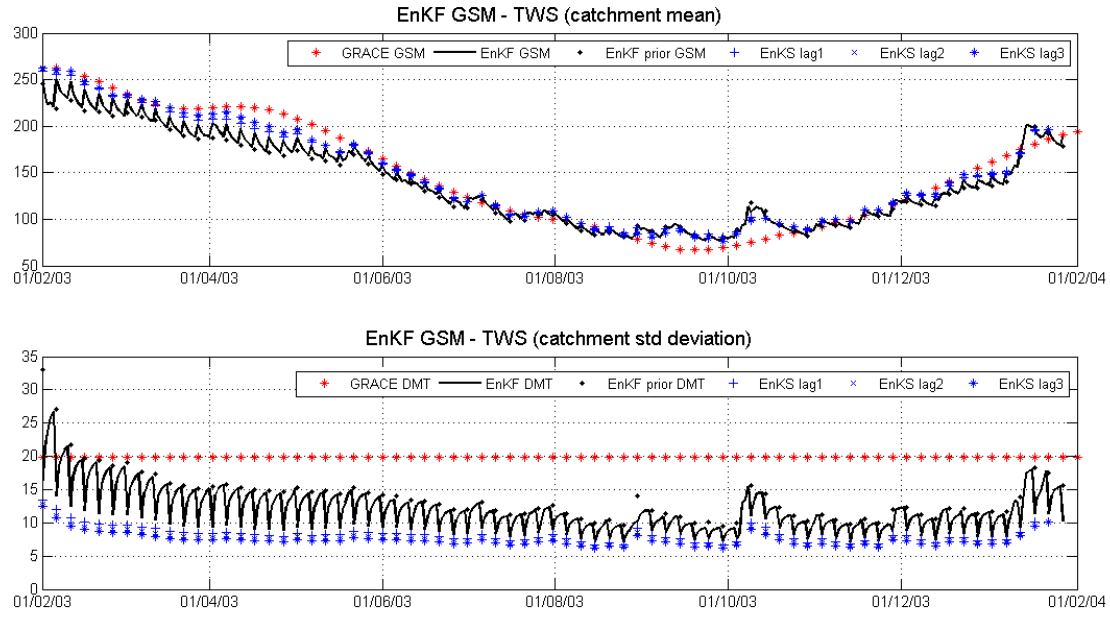

Figure 7-2 EnKF/EnKS GSM.

While the behaviours between the two experiments are similar one to another, there are differences in the magnitude of update as a result of the difference in observations values. Figure 7-3 shows the comparison between the two experiments. As can be seen in the first plot of Figure 7-3, the TWS estimate from both experiments generally agrees with each other, and the significant difference occurs during the wet season, which corresponds to difference in the peaks the two GRACE data sets during these times. In the first months of simulation (February – May 2003), the GRACE GSM observations are higher than the DMT1, and the EnKF GSM is higher than the DMT1 accordingly. As the simulation goes further in time, the GRACE DMT1 observations become higher than the GSM and thus the ENKF GSM gradually have higher values than the DMT1.

In the period between October 1st 2003 and November 31st 2003, the biggest difference between the two experiments is visible, where the EnKF GSM has much lower estimates than the EnKF DMT1. At this period, the GRACE DMT1 shows small peak in its observations, while the EnKF GSM just has a smooth increase of value as the wet season begins.

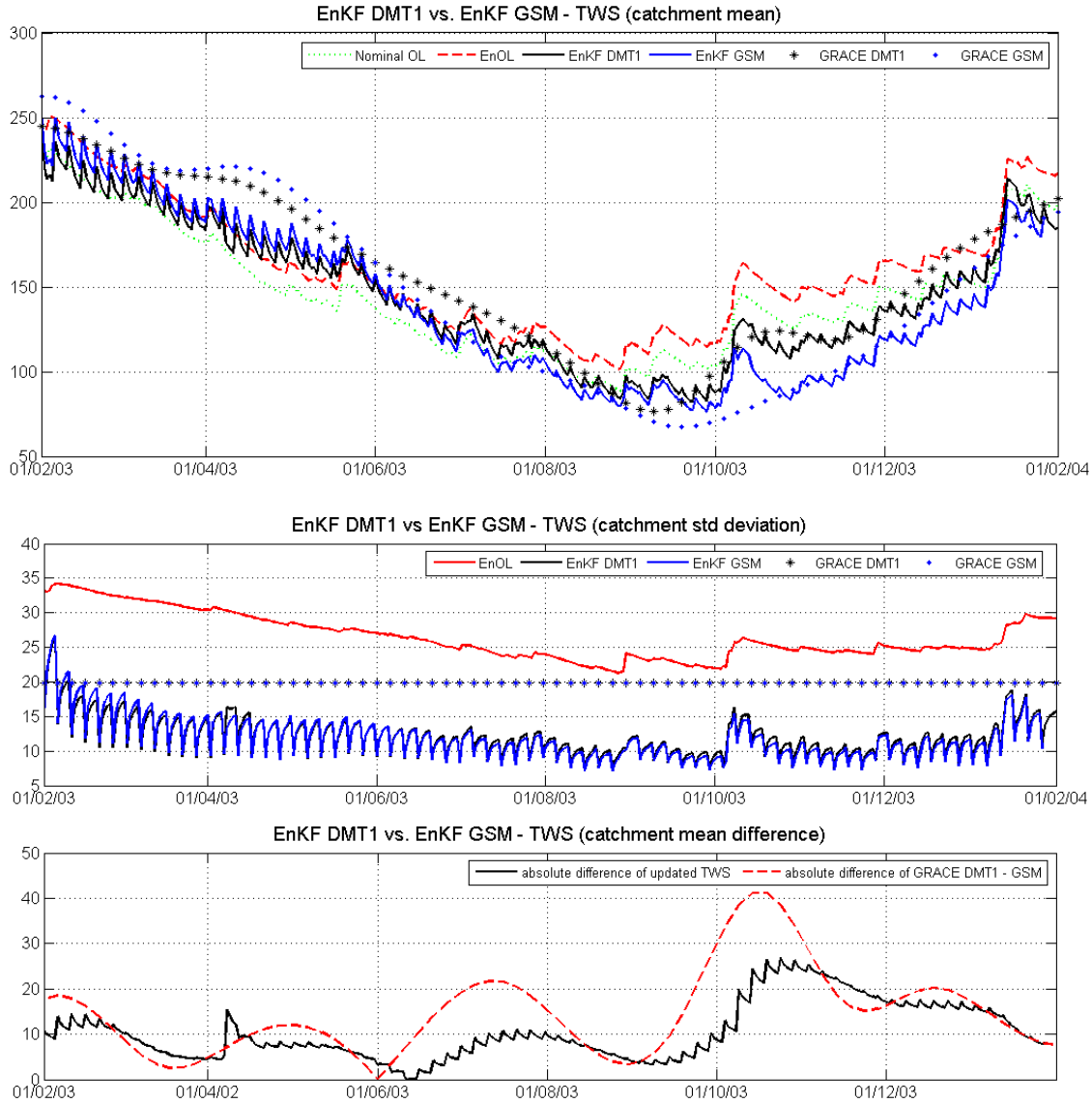

Figure 7-3 Comparison between EnKF DMT1 and EnKF GSM

Both the EnKF DMT1 and EnKF GSM generally have lower values compared to the EnOL, and closer towards the nominal OL. The third plot of Figure 7-3 shows the absolute catchment mean difference between the two experiments (i.e. difference regardless direction of update). Here it is visible that while difference in the observations are large, the updated TWS is generally reduced by constrain from the model. The EnKF works for both experiments, since it fulfils the expectation of reducing the ensemble variance and applying the different GRACE observations yields to different TWS estimates.

Figure 7-4 shows the update at one of the pixels (pixel 1, see Chapter 5), zoomed in at the first 2 months of the data assimilation for the GRACE GSM observation. Here it is visible that in using such a frequent observation interval, the ensemble variance of the model state generally continues to be reduced that the observations have less effect on the update. In other words, model estimate become very "accurate" and the filter trusts the model more. As the simulation progresses further, the update generally becomes less significant. The EnKS continues to update the TWS closer to the observations and further lowers the standard deviation for both experiments. The EnKS further reduces the standard deviation, but the amount of update is considerably small, and becomes less with larger lag.

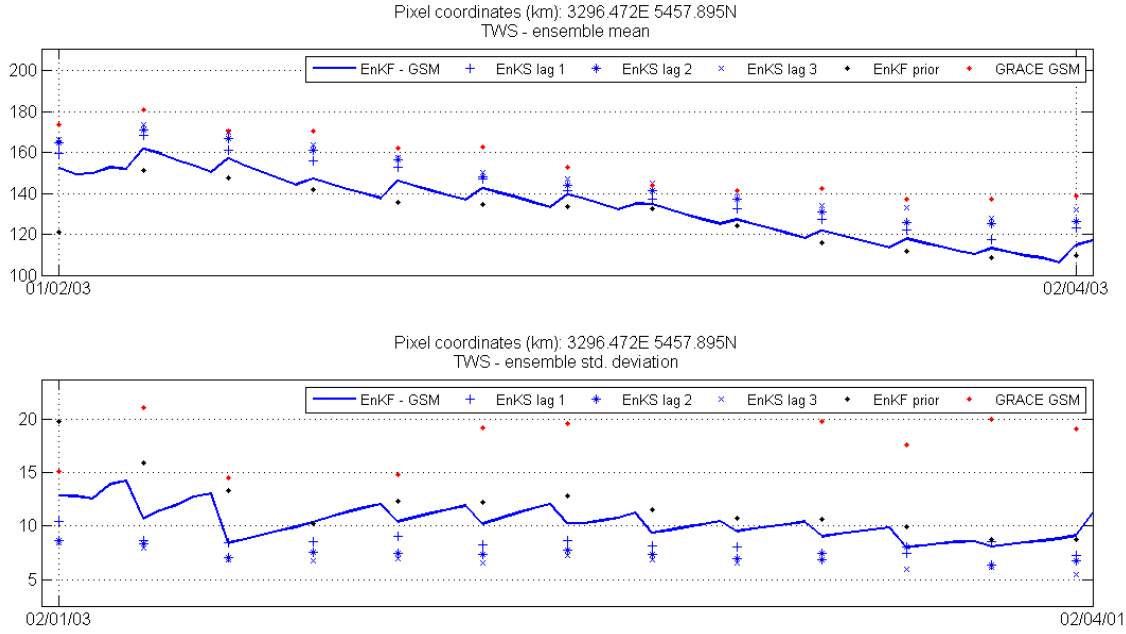

Figure 7-4 Zoomed in plot of EnKF GSM at pixel 1, showing the period of February 1st 2003 until April 2nd 2003.

Figure 7-5 gives the mean absolute update of the EnKF/EnKS over the simulation period (i.e. regardless direction of update). The mean update of the DMT1 is slightly higher than the GSM. The pattern of both experiments agrees with each other except on October 9th 2003 where EnKF DMT1 gives low update but EnKF GSM gives high update. This likely corresponds to the GSM observation being much lower than DMT1 at that time. Also visible in Figure 7-5 is how in general for both experiments the size of update decreases with larger EnKS lag.

The size of update is highest at the beginning of the simulation. Besides being the result of the decreasing ensemble variance, at this period (February – April 2003), both GRACE observations are much higher than the model compared to the dry period (June – August 2003), where GRACE and model are close to each other. As the season progresses to another wet period, the

update seems to gradually increase again. A longer simulation period would have been able to reveal if this pattern is repeated again in the next wet period.

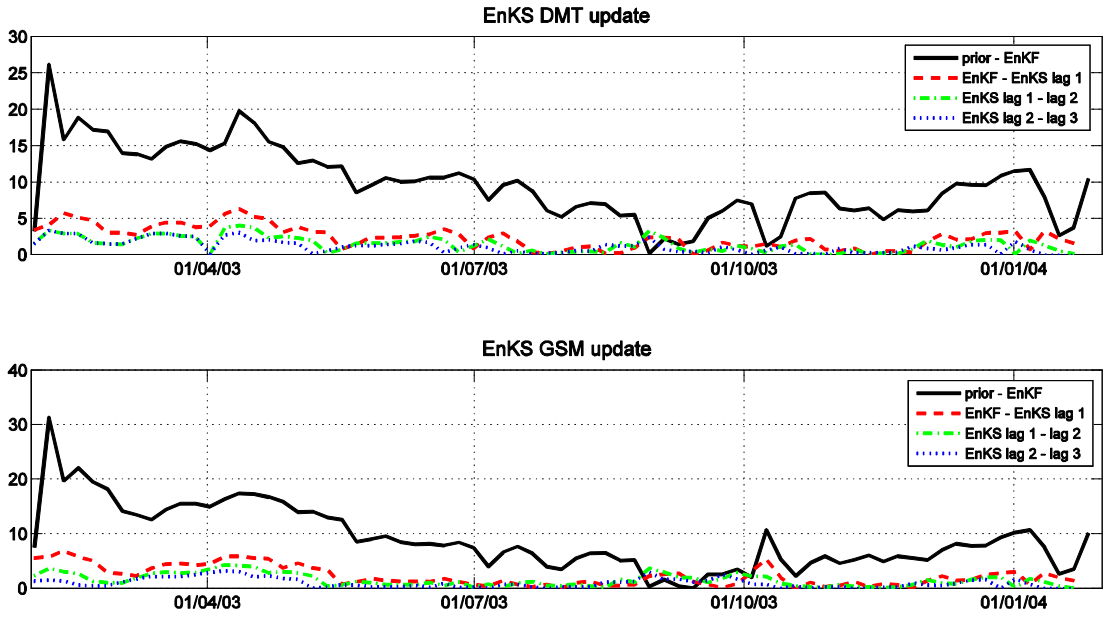

Figure 7-5 EnKF/EnKS mean absolute update

7.2 Additional short experiments

Seeing the results in the main experiment, 3 additional short experiments are done to see what happens if one of the terms is changed, which will be explained in the following sub sections. All 3 experiments are simulated for time period February 1st 2003 until August 31st 2003, using only the GRACE-DMT1 data.

Using observations every 10 days

The expectation in doing this experiment is that with using less frequent observation, the standard deviation of the ensemble will be allowed to grow, and thus the filter will use the observations to give a more significant update.

Figure 7-8 shows the results of this experiment at the catchment mean. The similar behaviour as the previous section occurs here. The standard deviation is reduced at the time of observation, and standard deviations are gradually reduced as the catchment becomes drier and Figure 7-9 compares it with the previous EnKF-DMT1 (using 5 days interval). They show that indeed the standard deviation grows more using less frequent interval, and therefore the size of update at the observation time is more significant. However the standard deviation grows quickly the first days after the update, and tends to stop growing afterwards.

The end result of this experiment is not much different than when using 5 days observation interval. At every 10 days, the updated TWS estimate is very close for both calculations. The computing time is however significantly reduced by approximately 1.4 times compared to updating every 5 days, making the EnKF DMT1 with 10 days interval an appealing procedure.

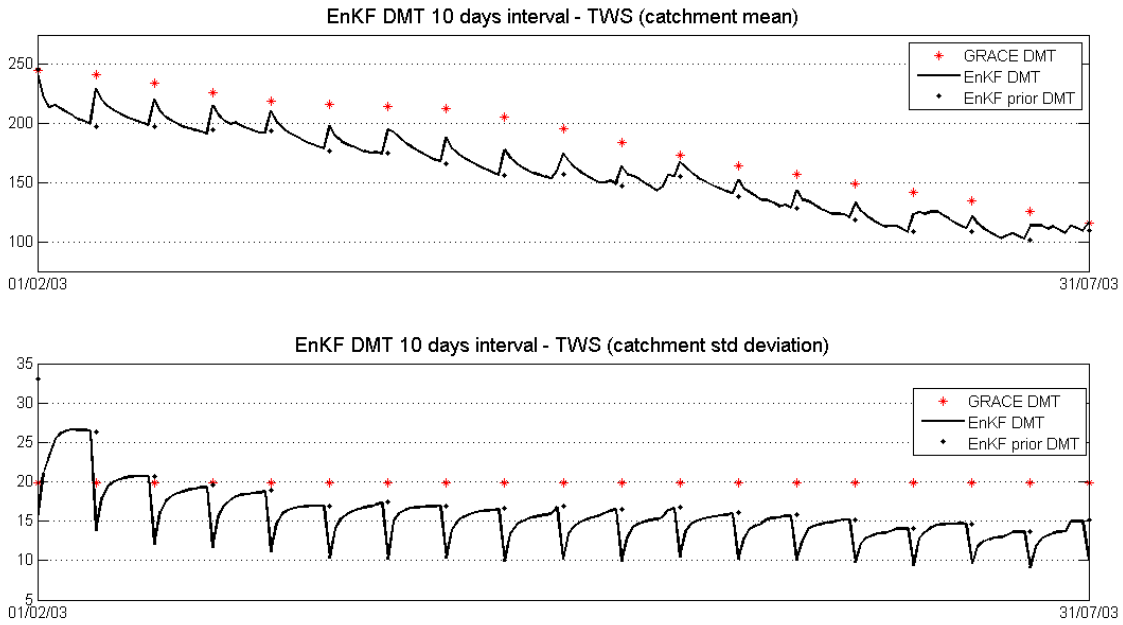

Figure 7-6 EnKF DMT with 10 days observation interval.

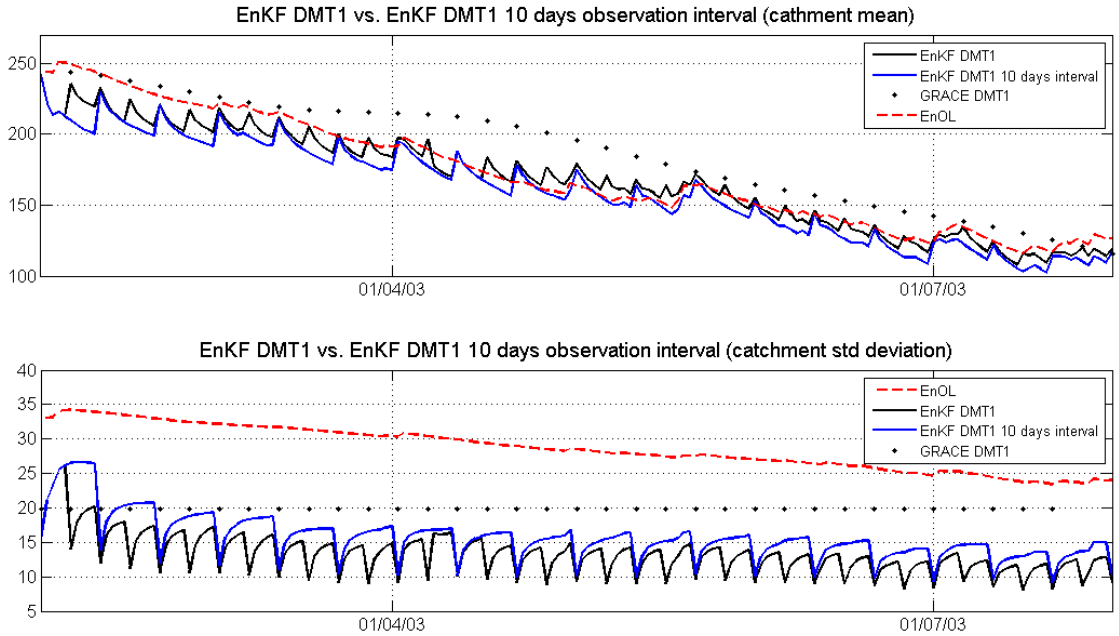

Figure 7-7 Comparison between the EnKF DMT using 5 days observation interval and using 10 days observation interval.

Assuming high observation accuracy

As mentioned earlier, 20 mm is the typical accuracy of GRACE observation. If the accuracy is assumed to be much higher, then the filter will update the model state very close to the observation. In this experiment, the standard deviation of GRACE is set to 2 mm, while the model parameters and forcing data remains the same. 10 days observation interval is again used since the previous experiment show similar result to the main experiment but with decreased computation time.

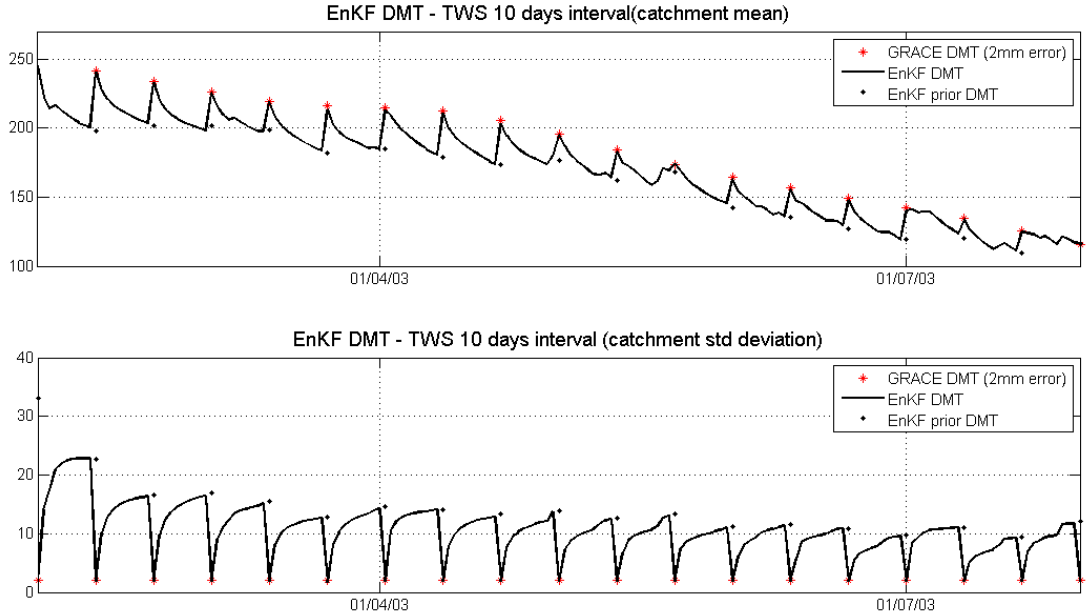

Figure 7-8 EnKF DMT with 10 days observation interval and 2 mm GRACE accuracy

Figure 7-8 shows the results of this experiment at the catchment. Clearly when the observation is much more accurate than the model state, the update draws the TWS very close to the GRACE observation.

Assuming very low parameter and forcing data accuracy

The next experiment is to assume that the model parameters and forcing data have very low accuracy. In this case the filter is again expected to update the model states very close to the observation.

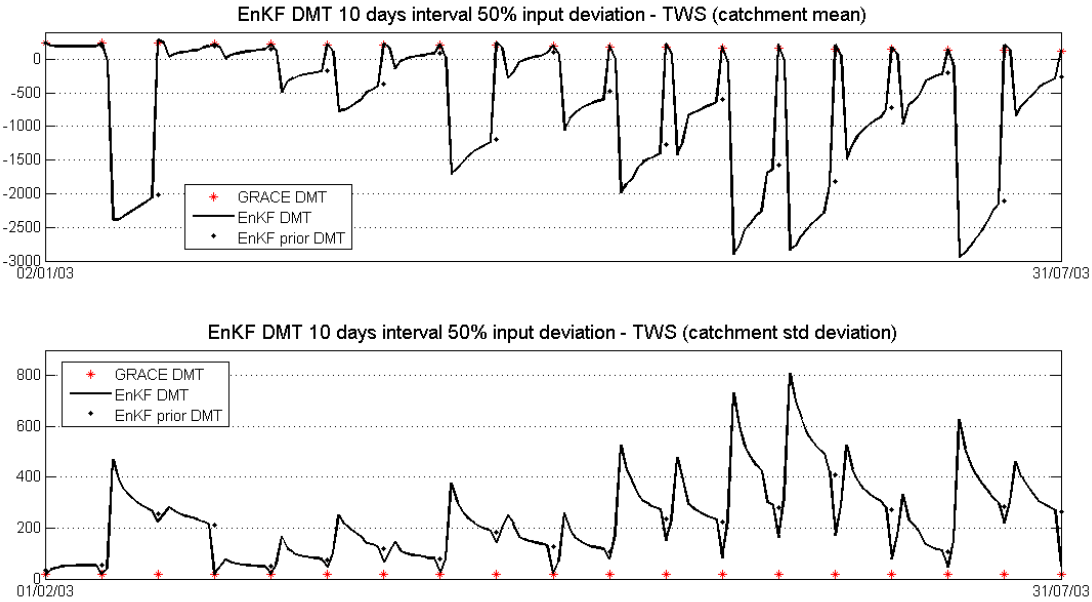

Figure 7-9 EnKF DMT with 10 days observation interval and 50% model input & parameter deviation

Figure 7-9 shows the results of this experiment. As can be expected, perturbing the forcing data and parameter so much results in extreme and physically unreasonable behaviour of the model. This experiment however is a good example on how well the EnKF works in correcting for this extreme behaviour, and draws the model state very close to the observations.

7.3 Comparison of discharge

So far it has been shown that the EnKF and EnKS have been successfully applied to assimilate GRACE observation to the HBV-96 model. However the remaining question is if assimilating GRACE observation actually improves the HBV-96 model? To answer this question, the data assimilation is validated by comparing the discharge calculated by the model after data assimilation to the best estimated discharge at 4 discharge measurement stations along the Rhine: Rees, Dusseldorf, Bingen, and Worms. Their locations are shown in Figure 7-10. The discharge data is hourly data in m^3/s units, obtained from Deltares (Weerts, 2009).

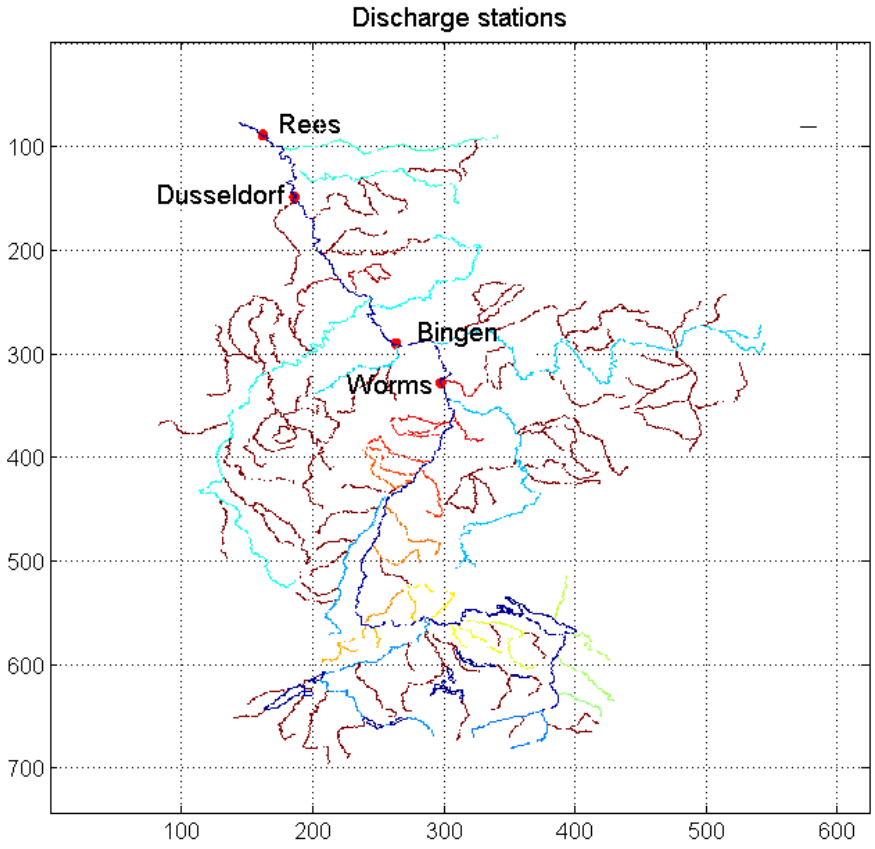

Figure 7-10 Discharge stations locations.

The results from stations Rees, Dusseldorf, Bingen and Worms are presented in Figure 7-11, 7-12, 7-13, and 7-14 respectively. Three plots are available for each station. The top plot of each figure shows the comparison between the hourly values of discharge and the daily values from the model estimated discharge from the nominal OL, EnOL, EnKF DMT1, EnKF GSM, and the EnKF DMT with 10 days interval. Since the model is in daily time step, the model estimated discharges are daily values. But in the figures, for ease of plotting they are plotted at the start of a day (i.e. at midnight).

At all stations, it is apparent that for the first months of data assimilation, the model estimated discharges are generally much larger than the measured discharge, with high jumps between the GRACE observation intervals. The model stabilises after some time, but still with the jumps in values. These jumps are most likely caused by the data assimilation update. At the observation times, the TWS storages are updated, meaning more water is added. As the model is propagated again, according to the model there is more water that needs to exit the storages as discharge. This results in high discharge value at one day after the observation day, as visible in the figures. The results at only the first day after the observation are given in the second plot of every figure.

Although there is a high discharge value at one day after the observation, the estimates are quickly reduced again at the next day. The third plot of each figure shows the estimated discharge at the time of GRACE observations. Here it can be seen that the model estimated discharges after data assimilation are in general still considerably lower than the validation data.

As already known in section 7.1, the most significant update happens at the first few months of the simulation, after which the update tends to have less impact to the model states. This is true when looking at the discharge on the days of the observation. The values of the first months are closer to the validation data compared to the EnOL. But as the model propagates further, they slowly converge to more or less the same magnitude as the EnOL, especially around September – October 2003. At this period, both GRACE data are close to the model (see Figure 7-3) and do not give much update to the model states. As the next wet period comes, the discharge estimates from the EnKF DMT1 and GSM gradually becomes closer to the measured discharge again.

Looking at the results of the two experiments, it is difficult at this point to conclude which one gives better update to the model states. While the EnKF GSM seems to give better update at the first months, the EnKF DMT1 gradually becomes closer to the validation data at the next wet period. A reason for this is that at the first wet period (February – April 2003) the GSM data is higher than DMT, thus giving more update. In contrast on the next wet period (November 2003 – January 2004) the DMT1 data is higher than the GSM data. Longer simulation period would be helpful to reveal the seasonal pattern and to come to a better conclusion.

It is interesting to observe the results on the different discharge stations. At Bingen (Figure 7-13) and Worms (Figure 7-14) which are approximetly in the middle of the catchment, the estimated discharge even at the day after the observation are generally lower than the measured discharge except on the first months. However this behaviour do not occur on the other two stations, Rees (Figure 7-11) and Dusseldorf (Figure 7-12), which are further south of the catchment. In these stations, at the day after the observation, the estimated discharges are higher than the measured discharges. This could be affected by the topography generally becoming lower towards southern part of the catchment, and more water is accumulated at the southern stations.

What is also interesting to see is that the EnKF DMT1 with 10 days interval has lower value compared to the EnKF DMT1 with 5 days interval. In section 7.2 it was noticed that at the end the updated TWS values at the 10 days interval are very close one another. But now it seems the observation interval has more impact on the non-directly updated model states such as discharge.

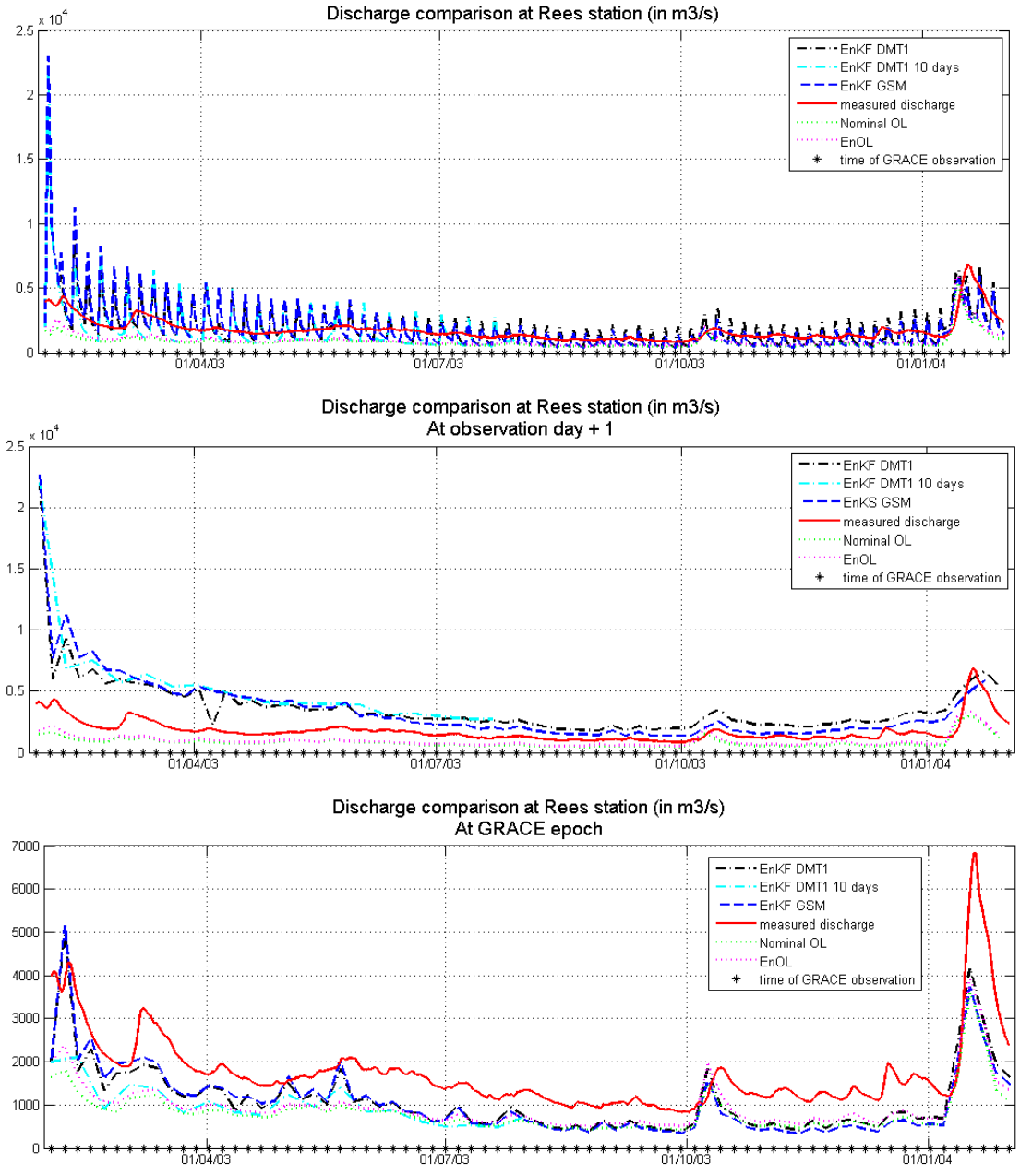

Figure 7-11 Discharge comparison at Rees station. Top: at model's daily time step. Middle: at one day after observations. Bottom: at days of observation.

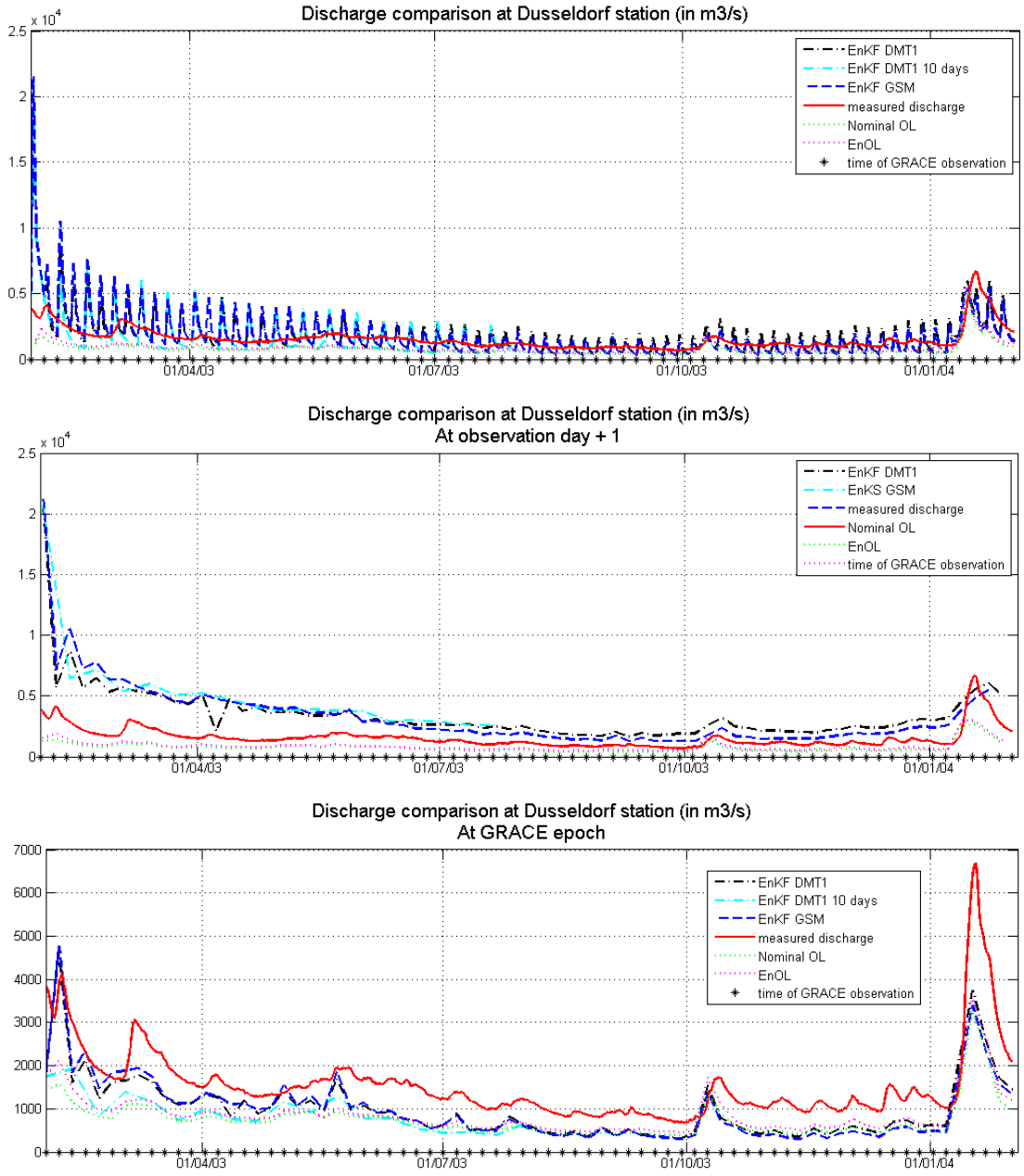

Figure 7-12 Discharge comparison at Dusseldorf station. Top: at model's daily time step. Middle: at one day after observations. Bottom: at days of observation.

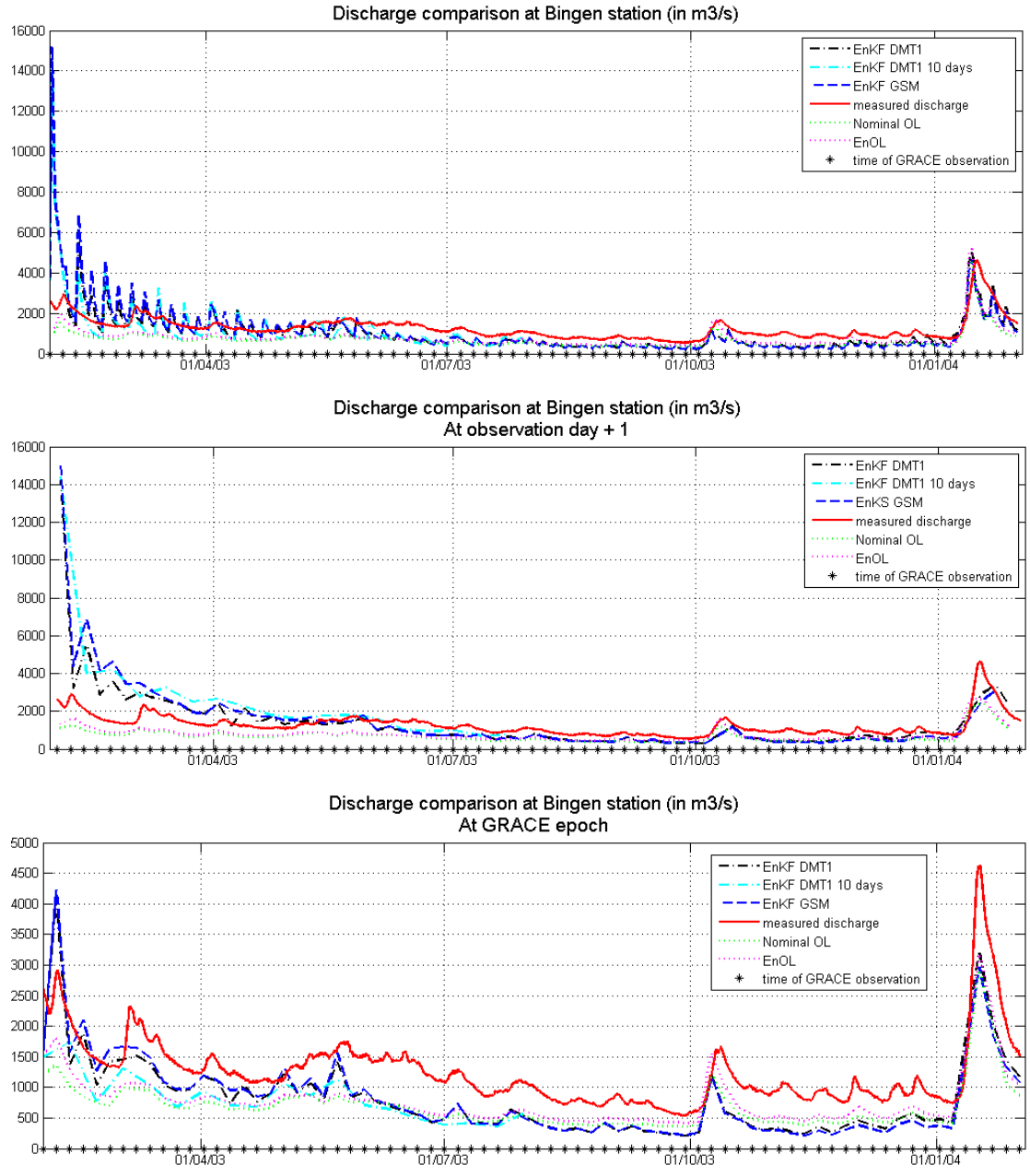

Figure 7-13 Discharge comparison at Bingen station. Top: at model's daily time step. Middle: at one day after observations. Bottom: at days of observation.

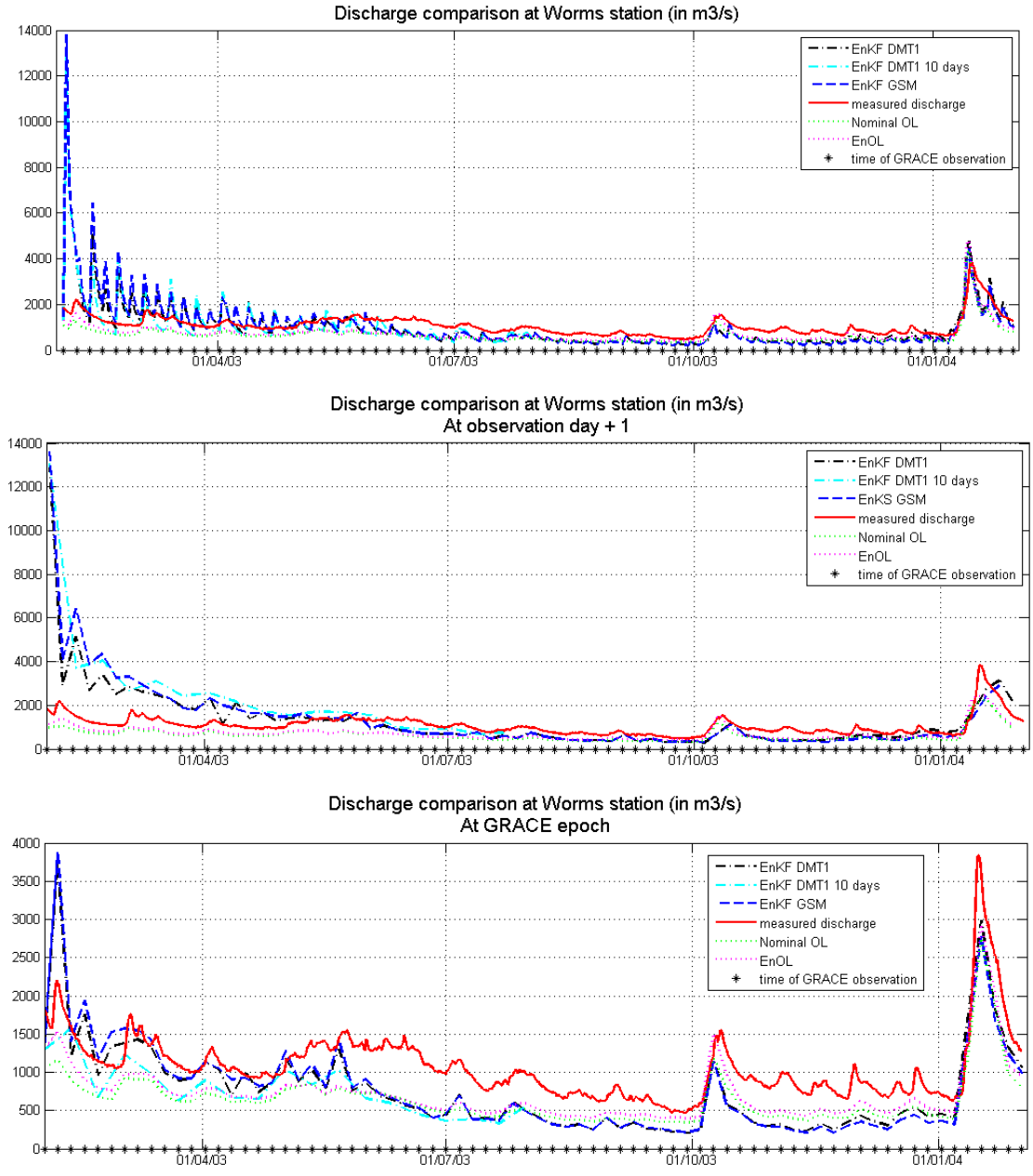

Figure 7-14 Discharge comparison at Worms station. Top: at model's daily time step. Middle: at one day after observations. Bottom: at days of observation.

In section 3.3, it was mentioned that the results of the EnKS is at least as good as the EnKF. To see whether this expectation holds, the results of EnKS DMT1 lag 3 are repropagated using the updated model states at observation times to obtain the full model states between observation times, including the discharge. Lag 3 was chosen since the update here already contains the update from lag 1 and 2. The resulting discharges are compared with the results from the EnKF DMT 1 and the EnOL, for two stations: Rees and Dusseldorf, as shown in Figure 7-15 and 7-16 respectively. The results from the other stations are similar to these two stations.

Again the discharges are high on the first day after each observation and then reduced, for the same reasons as the EnKF. If the EnKS has been used on every past days of the simulation instead of just the past observation days, the discharge estimates will be smoother between the observation days.

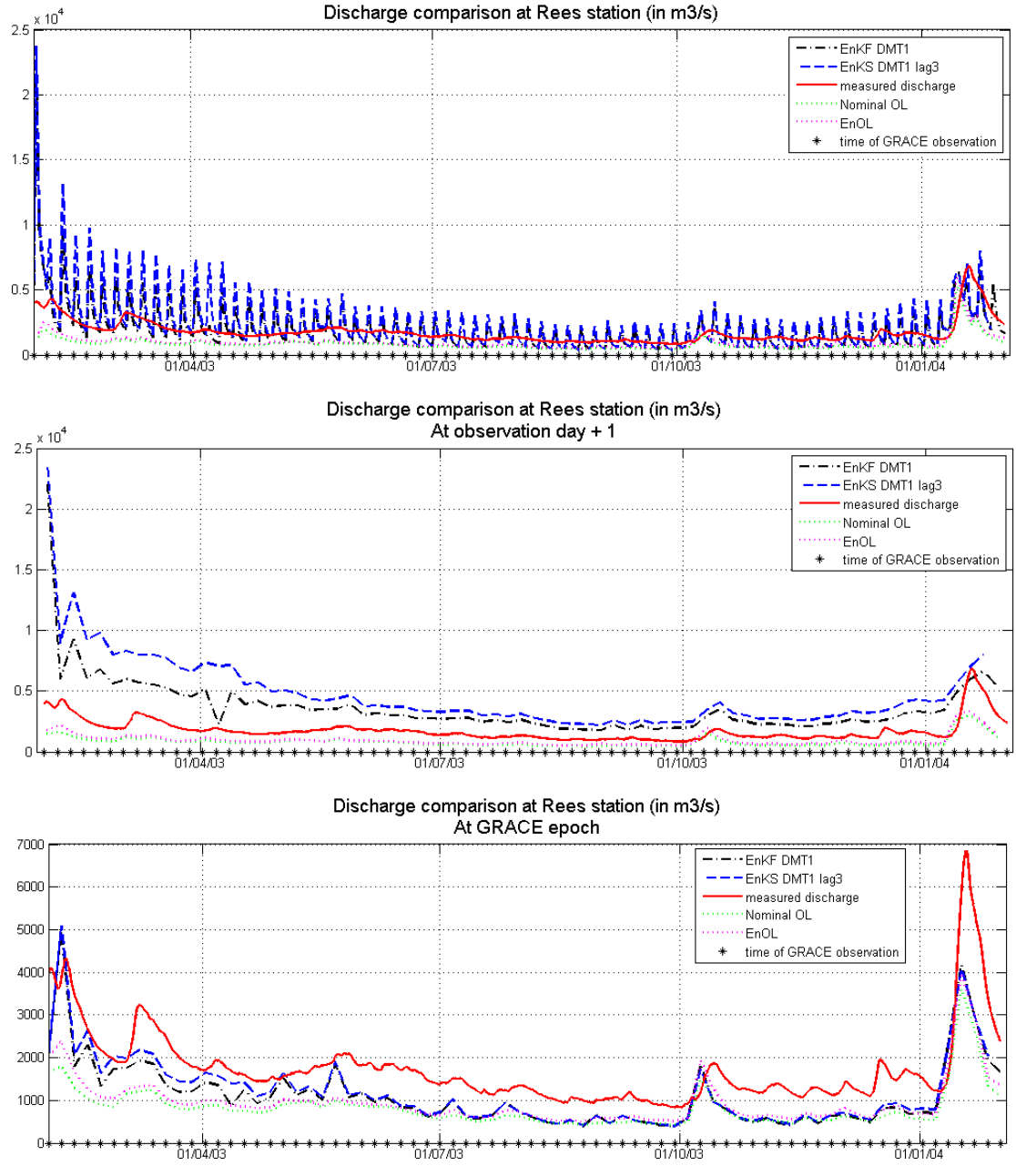

Figure 7-15 Discharge comparison at Rees station for the EnKS lag 3 Top: at model's daily time step. Middle: at one day after observations. Bottom: at days of observation.

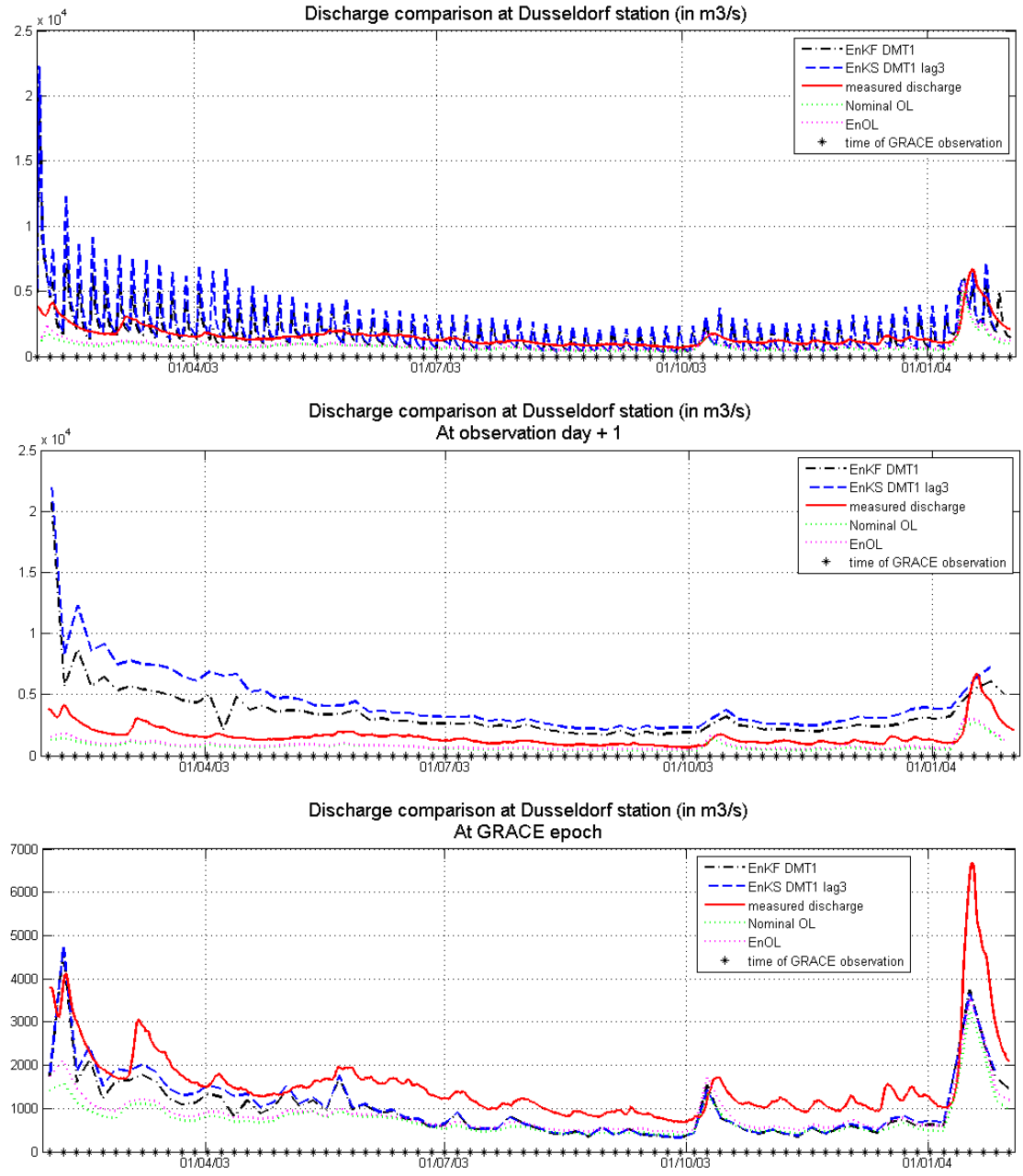

Figure 7-16 Discharge comparison at Dusseldorf station for the EnKS lag 3. Top: at model's daily time step. Middle: at one day after observations. Bottom: at days of observation.

What is visible from the comparison in the third plot of Figure 7-15 and Figure 7-16 is that again the most significant update occurs on the first few months. Except for the first observation intervals where the model estimated discharge far exceeds the measured discharge, the estimates from EnKS lag 3 are even closer to the measured discharge. This means that at least at this period, the EnKS does improve the discharge estimate. However as the simulation goes further in time, the EnKS lag 3 results converges to the EnKF, thereby the update became negligible.

7.4 Computing time and resources

A major constrain in this thesis is the computing resources. As the model was built in PCRaster the forcing data and parameters for each ensemble member are in the PCRaster map format, which is not very space-efficient. For illustration, a map at the size of the Rhine river basin (744*624 pixels) in PC Raster is ~1.8 MB in file size, while converting it into MATLAB's mat file uses only ~700kb. In a long simulation period, this is bound to lead to storage problems, which is one of the reasons for using only 30 ensemble members. Using a 32bit computer in Windows XP platform also means there are processing limitations due to the memory limitation of MATLAB for 32 bit computers, which needs careful handling.

In PC Raster it is not feasible to program the data assimilation, and therefore PCRaster is used as a call function in MATLAB, which at times requires file conversions, adding to the computing time. Students who will embark data assimilation of a PCRaster based model in the near future may want to try the new PCRaster Python extension which is planned to be officially launched within 2009 (University of Utrecht). This can eliminate the hassle of switching programming languages. The developers of PCRaster are currently developing the so called Python framework for spatio-temporal modelling which includes data assimilation functions (University of Utrecht). Although it seems that users are still bound to the PCRaster map format.

With respect to computing time, performing EnKS up to lag 3 compared to only EnKF only adds a small amount of time. Although it should be noted that if other states which are not directly updated in the EnKS is to be observed, repropagating the model is required, and this will add to the computing time with at least as much as an EnOL run. Significant time improvement is achieved from decreasing the observation interval. Table 7-1 gives the computing time comparison.

Process	**Relative time**
EnOL	0,9
EnKF (5 days interval)	1
EnKS (up to lag 3)	1,12
EnKF (10 days interval)	1,43

Table 7-1 Relative computing time.

8 Conclusions

The ensemble Kalman filter and smoother has been applied to assimilate the GRACE terrestrial water storage change data into a rainfall-runoff data, the HBV-96 model, on the Rhine river basin. The results has been shown in the previous Chapters, showing that the EnKF/EnKS fulfilled the expectation of combining the observation and model states into an updated state which has smaller variance than either the prior model state or the observation.

Some assumptions had to be taken during this research, with respect to generating the ensemble members for the model and the treatment of the GRACE TWS data. Using the 10 to 15% deviation size to perturb the forcing data was an educated guess of the quality of the data, since at the time there was very little knowledge on it. Perhaps for future work, this perturbation size can be obtained through comparison with other existing data, for instance the ECMWF[7] forecast (Gunter, 2009).

In the introduction of this thesis, there are three questions which are expected to be resolved with this thesis. The first one is the question of how to disaggregate the monthly GRACE observation in time. This was answered in section 6.1, by interpolating the converted-absolute GRACE TWS values into 5 days interval using spline interpolation, thereby avoiding having a single observation per month. Although the 5 days interval can be considered as an approximation to the GRACE footprint, perhaps in future studies this can be improved by taking into account the actual overpasses of the GRACE satellites over the Rhine river basin. This will require better knowledge of how GRACE TWS change data is processed.

The second question is how to separate the contribution of the TWS components from GRACE observation. This has been answered in section 6.4, by taking into account the storage boundaries implemented in the HBV-96 model.

The final and perhaps the most intriguing question is whether assimilation GRACE TWS change data into the HBV-96 model using the EnKF and EnKS works and actually improves the model state estimates. In terms of the EnKF and EnKS, the algorithm has been shown to perform as expected. The estimated TWS was updated towards the observation, and in the meanwhile the covariance is reduced to lower than either the prior TWS or the GRACE observation. This was proven further by the short experiments in Section 7.2.

From the results shown in Section 7.1, the update appeared to have the biggest impact on the first months of the simulation. As the simulation went further in time, the ensemble variance was significantly reduced that the model became more ‘accurate’ and the update became less significant. When the error covariance became higher due to precipitation event, the TWS is updated more significantly.

Here it can be seen that the HBV-96 model of the Rhine is very good that once the ensemble variance is reduced, it is difficult for the ensemble to grow much further again, even in the experiment of using longer observation intervals at which the standard deviation went to a plateau; and thus the update becomes less significant. It would be interesting if the experiment is conducted at a different basin where the model parameters and forcing data are not so well understood. Then it can be seen if the model would still be as ‘accurate’ after the first months of simulation as it was in this thesis.

[7] European Centre for Medium-Range Weather Forecasts

As the simulation started at the very wet period, the reducing variance was also affected by the wetness of the catchment (i.e. by precipitation event). The update appeared to be most negligible at the driest period, even after applying EnKS. This is combined with the GRACE observations at the dry period being considerably close the prior model state. Towards the end of the simulation, the catchment was beginning to become wet again, and the size of the update seemed to gradually become more significant again.

The same pattern is reflected in the estimated discharge in Section 7.3, where comparing the model estimated discharge to the validation data showed improvements in the beginning of the data assimilation, with the estimated discharge became closer to the validation data, but not maintained through simulation period, even when the EnKS was applied. The end of the simulation period showed a gradual improvement again.

With these findings, it is difficult to come to a definite conclusion. There is an indication of seasonality, since the update gradually became better again during the end of the simulation when the catchment became wet again. One year of simulation is clearly not enough to resolve whether this seasonality actually exists or not, and thus it is highly recommended to perform longer simulation period in future work.

This research has not been able to indicate which of the two GRACE data sets used in data assimilating provides better improvement to the model. The GRACE GSM data showed better agreement with the validation data at the beginning of the experiment, but the GRACE DMT1 data improved gradually towards the end of the simulation, which corresponds to the difference in peaks for the two data sets.

To further answer these questions, further study can be done by at least extending the simulation period, observe the seasonal pattern and get a better indication of the influence of the different GRACE data sets. The EnKS can be extended to longer lags, that the observations from different months influence the past states. Validation can also be extended to more discharge stations spread across the river basin, or by comparison with other data, such as remotely sensed soil moisture data.

9 Bibliography

Berglöv G. [et al.] Improvement HBV model Rhine in FEWS: Final report [Report] : Final report / SMHI. - 2009.

Beven K.J. and Bingley A.M The future of distributed models: model calibration and uncertainty prediction [Journal] // Hydrological Processes. - Vol. 6. - pp. 279-298.

Bohling Geoff Introduction to geostatistics and variogram analysis [Book]. - 2005. - http://people.ku.edu/~gbohling/cpe940/.

Crosson William L. [et al.] Assimilating remote sensing data in a surface flux-soil moisture model [Journal] // Hydrological processes. - 2002. - Vol. 16. - pp. 1645-1662.

CSR Gravity Recovery and Climate Experiment : Flight Configuration [Online] // GRACE. - 2004. - 16 July 2009. - http://www.csr.utexas.edu/grace/mission/flight_config.html.

Drécourt Jean-Philippe Data assimilation in hydrological modelling [Report] : PhD Thesis / Environment and Resources ; Technical University of Denmark. - 2004.

Dunne Susan and Entekhabi Dara An ensemble-based reanalysis approach to land data assimilation [Journal] // Water Resources Research. - Vol. 41.

Dunne Susan and Entekhabi Dara Land surface state and flux estimation using the ensemble Kalman smoother during the Southern Grat Plains 1997 field experiment [Journal] // Water Resources Research. - 2006. - Vol. 42.

Evensen Geir Sampling strategies and square root analysis schemes for the EnKF [Journal] // Ocean Dynamics. - 2004. - Vol. 54. - pp. 539-560.

Evensen Geir The Ensemble Kalman Filter: theoretical formulation and practical implementation [Journal] // Ocean Dynamics. - 2003. - Vol. 53. - pp. 343-367.

Famiglietti Jay Terrestrial Water Storage: Implications of the Decadal Survey [Presentation] // Satellite Observations of the Global Water Cycle. - [s.l.] : Earth System Science Department, University of California, Irvine and Jet Propulsion Laboratory, California Institute of Technology, 7 March 2007.

GFZ Global earth science data [Online] // Information systems and data center. - 16 July 2009. - http://isdc.gfz-potsdam.de/modules.php?name=product_type_overview.

Gunter B.C. . - 2009. - personal communication.

Güntner A Improvement of global hydrological models using GRACE data [Journal] // Surveys in Geophysics. - 2008. - Vol. 29.

Güntner Andreas [et al.] A global analysis of temporal and spatial variations in continental water storage. [Journal] // Water Resources Research. - 2007. - Vol. 43.

Hasan Shaakeel Terrestrial water storage change from temporal gravity variation [Report] : Ph.D. thesis / Wageningen University of Research. - 2009.

Hirschi Martin [et al.] Analysis of seasonal terrestrial water storage variations in regional climate simulations over Europe [Journal] // Journal of Geophysical Research. - 2007. - Vol. 112.

International Commission for the Hydrology of the Rhine (CHR) Impact of climate change on hydrological regimes and water resources management in the Rhine basin [Journal] / ed. Grabs W.. - 1997.

Klees R. [et al.] A Comparison of Global and Regional GRACE Models for Land Hydrology [Journal] // Surveys in Geophysics. - 2008a. - 4-5 : Vol. 9. - pp. 335-359.

Klees R. [et al.] A data-driven approach to local gravity field modelling using spherical radial basis function [Journal] // Journal of Geodesy. - 2008b. - 8 : Vol. 82.

Klees R. [et al.] The bias in GRACE estimates of continental water storage variations [Journal] // Hydrology and Earth System Sciences. - 2007. - Vol. 11. - pp. 1227-1241.

Klees R. [et al.] The design of an optimal filter for monthly GRACE gravity models [Journal] // Geophysics Journal International. - 2008c. - Vol. 175. - pp. 417-432.

Kroner C. and Jahr Th. Hydrological experiments around the superconducting gravimeter at Moxa Observatory [Journal] // Journal of Geodynamics. - 2006. - Vol. 41. - pp. 268-275.

Lindstorm G. [et al.] Development and test of the distributes HBV-96 hydrological model [Journal] // Journal of Hydrology. - 1997. - Vol. 201. - pp. 272-288.

McLaughin Dennis An integrated approach to hydrologic data assimilation: interpolation, smoothing, and filtering [Journal] // Advances in Water Resources. - 2002. - Vol. 25. - pp. 1275-1286.

Melching C.S. Reliability estimation [Book Section] // Computer models of Watershed Hydrology / ed. Singh V.P.. - [s.l.] : Water Resources Publications, 1995.

Reichle R.H., McLaughin D.B. and Entekhabi D. Variational data assimilation of microwave radio brightness observations for land surface hydrology applications [Journal] // IEEE Transactions on Geosciences adn Remote Sensing. - 2001. - 8 : Vol. 39. - pp. 1708-1718.

Reichle Rolf H., McLaughlin Dennis B. and Entekhabi Dara Hydrologic Data Assimilation with the Ensemble Kalman Filter [Journal] // Monthly Weather Reviews. - 2002. - Vol. 130. - pp. 103-114.

Rhine [Online] // Waterwiki.net. - 16 July 2009. - http://waterwiki.net/index.php/Rhine.

Riegger J. and Güntner A. Time variation in hydrology and gravity [Journal] // Earth, Moons and Planet. - 2005. - Vol. 94. - pp. 41-55.

Savenije H.H.G Hydrological modelling; CT4431 [Book]. - Delft : TU Delft, 2007. - p. 134.

Seo Dong-Jun, Koren Victor and Cajina Netfali Real-time variational assimilation of hydrologic and hydrometeorological data into operational hydrologic forecasting [Journal]. - 2003. - 3 : Vol. 4. - pp. 627-641.

SHMI [Online]. - 16 July 2009. - http://www.smhi.se/sgn0106/if/hydrologi/hbv.htm.

Singh Vijay P. and Woolhise David A. Mathematical Modeling of Watershed Hydrology [Journal] // Journal of Hydrologic Engineering. - 2002. - 4 : Vol. 7. - pp. 270-292.

Syed Tajdarul H. [et al.] Analysis of terrestrial water storage changes from GRACE and GLDAS [Journal] // Water Resources Research. - 22 February 2008. - Vol. 44.

Tapley B.D. [et al.] The gravity recovery and climate experiment: Mission overview and early results [Journal] // Geophysical Research Letters. - 2004. - Vol. 31.

University of Utrecht [Online] // PCRaster. - 16 July 2009. - http://pcraster.geo.uu.nl/.

Wahr J., Swenson S. and Velicogna I. Accuracy of GRACE mass estimates [Journal] // Geophysical Research Letters. - 2006. - Vol. 33.

Wahr John, Molenaar Mery and Bryan Frank Time variability of the Earth's gravity field: Hydrological and oceanic effects and their possible detection using GRACE [Journal] // Journal of Geophysical Research. - 1998. - Vol. 103. - pp. 30,205-30,229.

Weerts A. . - 2009. - personal communication.

Weerts A.H. and Serafy El G.Y.H. Particle filtering and ensemble kalman filtering for state updating with hydrological conceptual rainfall-runoff models. [Journal] // Water Resources Research. - 2006. - Vol. 42.

Weerts A.H., Meißner D. and Rademacher S. Input data rainfall-runoff model operational systems FEWS-NL & FEWS-DE [Report] / Deltares. - 2008.

Winsemius H.C. [et al.] Assesment of Gravity Recovery and Climate Experiment (GRACE) temporal signature over the upper Zambezi [Journal] // Water Resources Research. - 2006. - Vol. 42.

Zaitchik Benjamin F., Rodell Matthew and Reichle Rolf H. Assimilation of GRACE Terrestrial Water Storage Data into a Land Surface Model: Results for the Mississippi River Basin [Journal] // Journal of Hydrometeorology. - 2008. - Vol. 9. - pp. 535-548.

Appendix A Sensitivity study results

This appendix provides the maximum and minimum values of CV at the catchment and the 5 sample pixels, for the tested parameters in the sensitivity study (Chapter 5). These values are combined maximum and minimum for both tests (i.e. 2% and 5% deviations). Values from perturbing maxbas however, is not included as the results are all zero variability (CV = 0 everywhere). Next to this, for every parameter, a figure highlighting the most effected storage is provided to give a better view on its impact during the study period.

Perturbing *k4*

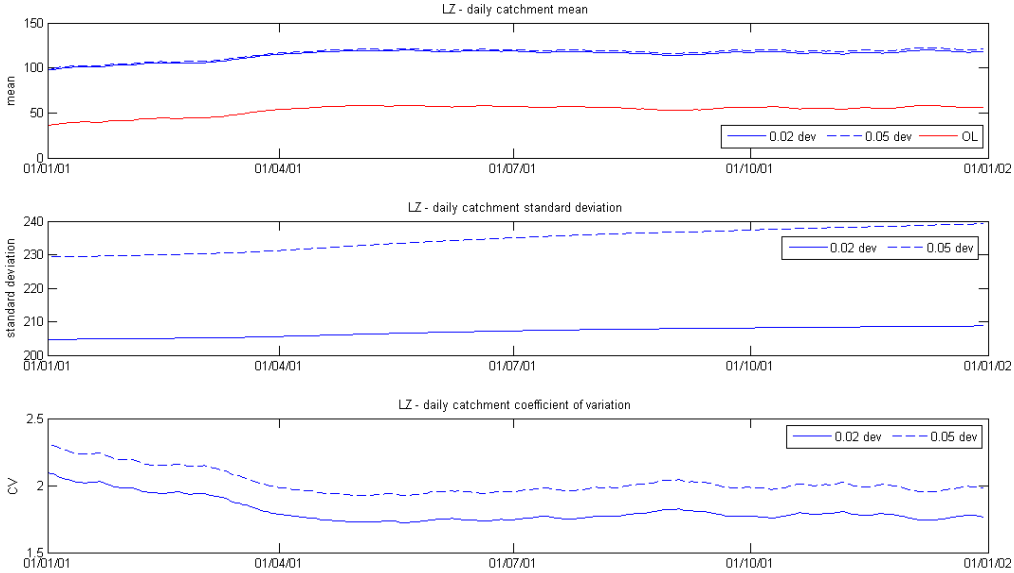

Figure A-1 Catchment statistics of lower zone storage (perturbed parameter: *k4*)

Table A -1 Coefficient of variation (perturbed parameter: *k4*)

	Output (1-4)							
	Snow cover		Soil Moisture		Interception Storage		Lower Zone Storage	
CV	Min	Max	Min	Max	Min	Max	Min	Max
Catchment	0	0	0	0	0	0	1.7235	2.3147
Pixel 1	0	0	0	0	0	0	0.0403	0.1001
Pixel 2	0	0	0	0	0	0	0.3108	0.7475
Pixel 3	0	0	0	0	0	0	0.0646	0.3213
Pixel 4	0	0	0	0	0	0	0.0328	0.0683
Pixel 5	0	0	0	0	0	0	0.0916	1.5412
	Output (5-8)							
	Upper Zone Storage		Runoff (Q)		Discharge (Qacc)		Base flow	
CV	Min	Max	Min	Max	Min	Max	Min	Max
Catchment	0	0	9.14E-04	0.1180	1.17E-05	0.0014	9.17E-04	0.1246
Pixel 1	0	0	2.47E-08	0.0046	2.46E-06	0.0005	1.82E-07	0.0131
Pixel 2	0	0	0	0.2219	0	0.0833	0	0.2219
Pixel 3	0	0	0	0.1243	0	0.0468	0	0.1243
Pixel 4	0	0	6.95E-08	0.0135	6.95E-08	0.0135	1.24E-07	0.0144
Pixel 5	0	0	0	0.2356	0	0.2356	0	0.2358

Perturbing *khq*

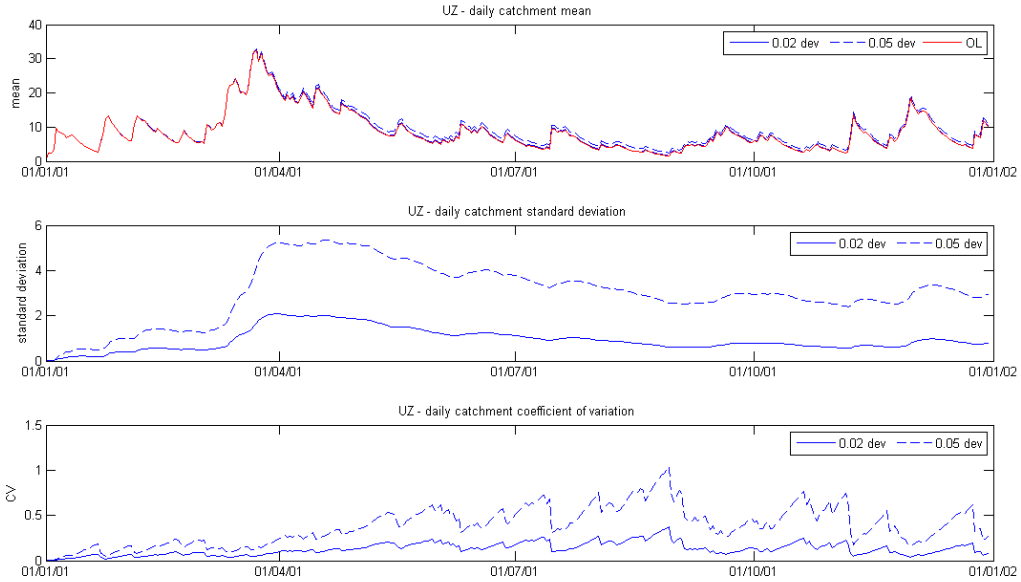

Figure A-2 Catchment statistics of upper zone storage (Perturbed parameter: *khq*)

Table A -2 Coefficient of variation (perturbed parameter: *khq*)

	Output (1-4)							
	Snow cover		Soil Moisture		Interception Storage		Lower Zone Storage	
CV	Min	Max	Min	Max	Min	Max	Min	Max
Catchment	0	0	0	0.0033	0	0	0	0.0272
Pixel 1	0	0	0	0.0016	0	0	0	0.0110
Pixel 2	0	0	0	0	0	0	0	0.0624
Pixel 3	0	0	0	0.0091	0	0	0	0.0960
Pixel 4	0	0	0	0.0122	0	0	0	0.1202
Pixel 5	0	0	0	0	0	0	0	0.0866
	Output (5-8)							
Pixel	Upper Zone Storage		Runoff (Q)		Discharge (Qacc)		Base flow	
CV	Min	Max	Min	Max	Min	Max	Min	Max
Catchment	0.0002	1.0353	0.0003	0.1225	4.91E-06	0.0035	0	0.0340
Pixel 1	0.0002	0.8789	0.0003	0.3557	1.01E-05	0.0017	0	0.0110
Pixel 2	3.09E-05	3.1622	0	0.3861	0	0.0970	0	0.0624
Pixel 3	9.59E-06	3.1622	0	0.2376	0	0.102	0	0.0960
Pixel 4	0.0002	3.1622	0.0001	0.1964	0.00011	0.1964	0	0.1202
Pixel 5	4.90E-06	3.1622	0	0.4804	0	0.4804	0	0.0866

Perturbing *beta*

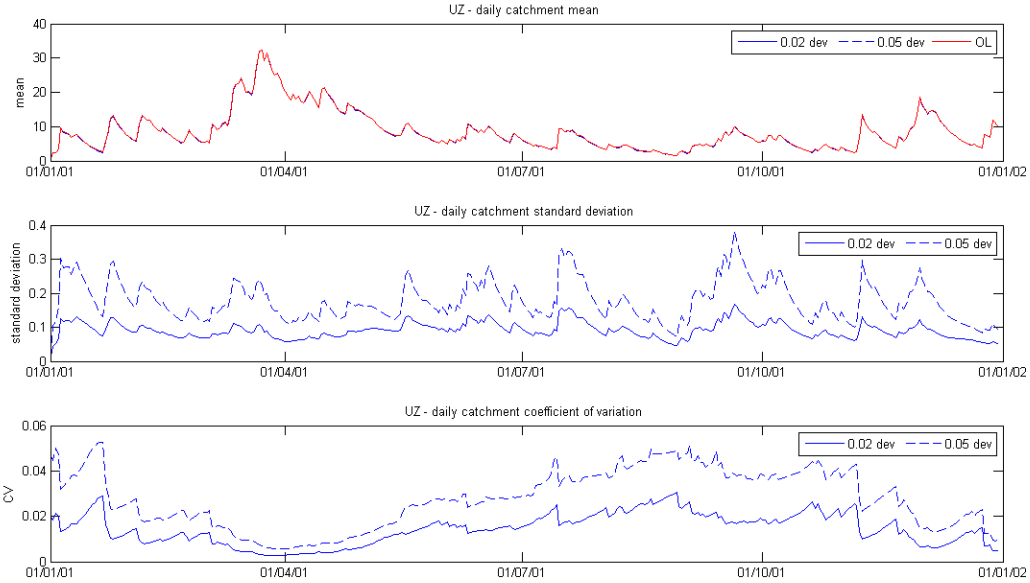

Figure A-3 Catchment statistics of upper zone storage (Perturbed parameter: *beta*)

Table A -3 Coefficient of variation (perturbed parameter: *beta*)

	Output (1-4)							
Pixel	Snow cover		Soil Moisture		Interception Storage		Lower Zone Storage	
CV	Min	Max	Min	Max	Min	Max	Min	Max
Catchment	0	0	9.45E-05	0.0140	0	0	2.51E-05	0.0138
Pixel 1	0	0	0.0006	0.0694	0	0	0	0.0973
Pixel 2	0	0	0	0.0122	0	0	0	0.0274
Pixel 3	0	0	0	0.0306	0	0	0	0.1161
Pixel 4	0	0	0.0002	0.0140	0	0	0	0.0906
Pixel 5	0	0	0	0.0160	0	0	0	0.0376
	Output (5-8)							
Pixel	Upper Zone Storage		Runoff (Q)		Discharge (Qacc)		Base flow	
CV	Min	Max	Min	Max	Min	Max	Min	Max
Catchment	0.0026	0.0527	0.0001	0.0363	3.62E-06	0.0027	3.97E-05	0.0223
Pixel 1	0.0018	3.1622	5.00E-04	0.1863	3.80E-06	0.0019	0	0.0973
Pixel 2	0.0007	3.1622	0	0.0315	0	0.0255	0	0.0274
Pixel 3	0.0023	3.1622	0	0.1161	0	0.0418	0	0.1161
Pixel 4	0.0001	3.1622	0.0003	0.0906	0.0003	0.0906	0	0.0906
Pixel 5	0.0019	3.1622	0	0.0376	0	0.0376	0	0.0376

Perturbing *fc*

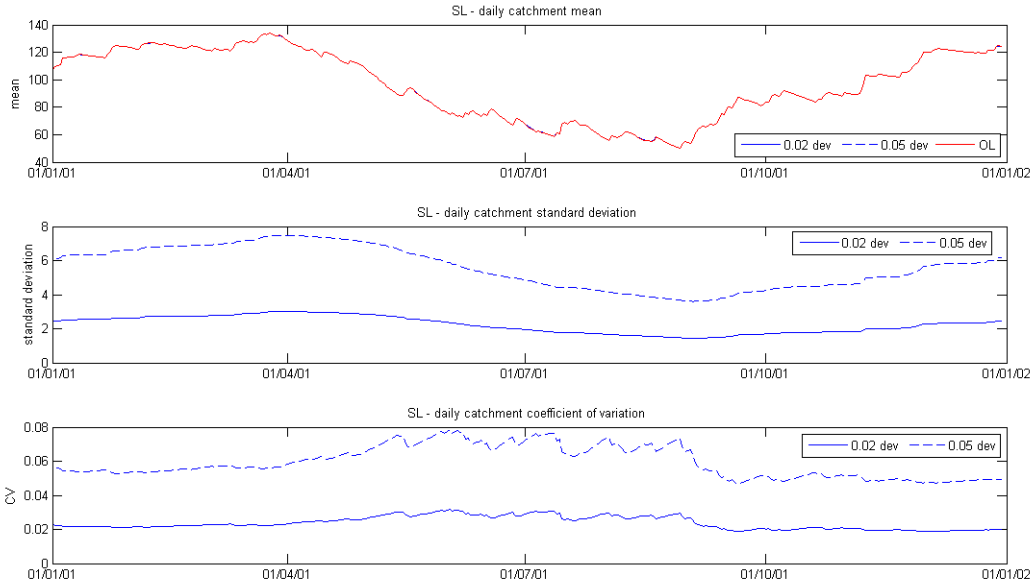

Figure A-4 Catchment statistics of soil moisture (Perturbed parameter: *fc*)

Table A-4 Coefficient of variation (perturbed parameter: *fc*)

	Output (1-4)							
	Snow cover		Soil Moisture		Interception Storage		Lower Zone Storage	
CV	Min	Max	Min	Max	Min	Max	Min	Max
Catchment	0	0	0.0187	0.0785	0	0	3.82E-06	0.0054
Pixel 1	0	0	0.0161	0.1723	0	0	0	0
Pixel 2	0	0	0.0167	0.2386	0	0	0	0.0385
Pixel 3	0	0	0.0235	0.1203	0	0	0	0.0187
Pixel 4	0	0	0.0174	0.0719	0	0	0	0.0222
Pixel 5	0	0	0.0179	0.0791	0	0	0	0.0091
	Output (5-8)							
	Upper Zone Storage		Runoff (Q)		Discharge (Qacc)		Base flow	
CV	Min	Max	Min	Max	Min	Max	Min	Max
Catchment	0.0019	0.0318	2.47E-05	0.0337	3.54E-07	0.0005	3.85E-06	0.0075
Pixel 1	1.04E-05	0.0649	3.43E-05	0.0357	8.57E-07	0.0004	0	0
Pixel 2	0.0003	3.1622	0	0.1128	0	0.0822	0	0.0385
Pixel 3	0.0001	3.1622	0	0.0401	0	0.0157	0	0.0187
Pixel 4	7.04E-06	3.1622	1.70E-05	0.0384	1.70E-05	0.0384	0	0.0222
Pixel 5	0.0005	3.1622	0	0.0305	0	0.0305	0	0.0091

Perturbing *perc*

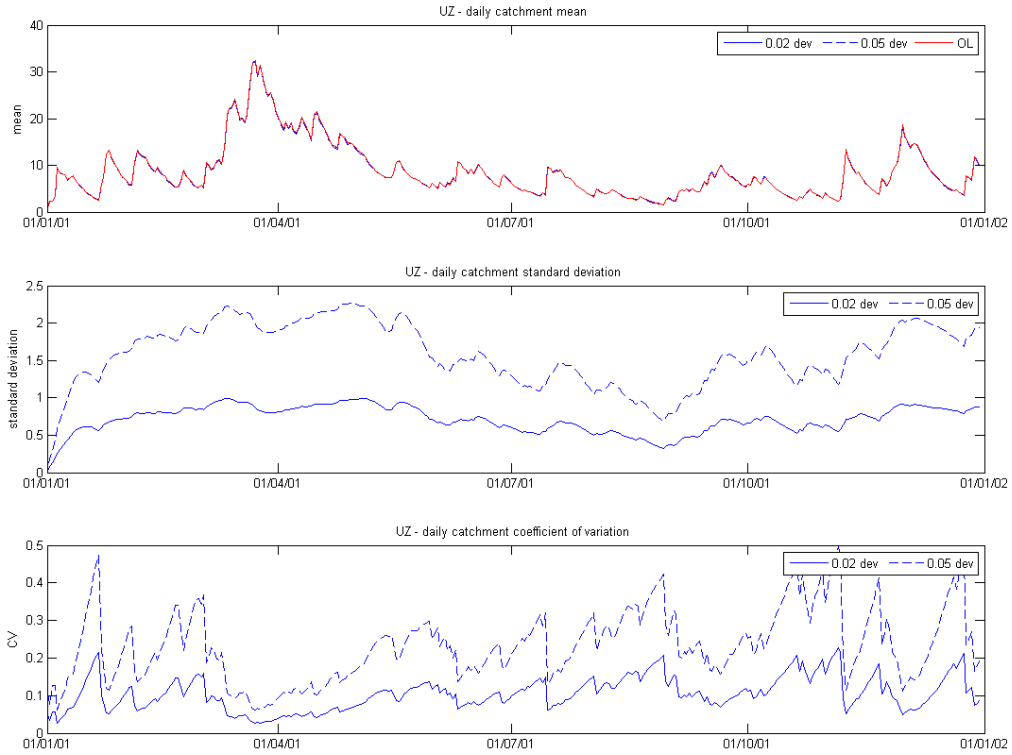

Figure A-5 Catchment statistics of upper zone storage (perturbed parameter: *perc*)

Table A-5 Coefficient of variation (perturbed parameter: *perc*)

	Output (1-4)							
	Snow cover		Soil Moisture		Interception Storage		Lower Zone Storage	
CV	Min	Max	Min	Max	Min	Max	Min	Max
Catchment	0	0	1.15E-05	0.0112	0	0	0.0006	0.1143
Pixel 1	0	0	0	0.0245	0	0	0.0158	0.9539
Pixel 2	0	0	0	0	0	0	0	0.1721
Pixel 3	0	0	0	0.0788	0	0	0	0.6453
Pixel 4	0	0	0	0.0692	0	0	0.0242	0.854
Pixel 5	0	0	0	0	0	0	0	0.1333
	Output (5-8)							
	Upper Zone Storage		Runoff (Q)		Discharge (Qacc)		Base flow	
CV	Min	Max	Min	Max	Min	Max	Min	Max
Catchment	0.0262	0.4968	0.00294	0.0882	4.02E-05	0.0013	0.0032	0.2129
Pixel 1	0.0176	0.7530	0.00012	0.3401	2.44E-05	0.0026	0.0158	0.9539
Pixel 2	0.0177	3.1622	0	0.2137	0	0.0483	0	0.1721
Pixel 3	0.0354	3.1622	0	0.3097	0	0.0909	0	0.6453
Pixel 4	0.0262	3.1622	0.00058	0.4056	0.00058	0.4056	0.0242	0.854
Pixel 5	0.0083	3.1622	0	0.0914	0	0.0914	0	0.1333

Perturbing *cflux*

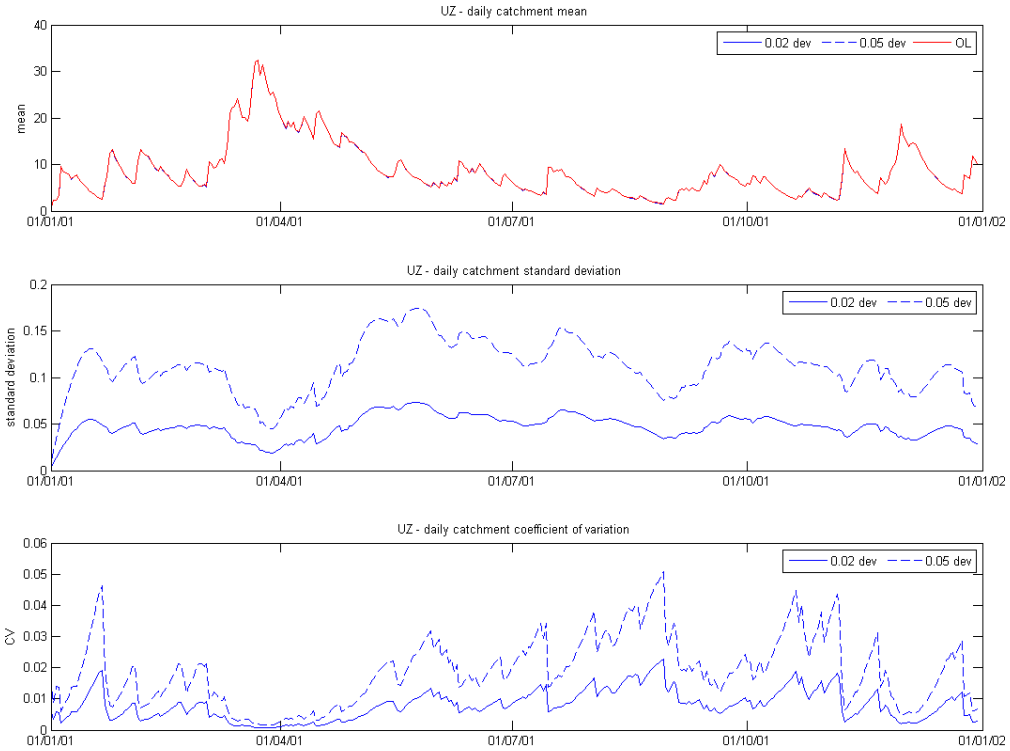

Figure A-6 Catchment statistics of upper zone storage (perturbed parameter: *cflux*)

Table A-6 Coefficient of variation (perturbed parameter: *cflux*)

	Output (1-4)							
	Snow cover		Soil Moisture		Interception Storage		Lower Zone Storage	
CV	Min	Max	Min	Max	Min	Max	Min	Max
Catchment	0	0	2.64E-05	0.0071	0	0	0	0.0048
Pixel 1	0	0	0.0001	0.0881	0	0	0	0.0158
Pixel 2	0	0	0	0.0030	0	0	0	0.0037
Pixel 3	0	0	0	0.0266	0	0	0	0.0604
Pixel 4	0	0	0.0001	0.0175	0	0	0	0.1139
Pixel 5	0	0	0	0.0038	0	0	0	0.0048
	Output (5-8)							
	Upper Zone Storage		Runoff (Q)		Discharge (Qacc)		Base flow	
CV	Min	Max	Min	Max	Min	Max	Min	Max
Catchment	0.0006	0.0507	3.42E-05	0.0130	4.76E-07	0.0001	0	0.0102
Pixel 1	8.18E-05	0.7484	9.57E-05	0.1835	1.41E-06	0.0006	0	0.0158
Pixel 2	1.29E-05	3.1622	0	0.0043	0	0.0067	0	0.0037
Pixel 3	9.54E-05	3.1622	0	0.0604	0	0.0270	0	0.0604
Pixel 4	0.0001	3.1622	0.0002	0.1139	0.0002	0.1139	0	0.1139
Pixel 5	6.79E-07	3.1622	0	0.0048	0	0.0048	0	0.0048

Perturbing *lp*

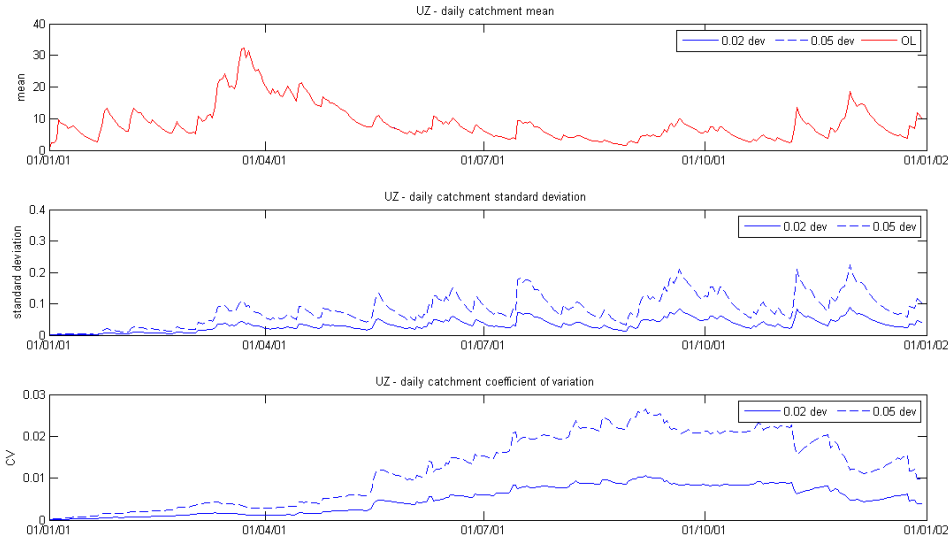

Figure A-7 Catchment statistics of upper zone storage (perturbed parameter: *lp)*

Table A-7 Coefficient of variation (perturbed parameter: *lp*)

	Output (1-4)							
	Snow cover		Soil Moisture		Interception Storage		Lower Zone Storage	
CV	Min	Max	Min	Max	Min	Max	Min	Max
Catchment	0	0	2.69E-05	0.0228	0	0	1.28E-07	0.0076
Pixel 1	0	0	3.65E-05	0.0432	0	0	0	0
Pixel 2	0	0	3.76E-05	0.0611	0	0	0	0.0172
Pixel 3	0	0	2.47E-05	0.0431	0	0	0	0.0206
Pixel 4	0	0	2.74E-05	0.0257	0	0	0	0.0551
Pixel 5	0	0	1.81E-05	0.0273	0	0	0	0.0231
	Output (5-8)							
	Upper Zone Storage		Runoff (Q)		Discharge (Qacc)		Base flow	
CV	Min	Max	Min	Max	Min	Max	Min	Max
Catchment	4.83E-05	0.0265	4.72E-07	0.0203	2.43E-08	0.0002	1.46E-07	0.0109
Pixel 1	3.96E-05	0.0598	1.47E-06	0.0383	8.58E-08	0.0002	0	0
Pixel 2	0.0003	3.1622	0	0.0329	0	0.0206	0	0.0172
Pixel 3	0.0001	3.1622	0	0.0206	0	0.0081	0	0.0206
Pixel 4	3.44E-05	3.1622	1.64E-06	5.63E-02	1.64E-06	0.0562	0	0.0551
Pixel 5	4.58E-05	3.1622	0	0.0231	0	0.0231	0	0.0231

Perturbing *icfi*

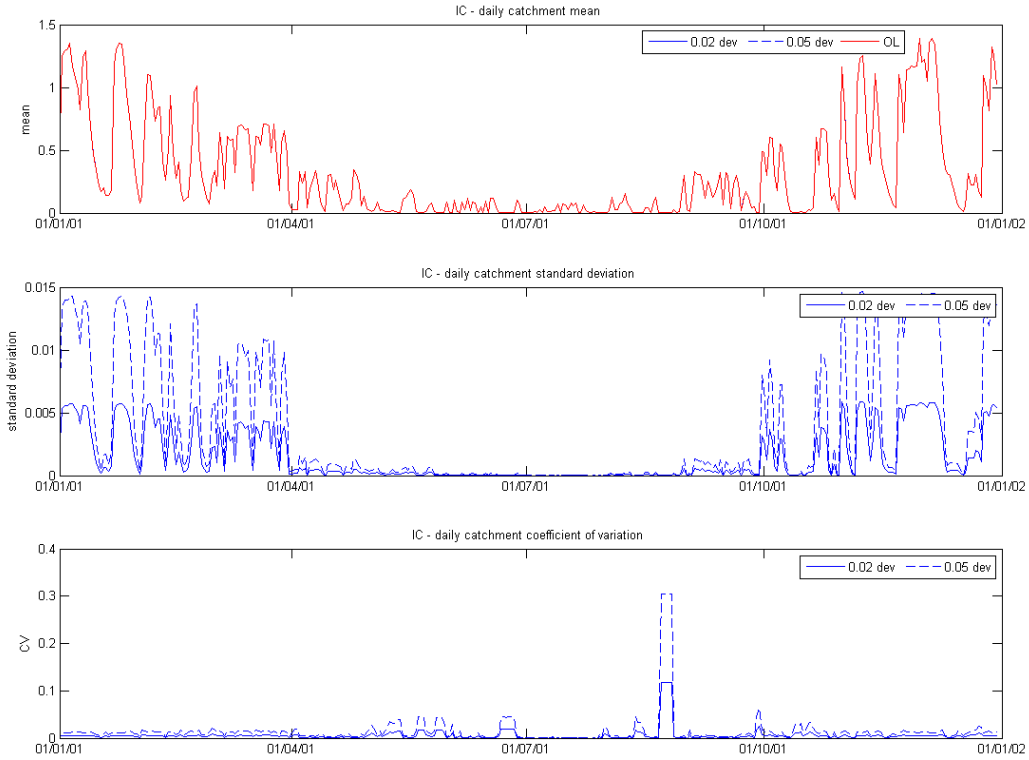

Figure A-8 Catchment statistics of interception storage (perturbed parameter: *icfi)*

Table A-8 Coefficient of variation (perturbed parameter: *icfi*)

	Output (1-4)							
	Snow cover		Soil Moisture		Interception Storage		Lower Zone Storage	
CV	Min	Max	Min	Max	Min	Max	Min	Max
Catchment	0	0	1.03E-05	0.0022	0	0.3051	6.25E-06	0.0021
Pixel 1	0	0	2.40E-05	0.0035	0.0136	3.1622	0	0
Pixel 2	0	0	0	0.0125	0	3.1622	0	0.0085
Pixel 3	0	0	0	0.0124	0.0109	3.1622	0	0.0201
Pixel 4	0	0	1.51E-05	0.0047	0	3.1622		
Pixel 5	0	0	0	0	0	0	0	0
	Output (5-8)							
	Upper Zone Storage		Runoff (Q)		Discharge (Qacc)		Base flow	
CV	Min	Max	Min	Max	Min	Max	Min	Max
Catchment	0.0002	0.0074	2.46E-05	0.0052	5.03E-07	8.19E-05	1.37E-05	0.0030
Pixel 1	0.0001	0.0150	6.36E-05	0.0106	6.25E-07	0.0001	0	0
Pixel 2	0.0001	3.1622	0	0.0099	0	0.0022	0	0.0085
Pixel 3	6.33E-05	3.1622	0	0.0201	0	0.0089	0	0.0201
Pixel 4	0.0001	3.1622	0	0.0275	0	0.0275	0	0.0275
Pixel 5	0	0	0	0	0	0	0	0

Perturbing *icfi*

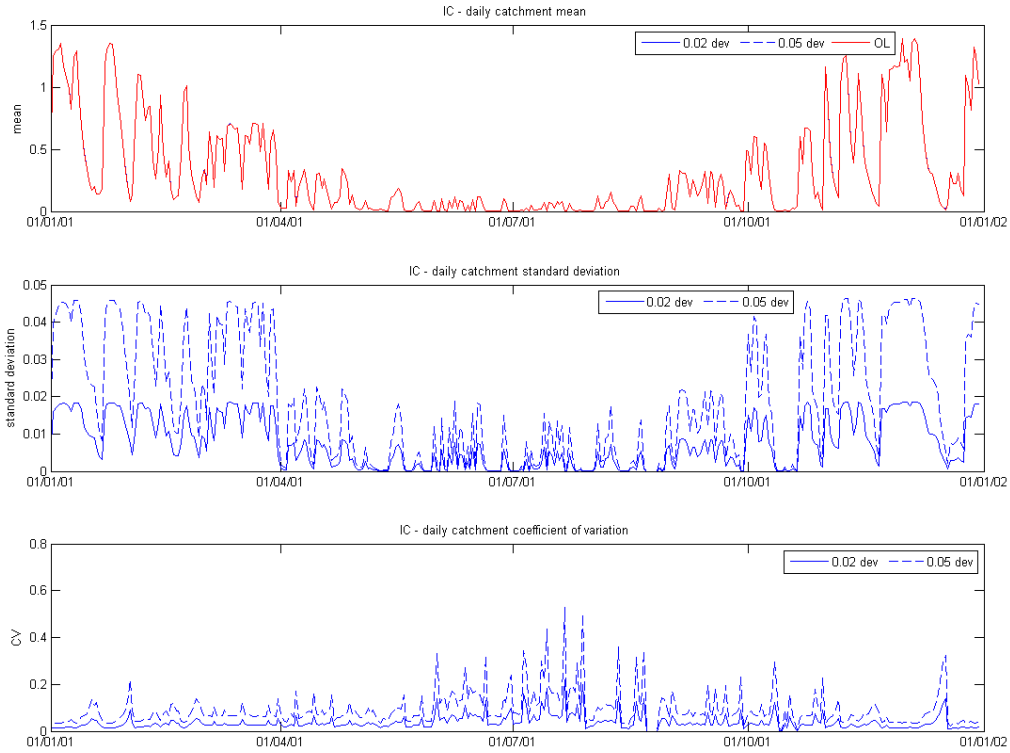

Figure A-9 Catchment statistics of interception storage (perturbed parameter: *icfo)*

Table A-9 Coefficient of variation (perturbed parameter: *icfo*)

	Output (1-4)							
	Snow cover		Soil Moisture		Interception Storage		Lower Zone Storage	
CV	Min	Max	Min	Max	Min	Max	Min	Max
Catchment	0	0	2.82E-05	0.0053	0	0.5296	1.08E-05	0.0026
Pixel 1	0	0	0	0	0	0	0	0
Pixel 2	0	0	0	0	0	0	0	0
Pixel 3	0	0	0	0	0	0	0	0
Pixel 4	0	0	0	0	0	0	0	0
Pixel 5	0	0	0	0.0077	0	3.1622	0	0.0150
	Output (5-8)							
	Upper Zone Storage		Runoff (Q)		Discharge (Qacc)		Base flow	
CV	Min	Max	Min	Max	Min	Max	Min	Max
Catchment	0.0005	0.0148	7.62E-05	0.0109	2.21E-06	0.0001	4.42E-05	0.0048
Pixel 1	0	0	0	0	3.63E-06	0.0004	0	0
Pixel 2	0	0	0	0	0	0.0084	0	0
Pixel 3	0	0	0	0	0	0	0	0
Pixel 4	0	0	0	0	0	0	0	0
Pixel 5	0.0001	3.1622	0	0.0150	0	0.0150	0	0.0150

Appendix B Variogram calculation

A semi-variogram (also commonly referred to as just variogram) characterises the spatial continuity of a dataset. It is based on modeling the squared differences in the data values as a function of the distances between the know points, and these variances are commonly represented as a graph (e.g. Figure B-1). Such a graph is helpful to build a mathematical model that describes the variability of the measure with location. For a complete explanation of building variogram, readers can refer to e.g. (Bohling, 2005).

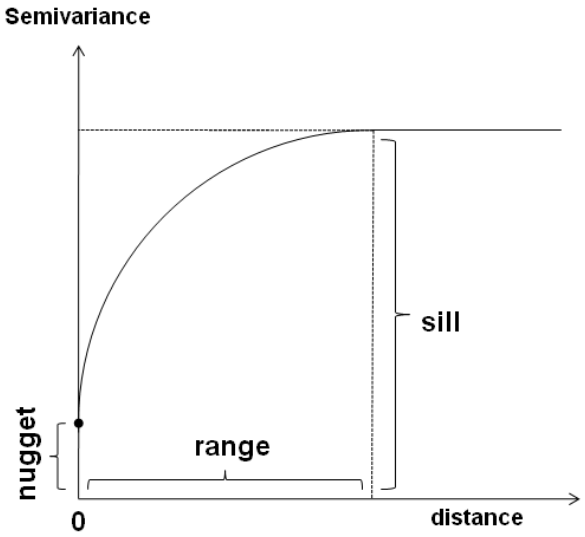

Figure B-1 Variogram

The variogram parameters of interest for this thesis are the range and the nugget. Range is the distance of which the maximum dissimilarity is reached, and can be interpreted as the correlation length to be used in the random perturbation generation.

Nugget is the height of the jump of the variogram at the discontinuity at the origin, which represents unresolved variation. This variation can be a mixture of spatial variation at finer scale than the sample spacing and measurement error. For the thesis purpose this can give indication of the standard deviation to also be used in the random perturbation generation.

The variogram parameters are calculated for Evapotranspiration, Precipitation, and Temperature. Data from one full year is considered to be sufficient to extract this information.

For one day, a random set of 2500 points are taken as sample to calculate variogram parameters of this day. This random sampling and calculation is done 10 times, and afterwards the mean of the parameters are calculated, resulting in daily mean parameters.

Within each month, maps for 10 days are taken as sample, and from the 10 daily mean parameters, the monthly mean parameters are calculated.

The process of calculating the variogram parameters in this thesis is illustrated in Figure B-2. The results for the three forcing data: temperature, precipitation, and evaptranspiration are given in Figure B-3, B-4, and B-5 respectively. The correlation lengths as used in section 6.2 are

the averages from the monthly values. This is done considering that except for the first months of 2001, the ranges are close to each other for each months.

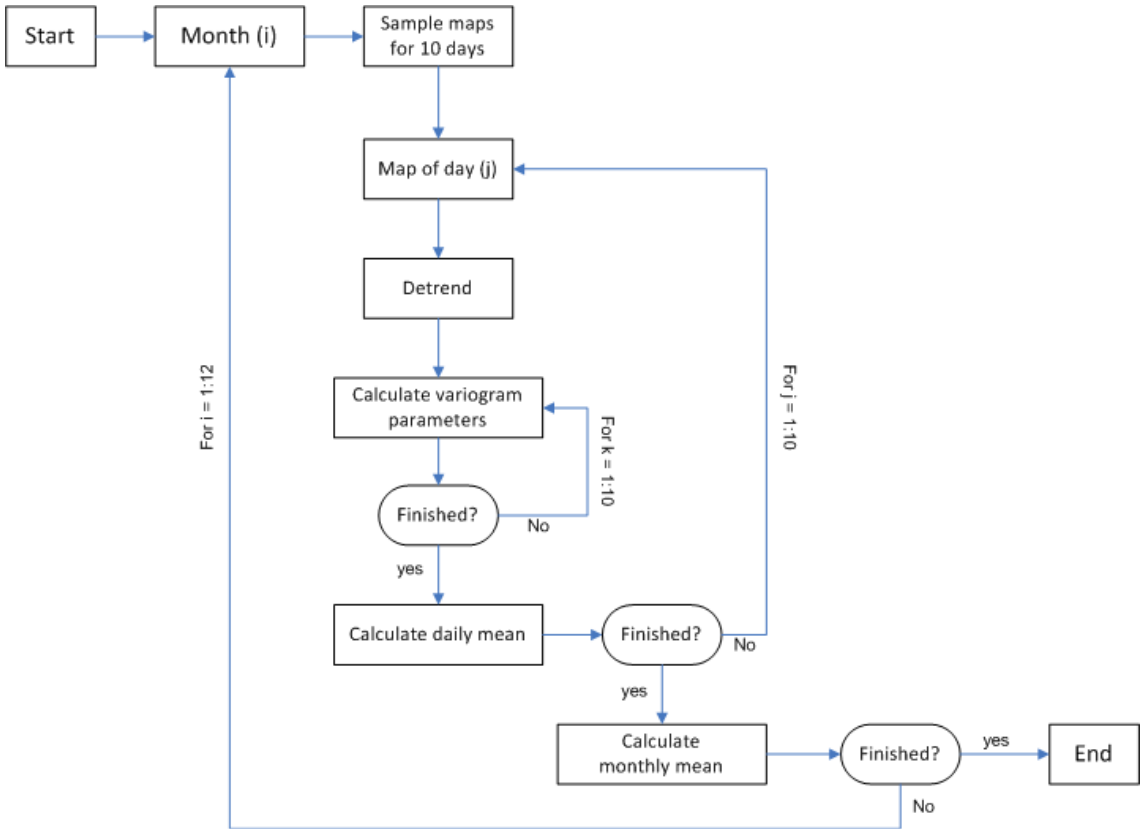

Figure B-2 Variogram calculation flow diagram.

Temperature

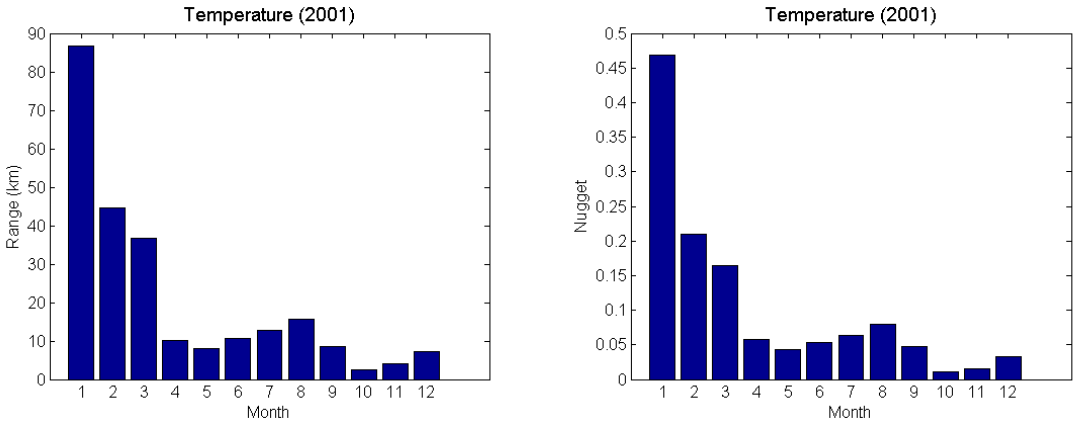

Figure B-3 Monthly mean range (left) and nugget (right) of temperature

Precipitation

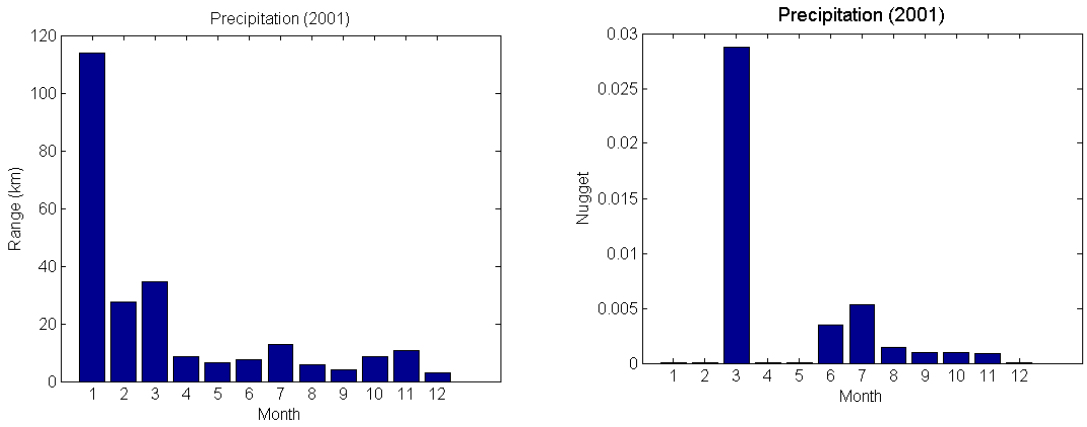

Figure B-4 Monthly mean range (left) and nugget (right) of precipitation

Evapotranspiration

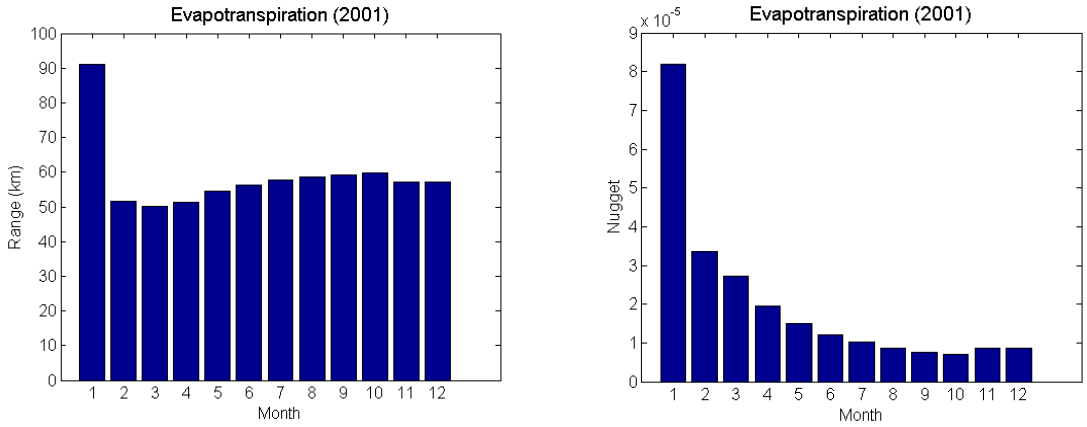

Figure B-5 Monthly mean range (left) and nugget (right) of evapotranspiration